NOVA SCHOOL OF SCIENCE & TECHNOLOGY

DEPARTAMENTO DE CIÊNCIAS DA VIDA

SARA LUCIANA DA SILVA CASCAIS

Licenciada em Bioquímica

MOLECULAR PHENOTYPING OF PROSTATE CANCER MICROENVIRONMENT, WITH EMPHASIS ON ASPARTOACYLASE EXPRESSION IN FIBROBLASTS

MESTRADO EM GENÉTICA MOLECULAR E BIOMEDICINA

Universidade NOVA de Lisboa

⟨Setembro⟩, ⟨2021⟩

NOVA SCHOOL OF SCIENCE & TECHNOLOGY

DEPARTAMENTO DE CIÊNCIAS DA VIDA

MOLECULAR PHENOTYPING OF PROSTATE CANCER MICROENVIRONMENT, WITH EMPHASIS ON ASPARTOACYLASE EXPRESSION IN FIBROBLASTS

SARA LUCIANA DA SILVA CASCAIS

Licenciado em Bioquímica

Orientador:	Mireia Castillo-Martin, Doutora Group Leader – Molecular and Experimental Pathology, Champalimaud Centre for the Unknown
Coorientadores:	Alexandra R Fernandes, Professora Doutora Assistant Professor, Department of Life Sciences, NOVA School of Science and Tecnhonology | FCT Nova

MESTRADO EM GENÉTICA MOLECULAR E BIOMEDICINA

Universidade NOVA de Lisboa
⟨Setembro⟩, ⟨2021⟩

Molecular Phenotyping of Prostate Cancer Microenvironment, with emphasis on Aspartoacylase expression in fibroblasts

Agradecimentos

Gostaria de expressar a minha maior gratitude ao grupo "Molecular and Experimental Pathology" da Fundação Champalimaud, que me acolheu desde o primeiro dia, e tornou este caminho muito mais agradável. Um obrigado especial à Mireia Castillo-Martin, que desde o primeiro dia me impressionou com a sua personalidade simples, criativa e acolhedora. Grata por todos os ensinamentos partilhados e por toda a confiança que depositou no projeto e na minha forma de investigar. Uma nota especial de agradecimento às minhas colegas: Ana, Andreia, Cátia e Inês; tornaram os meus dias mais animados e leves, e partilharam os desafios, dificuldades e contratempos inerentes a este percurso. Em conjunto, aprendemos a verdadeira importância da perseverança e resiliência.

Este trabalho não seria possível sem a ajuda de várias plataformas da Fundação Champalimaud: agradeço à "Advanced BioImaging and BioOptics Experimental Platform", em especial à Anna Pezzarossa pela ajuda crucial na análise das imagens de imunofluorescência; à plataforma de "Anatomy and Histology" por atender sempre aos meus pedidos de cortes histológicos sem fim, com uma simpatia inigualável e ao "Champalimaud Foundation Biobank" pelas amostras humanas disponibilizadas para que este projeto pudesse ser reproduzível.

Um obrigado à Faculdade de Ciências e Tecnologias da Universidade Nova de Lisboa, por todas as ferramentas disponibilizadas e pela preparação fornecida.

Agradeço a todos os meus amigos e colegas, que de forma direta e indireta me ajudaram a traçar este caminho. Um obrigado especial à Ana Moura, a minha eterna "lab partner", que apesar da distância, foi sempre um apoio incondicional, presente nos momentos mais desafiantes. Obrigado por me relembrares que admitir as nossas fraquezas e fragilidades é um grande passo para as ultrapassarmos. À Cátia Rebelo, a amizade mais espontânea deste percurso. Obrigado pelo companheirismo autêntico, pela liberdade das nossas conversas e por todos os planos traçados em conjunto. À minha amiga de infância, Beatriz Cardoso, por me incentivar, de uma forma tão genuína e inata, a percorrer um caminho que me faz sentir realizada. Ao Barbosa, por me ensinar a beleza por detrás da estranha ordem das coisas, por acreditar em mim e mesmo sem saber, foi uma das minhas maiores fontes de motivação e segurança. A todos os meus amigos, cujo nome não enumerei, um enorme obrigado; seguem no meu coração.

Aos meus irmãos, João e Andreia, por serem o meu "easy like a Sunday Morning", por serem um apoio verdadeiro e sincero. À minha tia Tita, pelo seu incentivo constante, por acreditar nos meus sonhos e partilhar a alegria por detrás de cada desafio aceite. Obrigado por cuidar de nós de uma forma incondicional e dedicada.

Dedico esta tese à minha mãe Alice e ao meu pai João, por serem a minha maior fonte de inspiração, o meu porto seguro, a minha força, os meus guias. Ao meu pai, por ser o oceano calmo, o apoio absoluto, a confiança verdadeira. À minha mãe, por ser a mulher forte e determinada que nos presenteia com uma energia vibrante. Obrigado pelo abraço forte e certo, que me faz ter a saudade mais intensa e o desejo mais afiado de conquistar. Obrigado por todos os valores que me transmitiram, por apostarem sempre na minha educação e formação e por me terem proporcionado a liberdade de voar atrás dos meus sonhos.

Para o meu avô Manel e a minha avó Alice, as estrelinhas mais brilhantes do céu. Aquilo que sou e a forma como vejo o mundo a eles lhe devo. Obrigado, avô, por me sentares no teu colo a ler as grandes enciclopédias e livros de história, o que fez de mim uma pessoa curiosa e sonhadora. E a ti avó, por me mostrares que a dedicação não tem medida, e que o amor é a forma mais bonita de conquistar o mundo. Para sempre grata.

“Every scientist dreams of doing something that can help the world”

Tu Youyou, Nobel Prize in Physiology or Medicine 2015

Resumo

O cancro da próstata (CaP) é o cancro mais comum e a segunda principal causa de morte por cancro em homens, estando 90% da mortalidade associada ao desenvolvimento de doença metastática, após a ineficiência de uma combinação de regimes terapêuticos disponíveis. Recentemente, foi demonstrado que o microambiente tumoral (MT) e as alterações metabólicas associadas às células que o compõem desempenham um papel determinante na tumorigénese.

A realização de um screening genético com o intuito de identificar alterações na expressão génica associadas a pior prognóstico e maior capacidade de metastização revelou que a Aspartoacilase (ASPA) poderá estar relacionada com uma maior agressividade da doença. O principal objetivo deste projeto é caracterizar o MT do CaP usando microscopia multiespectral, estabelecendo uma correlação das características do MT com os estágios da doença e o quadro clínico dos pacientes. Ao recorrer à técnica de imunofluorescência pretende-se desvendar um possível fenótipo que poderá prever o desenvolvimento de metástases antes da sua manifestação clínica.

Uma coorte de 123 amostras humanas, que inclui hiperplasias benignas da próstata (n = 20), CaP primários (n = 85) e metastáticos (n = 18), foi caracterizada imunofenotipicamente usando um painel otimizado de 5 biomarcadores (ASPA, CD31, CD68, Citoqueratina 18 e Desmina). Recorrendo a uma Multiplex de Imunofluorescência, foi possível avaliar a expressão de ASPA no MT, bem como as populações de fibroblastos (Desmina) e macrófagos (CD68). O marcador CD31 foi incluído com o intuito de determinar a densidade vascular nas amostras em estudo. O sinal de Citoqueratina 18 permitiu identificar as células tumorais, guiando a aquisição de imagens microscópicas. Em particular, áreas estromais entre as glândulas tumorais e na periferia dos ninhos tumorais foram adquiridas e analisadas recorrendo a softwares adequados.

Os nossos resultados demonstram que a expressão de ASPA co-localiza fortemente com a população de fibroblastos e diminui significativamente com a progressão tumoral. É também evidente um infiltrado de macrófagos abundante, principalmente nas regiões intratumorais, podendo correlacionar-se com pior prognóstico dos doentes. Verifica-se aumento da densidade vascular com a evolução da doença, mas não há co-localização entre a expressão da enzima e a expressão de CD31, sugerindo que os vasos sanguíneos não estão envolvidos no fenômeno de expressão da enzima no MT. Além disso, é demonstrado que o ASPA é um biomarcador de pior evolução clínica, uma vez que os pacientes com os menores níveis de expressão de ASPA são mais propensos a apresentar uma evolução menos favorável da doença, principalmente no que se refere à sobrevivência livre de metástases.

O cenário descrito pode ser atribuído à desregulação da enzima ou à acumulação do seu metabolito N-acetil-aspartato (NAA), que poderá ser responsável pela emissão de sinais

moleculares que culminam na ativação de vias metabólicas das células tumorais, levando à manifestação de um fenótipo mais agressivo da doença.

Ao adotar uma abordagem de diagnóstico e terapêutica orientada por biomarcadores, caminhamos no sentido de uma medicina mais precisa, oferecendo o benefício máximo para cada paciente.

Palavras-chave: Cancro da Próstata, Metástases, Aspartoacilase, Microambiente Tumoral, Imunofluorescência, Microscopia Multiespectral, Biomarcadores.

Abstract

Prostate Cancer (PCa) is the most common cancer and the second leading cause of death by cancer in males, being 90% of PCa related mortality due to development of metastatic disease, after failure of a combination of therapeutic regimens. Recently, it has been demonstrated that tumour microenvironment (TME) and the metabolic changes associated to the cells that compose PCa play an important role in tumourigenesis.

A genetic screen to identify alterations in gene expression associated with poor prognosis and higher capacity of metastasis revealed Aspartoacylase (ASPA) as a possible candidate of aggressiveness. The main goal of this project is to characterize the PCa TME using Multispectral Microscopy to establish a correlation of TME features with disease stages and patients' outcome and ultimately unravel a possible phenotype which could predict metastasis before clinical manifestation.

A cohort of 123 samples from Benign Prostate Hyperplasia (BPH) (n= 20), primary (n=85) and metastatic PCa (n=18) were immunophenotypically characterized using an optimized panel of 5 biomarkers (ASPA, CD31, CD68, Cytokeratin 18 and Desmin). Using Multiplex Immunofluorescence (mPlex IF), it was possible to assess the expression of ASPA in the TME, as well as the populations of fibroblasts (Desmin) and macrophages (CD68). CD31 was also included to determine the status of vessel density in the samples. Cytokeratin 18 signal enabled the identification of tumour cells, guiding the acquisition of microscopical images. Stromal areas in between the tumour glands and in the periphery of the tumour nests were acquired and analysed using proper softwares.

Our results demonstrate that ASPA expression strongly co-localizes with fibroblasts, and significantly decreases with tumour progression. A macrophage infiltrate is also evident, especially in intratumoral regions, showing a tendency to correlate with poor prognosis. Vascular density also increases but there is no co-localization between ASPA and CD31, meaning that blood vessels are not involved in the phenomenon of expression of the enzyme in the TME. Moreover, it is demonstrated that ASPA is a biomarker of poor clinical outcome, once those patients with the lowest levels of ASPA expression are more prone to experience less favorable disease outcome, especially in what concerns metastasis-free survival.

The observed scenario may be attributed to the downregulation of ASPA or to the accumulation of its metabolite N-acetyl-aspartate (NAA) that may give molecular signals for tumour cells to activate molecular pathways that culminate in a more aggressive phenotype.

By adopting a biomarker-driven precision therapy approach and using prognostic and predictive treatment biomarkers, physicians could more accurately assign patients to the best available standard of care that offer the maximal benefit for each patient.

Key words: Prostate Cancer, Metastasis, Aspartoacylase, Tumour microenvironment, Immunofluorescence, Multispectral Microscopy, Biomarkers.

List of Contents

List of Figures

List of Tables

Glossary of abbreviations

α

α-SMA α-Smooth Muscle Actin

A

ADT Androgen Deprivation Therapy

AR Androgen Receptor

ASPA Aspartoacylase

AWD Alive with disease

AWOD Alive without disease

B

BPH Benign Prostatic Hyperplasia

BR Biochemical recurrence

BRFS Biochemical recurrence-free survival

BSA Bovine Serum Albumin

bGS biopsy-based Gleason score

C

CAFs Cancer Associated Fibroblasts

CHD1 Chromodomain Helicase DNA binding protein

CLR Clinical Recurrence

CRPC Castration Resistant Prostate Cancer

D

DFS Disease-free survival

DOD Death of disease

DOOD Death of other causes

DRE Digital Rectal Examination

DSFS Disease specific-free survival

E

ERG ETS Related Gene

ETS E26 Transformation Specific Fusions

EZH2 Enhancer of Zeste Homolog 2

F

FAP Fibroblast Activation Protein

FFPE Formalin-Fixed Paraffin Embedded

FOXA1 Fork head box A1

G

G2 Gleason Score 2

G3 Gleason Score 3

G4 Gleason Score 4

G5 Gleason Score 5

H

H&E Hematoxylin & Eosin

M

mPlex IHC/IF Multiplex Immunohistochemistry/Immunofluorescence

MFS Metastasis-free survival

MSCs Mesenchymal Stem Cells

N

NAA N-acetyl-aspartate

O

OS Overall survival

P

PBS Phosphate Saline Buffer

PCa Prostate Cancer

PIA Proliferative Inflammatory Atrophy

PIN Prostatic Intraepithelial Neoplasia

PSA Prostate Specific Antigen

PTEN Phosphatase and Tensin homolog

R

Ress Ressection

ROIs Regions of Interest

RT Room Temperature

RB1 Retinoblastoma protein 1

S

SD Standard Deviation

SPOP Speckle Type BTB/POZ Protein

Str Far Stroma far from the prostatic glandular structures

Str Hyp Stroma close to the hyperplasic glands

Str Met Stroma close to the metastatic cells

Str Tum Stroma close to the malignant cells

T

TAMs Tumour associated macrophages

TME Tumour Microenvironment

TMPRSS2 Transmembrane protease, serine 2

TNM Tumour, Nodes, Metastasis classification

TP53 Tumour protein p53

TUR Transurethral resection

Introduction and Literature Survey

Prostate Cancer

Epidemiology

Cancer may be defined as the uncontrolled division and spread (metastasis) of abnormal cells within the body. It is the second leading cause of death globally, being responsible for an estimated 10 million deaths in 2020. Worldwide, about 1 in 6 deaths is due to cancer (World Health Organization). Overall, the burden of cancer incidence and mortality is rapidly growing worldwide; this reflects both aging and growth of the population as well as changes in the prevalence and distribution of the main risk factors for cancer, several of which are associated with socioeconomic development [1].

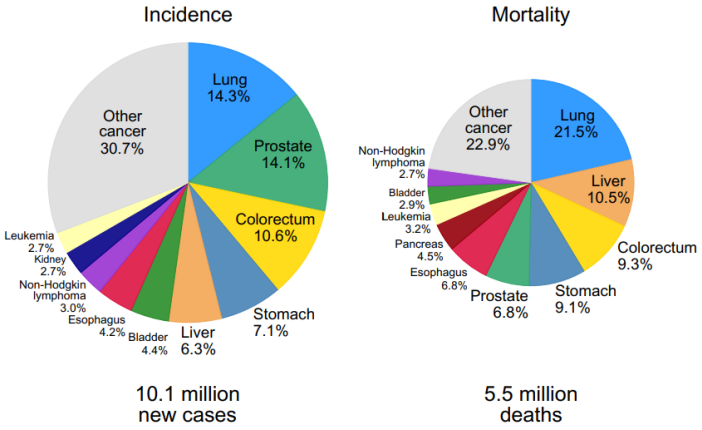

Figure 1: Distribution of cases and deaths for the most common cancers in 2020 for men. *The area of the pie chart reflects the proportion of the total number of cases or deaths. PCa has an incidence of 14.1% and a mortality rate of 6.8% (GLOBOCAN 2021).*

PCa is the most prevalent form of non-cutaneous cancer in men and is a leading cause of cancer-related death among men (Figure 1) [2,3]. While tumours with low pathological grade and stage – that are confined to the prostate at the time of diagnosis – are usually cured, others with advanced "International Society of Urological Pathology" grade groups and metastasis convey a poorer prognosis [4]. Around 90% of PCa related mortality is due to development of metastatic disease after the failure of a combination of therapeutic regimens [5].

Hallmarks of PCa include its multifocality, multiclonality and its notable inter- and intra-individual heterogeneity; due to these features, PCa management is a major challenge, and thus, further elucidation of the unique biology of this disease is urgently needed [6].

Prostate Cancer Carcinogenesis

The human prostate is a walnut-sized organ that is located just below the bladder surrounding the urethra (Figure 2). Its main functions are producing approximately one third of the seminal fluid as well as supplying nutrients, enzymes, and ions to ensure the survival of spermatozoa until reproduction [2].

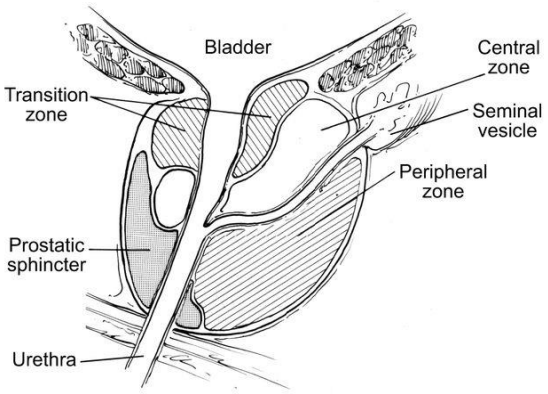

Figure 2: Overview of prostate anatomy (*adapted from Cunha et al. (1987) and McNeal (1969) and reproduced from Abate-Shen and Shen (2000)).*

Structurally, prostate is two-thirds glandular and the remaining third is fibromuscular. The cellular composition includes basal cells, anchored on top of the basement membrane; neuroendocrine cells; epithelial cells; and secretory luminal cells (Figure 3). Under the basement membrane, stroma is occupied by fibroblasts, myofibroblasts and smooth muscle cells. Almost all prostate cancers are adenocarcinomas, meaning that they develop from the basal and luminal cells [2,7,8].

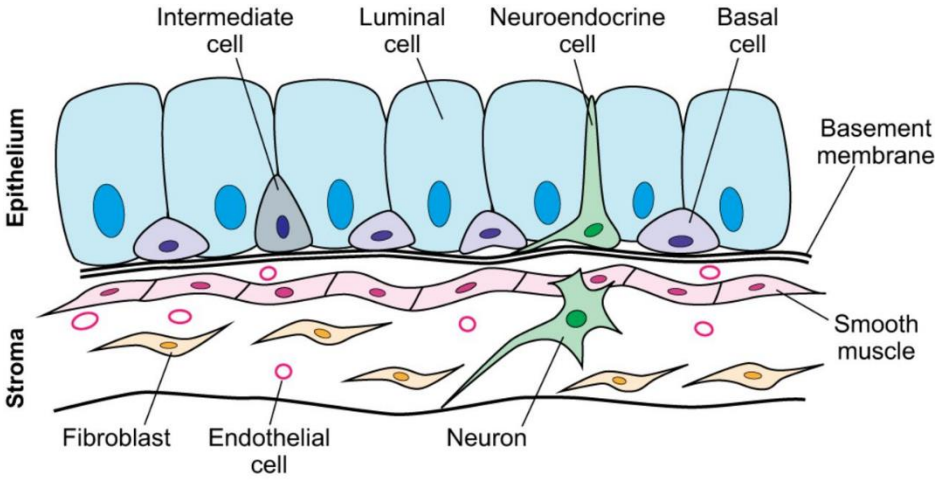

Figure 3: Cellular types composing the adult prostate. *The epithelial compartment is composed of basal cells that line the basement membrane, secretory luminal cells, and rare intermediate and neuroendocrine cell populations. These epithelial ducts are adjacent to a stromal compartment that includes smooth muscle cells, fibroblasts, and vascular and neural components (Toivanen & Shen, 2017).*

Malignant transformation of the prostate follows a multistep process, initiating as prostatic intraepithelial neoplasia (PIN) followed by localized PCa and then advanced PCa with local invasion, culminating in metastatic PCa, via spreading to surrounding tissue and finally to other parts of the body via the lymphatic system and vascular system (Figure 4) [2].

Most notably, regions of focal atrophic prostate epithelium can often be identified in aging men, frequently in association with an inflammatory response. Such regions usually display increased epithelial proliferation and have been termed ‘‘proliferative inflammatory atrophy’’ (PIA). Regions of PIA are also often located in proximity with PIN and adenocarcinoma, and thus PIA has also been proposed to represent a precursor lesion for prostate cancer (Figure 4) [9].

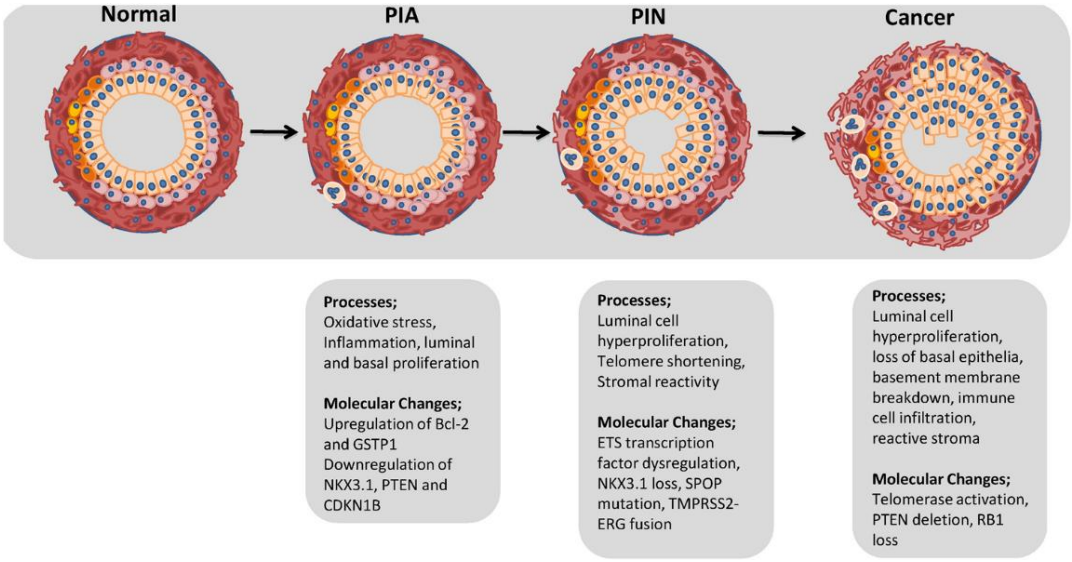

Figure 4: Phenotypic, microenvironmental and molecular changes during PCa carcinogenesis *(Packer & Maitland, 2016).*

During the process of malignant transformation, cells gradually evolve from the benign to the malignant phenotype. PCa presumably develops due to genetic and epigenetic insults accumulated by a single cell, which then proceeds to generate an extensively heterogeneous tumour. With time, an increase in number and severity of genomic alterations adds molecular complexity and is associated with progression to metastasis [7].

Multiple studies have identified recurrent somatic mutations, copy number alterations, and oncogenic structural DNA rearrangements in primary PCa (summarized in Table 1). These include point mutations in Speckle Type BTB/POZ Protein (SPOP), Fork head box A1 (FOXA1), and in Tumour Protein p53 (TP53); copy number alterations involving c-Myc binding protein homolog (MYC), Retinoblastoma protein (RB1), Phosphatase and Tensin homolog (PTEN), and Chromodomain-helicase-DNA-binding protein 1 (CHD1); and E26 transformation-specific (ETS) fusions, among other biologically relevant genes [10]. Genomic studies of metastatic prostate cancers demonstrated additional alterations in Androgen Receptor (AR) [11] and in the androgen signalling pathway [10].

AR is required for the normal functioning of the prostate; however, it attains an autonomous activation in case of PCa. It has been observed that PCa is highly dependent on AR function in its early stages (both localized and metastatic). Apparently, this is because many molecular alterations that occur in early stages of PCa involve genes that are androgen-dependent [12].

Table 1: Molecular alterations associated with PCa initiation and progression. Development of sophisticated techniques for genome analysis enabled the identification of the main gene alterations driving the development of PCa. The tumour of each patient may display a sum of the alterations briefly presented below (adapted from Perdomo et al., 2018; Robinson et al., 2015; Shen & Abate-Shen, 2010; Spratt at al., 2016).

Molecular Alteration	
Androgen signalling	AR binds testosterone to stimulate the transcription of androgen-responsive genes and regulates the growth of both normal prostate gland and PCa. Two major types of genetic alterations in AR occur in hormone refractory cancers: somatic mutations that result in decreased specificity of ligand-binding and inappropriate receptor activation by estrogens, progestins, adrenal androgens, glucocorticoids, and/or AR antagonists; and genomic amplification of the AR gene, which can maintain an active androgen signalling axis even with very low levels of androgens. Germline polymorphisms in the trinucleotide repeat of the AR gene, which probably affect AR activities, have also been linked to increased PCa risk, whereas other germline mutations are rare.
Akt/mTOR and MAPK signalling	The MAPK/ERK pathway is involved in cell survival, cell-cycle progression, tumour dissemination, and resistance to therapy. Data from preclinical research suggests an association with more aggressive disease in certain genetic contexts. BRAF is the most altered MAPK gene in PCa, with gene fusions or activating mutations present in 2–3% of tumours.
BRCA1 and BRCA2	These tumour suppressor genes normally help repair mistakes in a cell's DNA (or cause the cell to die if the mistake can't be fixed). Inherited mutations in these genes more commonly cause breast and ovarian cancer in women. But changes in these genes (especially BRCA2) also account for a small number of PCa.
CHD1	The CHD1 protein is involved in chromatin remodelling, and is commonly deleted in primary tumours, often coincides with SPOP mutation.
Developmental signalling pathways	Prostate tumours express a wide range of genes normally expressed during embryonic/ neonatal organogenesis, suggesting that cancer progression reactivates embryonic developmental programs of gene expression. Elevated canonical Wnt signalling may play a role in the emergence of castration resistance. Alterations in the Wnt signalling pathway are also common in PCa, both in the primary setting and in patients with metastatic PCa, where it is present in approximately 18% of patients. Canonical Wnt signalling is an evolutionarily conserved pathway that has been implicated in cancer stem-cell maintenance, epithelial-to-mesenchymal transition, embryonic development, and homeostasis in adults.

Enhancer of zeste homolog 2 (EZH2)	EZH2 encodes a histone lysine methyltransferase that participates in histone methylation and, ultimately, transcriptional repression. It is frequently up regulated in advanced PCa, in some cases through gene amplification.
FOXA1	FOXA1 is a chromatin remodeler that provides genomic access to AR for its binding, therefore, regulating AR driven transcription. Mutations in FOXA1 are found in 4% of PCa; most of these are missense mutations, although there are some truncating mutations. These events are predicted to affect interaction of other chromatin bound factors associated with FOXA1. It is responsible for the promotion of cell growth in an AR-dependent manner and inhibits cell motility in an AR independent way. Mutations in FOXA1 have shown to abrogate the ability of FOXA1 to repress cell motility, consistent with an oncogenic function. In general, tumours with FOXA1 mutation show similar molecular features to SPOP-mutant tumours, including patterns of gene expression, genomic aberrations, and DNA methylation.
Homeobox protein NKX-3.1	NKX3-1 is an androgen-regulated, prostate-specific homeobox gene, critical for the prostate epithelial differentiation and tumour suppression. Down-regulation of the NKX3.1 homeobox gene represents a frequent and critical event in prostate cancer initiation; there is substantial evidence that NKX3.1 undergoes epigenetic down-regulation, through promoter methylation.
MYC Proto-Oncogene	MYC is responsible for the regulation of cell proliferation. This amplified gene is frequently present in PCa, and its expression in prostatic cells has been associated with immortalization. MYC is seen to be upregulated in early prostate tumours and its locus is frequently amplified in advanced cancers.
Oncogenic tyrosine kinases	In prostate cancer, aberrant tyrosine kinase signalling has been associated to aggressive disease, progression to metastasis, and castration resistance, and, consequently, has been implicated as a key therapeutic target in patients with advanced disease.
PTEN	PTEN is a tumour suppressor gene frequently mutated or deleted in many cancers, including PCa. Point mutations and epigenetic silencing associated with PTEN have also been identified. PTEN deletions have been found in up to 20% of patients with PCa and have been associated with earlier biochemical relapse, metastasis, resistance to castration, presence of ERG gene fusions and the accumulation of nuclear TP53. PTEN is the reciprocal phosphatase of PI3K. Reduced removal of PI3K phosphorylations causes unchecked AKT activation that allows for increased cell survival and proliferation.
PI3K pathway	PI3K pathway is a critical regulator of proliferation, survival, metabolism, angiogenesis, and immune function. It is commonly dysregulated in patients with PCa. Hyperactivation of the pathway through loss of PTEN acts as a negative regulator of PI3K signalling as by far the most common PI3K aberration observed in patients with PCa.
Retinoblastoma protein (RB1)	RB1 is important for controlling the R-point, which is a decisive point in late G1 phase during which the cell is committed to undergo division. It is mutated in at least 30% of prostate tumours.
SPOP	SPOP is required for ubiquitination and further degradation of various proteins; it is also involved in maintaining genomic stability by modulating double strand break (DSB) repair. Consequently, mutant SPOP impairs homology directed or DSB repair. SPOP is mutated in 6–15% of primary cancers.

Telomerase	The protection of chromosome ends by inappropriate activation of telomerase prevents replicative senescence in highly proliferative cancer cells. Telomerase expression switching on occurs during PIN and early prostate cancer.
Transmembrane protease, serine 2 (TMPRSS2) – ETS related gene (ERG) translocations	The most common of these rearrangements creates a TMPRSS2-ERG fusion gene, resulting in expression of N-terminally truncated ERG protein under the control of the androgen-responsive promoter of TMPRSS2. The ETS proteins are developmental transcription factors that affect proliferation, migration, and transformation of cells. These gene fusions are seen in over half of all PCa.
TP53	TP53 is a tumour suppressor gene that plays an important role in response to cellular damage. This suppressor is often mutated in genitourinary cancers. In addition, different tumour suppressive pathways are associated with TP53, and some examples are the response to DNA damage, cell senescence and apoptosis.

Risk Factors

There are recognised risk factors associated with PCa development, such as: advanced age, ethnicity, genetic factors, and family history. Other aspects such as diet and physical activity may be determinant for the presence and progression of the disease [16–18].

Of note, for African men, the incidence rates are higher when compared to caucasian men, and family history of PCa significantly increases risk, being one of the most heritable cancers, with many susceptibility loci associated. Behind this disparity may be differences in social, environmental, and genetic factors, confirming the heterogeneity of alterations associated with disease initiation and progression. Underdiagnosis, differences in the screening methods and differences in healthcare access may contribute to variations in incidence among different populations [8,18,19].

The incidence and mortality of PCa is also strongly correlated with increasing age, being the average age at diagnosis of 66 years. The relationship between PCa and advanced age likely reflects the interplay of environmental, physiological, and molecular influences with normal consequences of aging that presumably exacerbate the effects of these influences. Moreover, various studies have described gene expression changes associated with aging, particularly in the prostatic stroma, including genes involved in inflammation, oxidative stress, and cellular senescence [20–22].

Symptoms and Diagnosis

Indolent prostatic neoplastic lesions may be asymptomatic or present with lower urinary tract symptoms. In contrast, advanced tumours may cause more severe symptoms related to multi-organ spread such as vertebral fractures or spinal cord compression [23]. The most frequent complaints are difficulty with urination, increased frequency, and nocturia; symptoms that may also arise from prostatic hypertrophy. More advanced stage of the disease may present with urinary retention and back pain, as axis skeleton is the most common site of bony metastatic disease [2].

The detection of PCa is frequently made based on elevated plasmatic levels of prostate-specific antigen (PSA > 4 ng/mL), a glycoprotein normally expressed by prostate tissue but augmented in cases of cancer. However, because men without cancer have also been found with elevated PSA, a tissue biopsy is required to confirm the presence of disease. Digital Rectal Exams (DRE) together with PSA monitoring are the well-established and minimally invasive clinical tests for the screening and tracking of PCa [2,24].

Imaging tests such as Computed Tomography scan and Magnetic Resonance Imaging are valuable approaches for helping in the diagnosis of prostate cancer. Positron Emission Tomography – Computed Tomography scan and bone scan may be helpful in detecting distant metastasis [25].

Tumour Staging and Grading

Several different grading systems have been proposed for PCa, but pathologists today use the Gleason grading system and the Prognostic Gleason grade grouping [26].

As mentioned above, men who have elevated PSA levels typically undergo biopsy to assess the potential presence of PCa. Following biopsy, histopathological grading of prostate tissue is performed by Gleason scoring, which classifies tumours from 1 to 5 (well to poorly differentiated, respectively) based on their most prevalent architecture (Figure 5), and assigns a combined score that is the sum of the two most common patterns [24,27,28]. Of note, this grading system demonstrates to have prognostic implications in PCa patients [29].

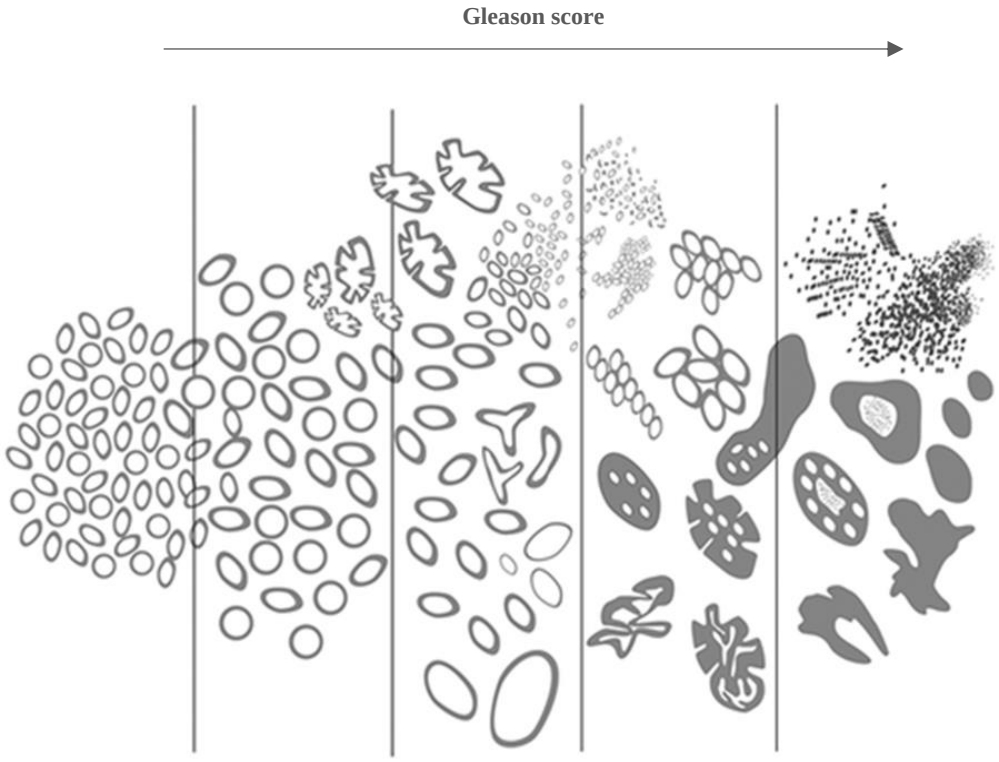

Figure 5: Gleason grading system. *Pathologists evaluate prostate biopsy samples and grade tumour regions based on defined architectural patterns (reproduced from Indiana University, 2015).*

Other than the grade, PCa is also classified by their stage using the Tumor, Nodes, Metastasis classification (TNM; Table 2) [30], which has to do with the status of the primary tumours, from organ-confined to locally invasive (T1–4), with or without lymph node involvement (N0 or 1), and the presence and degree of distant metastases (M0 and 1a–c) [31].

Several nomograms have been developed to guide therapy and predict outcome following radiotherapy: one of the most popular classifications is the D'Amico risk classifier, dividing patients according to pre-treatment PSA, clinical stage and biopsy-based Gleason score (bGS) into three categories: low-risk (PSA <10 ng/ml and cT1-cT2a and bGS ≤6) , intermediate-risk (PSA 10–20 ng/ml or cT2b or bGS 7) and high-risk (PSA >20 ng/ml or clinical stage ≥ cT2c or bGS ≥8) [32].

Table 2: The TNM Staging System for PCa. Tumour staging TNM summarizes data on the extent of the tumour burden (T), presence of cancer cells in draining and regional lymph nodes (N) and evidence of metastasis (M). This classification has been shown to be valuable in estimating the outcome of patients with a variety of cancers (adapted from Buyyounouski et al., 2017).

Classification	Definition
Clinical (cT)	
T Category	
Tx	Primary tumour cannot be assessed
T0	No evidence of primary tumour
T1	Clinically inapparent tumour that is not palpable
T1a	Tumour incidental histologic finding in 5% or less of tissue resected
T1b	Tumour incidental histologic finding in more than 5% of tissue resected
T1c	Tumour identified by needle biopsy found in one or both sides, but not palpable
T2	Tumour is palpable and confined within prostate
T2a	Tumour involves one-half of one side or less
T2b	Tumour involves more than one-half of one side but not both sides
T2c	Tumour involves both sides
T3	Extraprostatic tumour that is not fixed or does not invade adjacent structures
T3a	Extraprostatic extension (unilateral or bilateral)
T3b	Tumor invades seminal vesicle(s)
T4	Tumour is fixed or invades adjacent structures other than seminal vesicles, such as external sphincter, rectum, bladder, levator muscles, and/or pelvic wall
Pathologic (pT)	
T Category	
T2	Organ confined
T3	Extraprostatic extension
T3a	Extraprostatic extension (unilateral or bilateral) or microscopic invasion of bladder neck
T3b	Tumour invades seminal vesicle(s)
T4	Tumour is fixed or invades adjacent structures other than seminal vesicles, such as external sphincter, rectum, bladder, levator muscles, and/or pelvic wall
N Category	
Nx	Regional lymph nodes were not assessed
N0	No positive regional lymph nodes
N1	Metastases in regional lymph node(s)
M Category	
M0	No distant metastasis
M1	Distant metastasis
M1a	Nonregional lymph node(s)
M1b	Bone(s)
M1c	Other site(s) with or without bone disease

Metastatic Prostate Cancer

Despite the high long-term survival in localized PCa, metastatic PCa remains largely incurable even after intensive multimodal therapy. 5-year relative survival rate for metastatic PCa patients is only 28%, while it is 99% for patients with localized disease [33,34]. The lethality of advanced disease is driven by the lack of therapeutic regimens capable of generating durable responses in the setting of extreme tumour heterogeneity on the genetic and cell biological levels [8].

In the last decade, the treatment of castration resistant PCa (CRPC) has evolved with the addition of upfront intensification with novel hormonal therapies (abiraterone, enzalutamide, apalutamide) or docetaxel in addition to androgen deprivation therapy – the backbone of systemic treatment [35].

Although several new strategies to inhibit AR signalling have recently been developed, CRPC remains incurable, and better treatments are needed. Important to highlight that intratumoral heterogeneity within a given patient is now recognized as an equally important factor in dictating drug response and disease relapse. This intratumoral heterogeneity manifests on many levels and includes genomic and developmental cell variability within the cancer cell compartment as well as the diversity of numerous TME cell types and their complex heterotypic interactions [8].

Treatment

The treatment of PCa depends on the grade, stage and patient's age and ranges from active surveillance to a mix of surgery, chemotherapy, radiation, and/or Androgen Deprivation Therapy (ADT) [36].

When PCa is diagnosed, conventional treatment regimens include surgical excision of the prostate (radical prostatectomy), or irradiation through external beam therapy or implantation of radioactive ''seeds'' (brachytherapy). In the case of advanced cancer, these regimens are usually followed or substituted with ADT which initially will reduce tumour burden and/or circulating PSA to low or undetectable levels, chemotherapy, or immunotherapy to boost the immune system [2,37].

ADT remains a gold standard in PCa with an initial response rate of approximately 80%. Subsequently, as a response to ADT, patients develop resistance and progress to ADT resistance. CRPC occurs in 10-20% of patients and has a medium survival rate of around 14 months [12].

Tumour Microenvironment

Significant intratumoral heterogeneity is also reflected in the diversity of cell types and the composition of the extracellular matrix comprising the tumour microenvironment (TME). TME cell types include cancer associated fibroblasts (CAFs), mesenchymal stem cells (MSCs), immune cells, and blood and lymphatic vascular cells (Figure 6). TME composition plays essential roles in regulating cancer cell proliferation, angiogenesis, invasion, metastasis, immune evasion, and resistance to therapeutics and is mediated by signalling cross-talk between cancer cells and distinct stromal populations through direct cell contact and/ or secreted factors such as cytokines, chemokines, and growth factors [38,39]. The different functions of the distinct TME cells

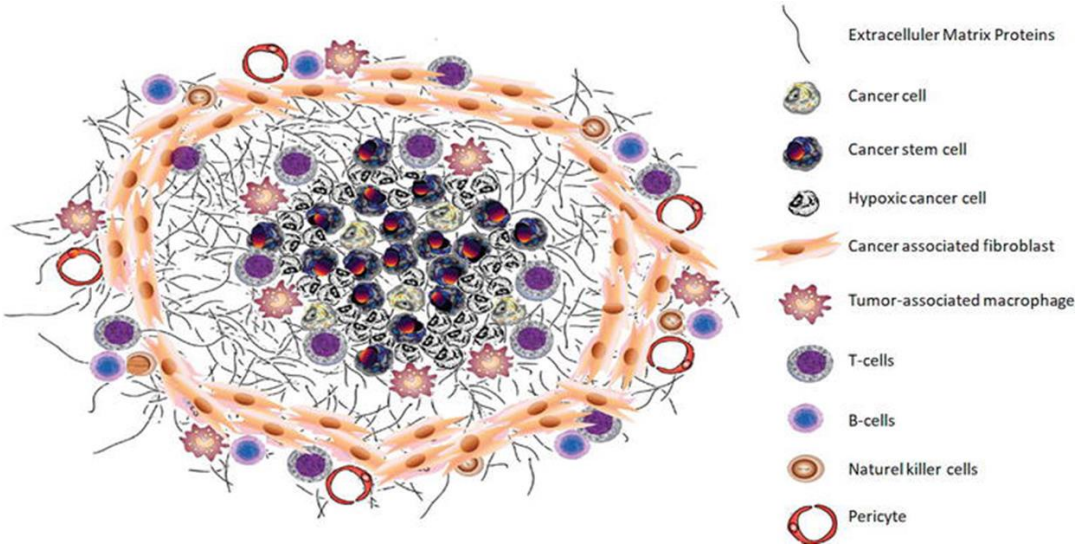

Figure 6: Schematic view of the TME. *The tumour ecosystem consists of different cell types (tumour cells, non-tumour cells), chemical and physical factors. Tumour growth and metastasis requires an appropriate support structure, known as TME (Eskiizmir & Özgür, 2018).*

are summarized in Table 3.

Table 3: Different cell types present in the TME and their role in cancer. Anti-tumourigenic function is presented in white and pro-tumourigenic role in blue (adapted from Balkwill et al., 2012; Quail & Joyce, 2013; Hanahan & Coussens, 2012; Shiao et al., 2016).

Cell Type	Roles in Cancer
B Cells	Antibody-mediated lysis of tumour cells.
	Supress T cell functions. Promote tumour growth and progression. Release inhibitory cytokines; production of pro-tumorigenic lymphotoxin.
Dendritic Cells	Release cytotoxic cytokines. Antigen presentation to T cells.
	Supress anticancer immune responses. Stimulate inflammatory cytokine production.
Fibroblasts	Limited.

	Enhance the proliferation and invasiveness, encourage the acquisition of therapeutic resistance and immune evasiveness. Support tumourigenesis and subsequent tumour growth; accelerate extracellular matrix deposition and turnover.
Macrophages	Cancer cell killing. Antigen presentation to T cells. M1 macrophages are pro-inflammatory and anti-tumourigenic.
	Promote angiogenesis, tumour proliferation, chemotaxis, invasiveness, and metastasis. M2 macrophages are anti-inflammatory and pro-tumourigenic.
Mast Cells	Limited.
	Mitogenic, pro-angiogenic, pro-invasive, recruit other immune cells, supress cytotoxicity activity.
MSCs	Limited.
	Promote tumour growth. Differentiate into CAFs to promote metastasis
Monocytes	Limited.
	Pro-angiogenic, pro-invasive, pro-metastatic, supresses cytotoxic activity.
Natural Killer Cells	Release cytotoxic cytokines. Directly cytotoxic to cancer cells.
	Limited.
Neutrophiles	Anti-metastatic, cancer cell killing. N1 neutrophils are pro-inflammatory and anti-tumourigenic.
	Mutagenic, mitogenic, recruit Immune cells, pro-angiogenic, pro-invasive, pro-metastatic. N2 neutrophils are anti-inflammatory and pro-tumourigenic.
Pericytes	Limited.
	Modulate angiogenesis and cell transit, support vascular functionality.
Platelets	Limited.
	Pro-metastatic, pro-angiogenic.
T Cells (CD8+, CD4+)	Directly lyse cancer cells. Release cytotoxic cytokines.
	Release tumour promoting cytokines.
T regulatory	Release tumour promoting cytokines.
	Supress anticancer immune responses. Stimulate inflammatory cytokine production.
Vascular Endothelial Cells	Limited.
	Angiogenesis for blood supply of oxygen and nutrients; produce paracrine trophic. functions; recruit Infiltrating Immune cells; modulate cancer cell dissemination and seeding.

Stromal cell populations have diverse functional properties, contributing to the core and emergent hallmarks of cancer, namely, sustaining proliferative signalling, evading growth suppressors, resisting cell death, enabling replicative immortality, inducing angiogenesis, activating invasion and metastasis, reprogramming energy metabolism, and evading immune destruction [39].

In PCa, various signalling molecules (androgen, fibroblast growth factor, and transforming growth factor beta) are involved in these heterotypic and homotypic interaction networks across cancer cells and stromal cells [43–45].

Stromal changes occur as an early phenomenon in prostate carcinogenesis. Of note, in PCa, the reactive stroma consists largely of CAFs. This population has been observed in PIN and their numbers increase as tumours progress to a higher-grade [46,47]. Fibroblasts are key players in the prostatic stroma. They maintain the integrity of epithelial cells by constantly remodelling and interacting with different elements within the organ [48]. The proposed activity of CAFs in response to its interaction with tumour cells leads to the formation of an uncontrolled "reactive stroma" stimulating cancer cell proliferation, aggressiveness, and affecting response to treatment [49].

Immune cells are normal residents of a healthy prostatic tissue and play a protective role against infiltrating pathogens [50]. However, histological studies have shown that high-grade PCa is associated with increased stromal immune cell infiltrates with difference in cellular types according to tumour stage [51].

In particular, tumour associated macrophages (TAMs) shape the characteristics of the TME by producing various humoral factors and expressing regulatory molecules that promote the growth, metastasis, and invasion of tumour cells as well as their immunosuppressive effects and immune escape [52]. Therefore, a high frequency of TAMs generally correlates with poor clinical outcome in cancer patients [53]. Moreover, macrophages exhibit differences in ontogeny, differentiation status, and distribution within tumour tissues [54].

From the late 1990s, a M1/M2 classification based on the activating condition of macrophages was introduced [55]. It has been accepted that M1 macrophages are pro-inflammatory cells involved in anti-microbial host defence, and they can be differentiated *in vitro* by stimulation with Toll-like receptor ligands as well as Th1 response-related interferon (IFN-α/β) or IFN-γ [56]. On the other hand, M2 macrophages generally counteract inflammatory responses and promote tissue repair [57]. The majority of TAMs associated with prostate cancer lesions are pro-tumour and M2-like. Similar to M2s, these TAMs promote tissue remodelling, cell growth and proliferation, and supress a CD8+ cytotoxic T cell response which all together support tumours. Given their pro-

tumour functions and their prevalence in PCa, targeting pro-tumour M2-like TAMs provides a pressing and promising adjunct therapeutic strategy [58].

Prostatic tumorigenesis is dependent, to a certain extent, on angiogenesis upregulation. Formation of blood vessels is a crucial phenomenon to support cancerous cell viability and growth. In normal prostatic tissue, there exists a balanced interaction between endothelial cells, pericytes, and smooth muscle cells. However, tumour vasculature is characterized by aberrant formation of immature leaky blood vessels that lack covering pericytes [59,60]. It was demonstrated that endothelial cells are a main component of the TME for their role in stimulating metastatic activity via suppressing both AR expression and transcriptional activity, hence proposing that their inhibition could hinder PCa progression [61]. A high level of angiogenesis within a tumour may therefore be indicative of its aggressiveness [62].

Epithelial cells are not the only players contributing to PCa tumorigenesis. As mentioned previously, immune and non-immune cells also play a pivotal role in pathogenesis and disease progression [63]. Characterizing the interplay between malignant tumour cells and surrounding cell populations and how those relationships are influenced over time by treatments may open doors to a better understanding of the TME and elucidate biomarker signatures helpful for diagnosis and treatment. The contribution of stromal– epithelial crosstalk to PCa initiation and progression provides the impetus for combinatorial microenvironment-targeting strategies [43]. Thus, defining molecular biomarkers for PCa that can aid in diagnosis and distinguishing patients who require aggressive therapy from those who should avoid overtreatment is a significant unmet need. Mechanisms underlying the development of PCa are not confined to cancer epithelial cells, but also involve the TME [64].

Notably, strategies to therapeutically target the TME have emerged as a promising approach for cancer treatment in recent years due to the critical roles of the TME in regulating tumour progression and modulating response to standard-of-care therapies (Figure 7). It includes immunotherapy, antiangiogenic drugs, and treatments directed against cancer-associated fibroblasts and the extracellular matrix [65].

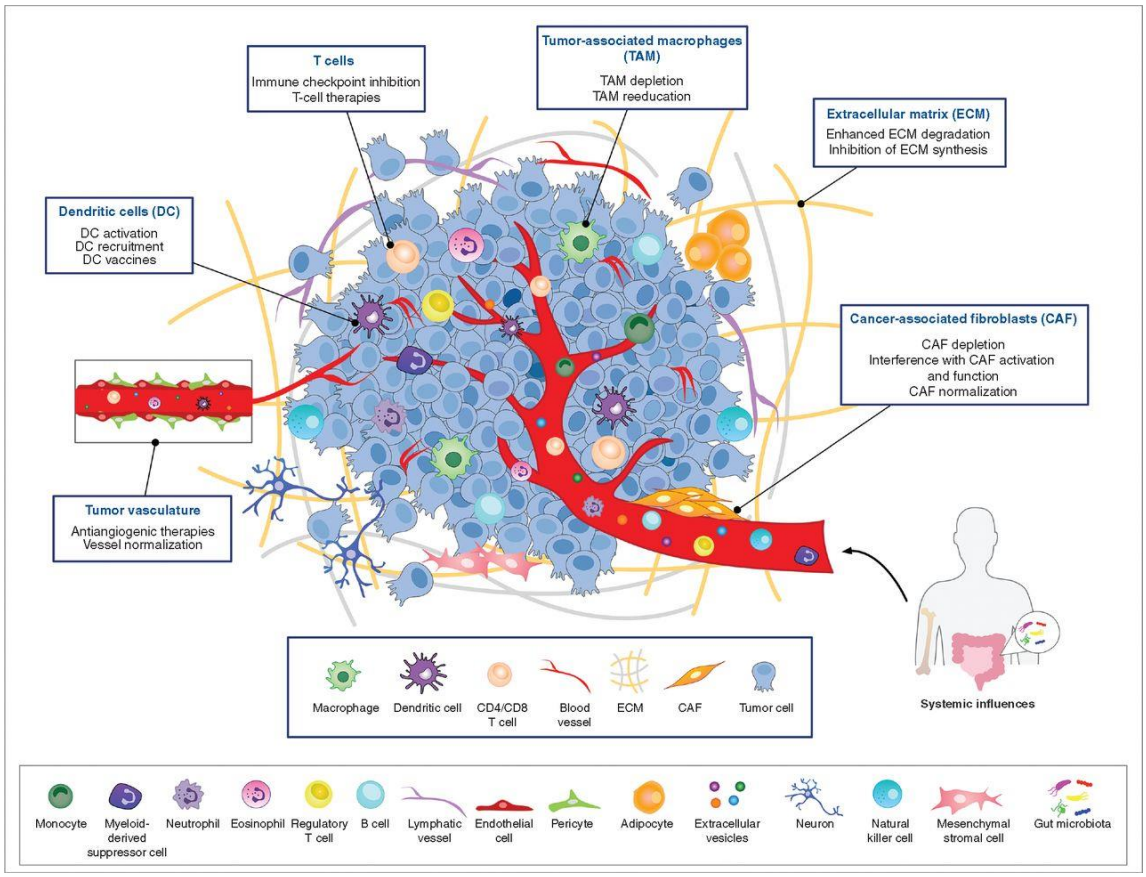

Figure 7: TME is composed of diverse cell types and secreted factors that represent targets for anticancer therapies. *As each of these cell types can contribute to the regulation of tumour progression and therapeutic response in unique ways, multiple therapies directed to the TME have been developed in recent years (Bejarano, 2021).*

Tumour Metabolism

Aberrant proliferation of cancer cells is supported by enhanced adaptation to nutrient microenvironment mediated by alterations in energy metabolism [66]. This metabolic rewiring and gene deregulation are both hallmarks of cancer and are addictive for tumour cells [38]. Thus, the crosstalk between gene expression and metabolism are fundamental aspects of cellular adaptation to nutritional changes during tumorigenesis [67].

It is important to highlight the existing metabolic heterogeneity among the cells in a tumour. This heterogeneity is behind the different behaviour of different populations in a tumour, including resistance to therapeutics and capacity to evolve to a higher stage. Of note, it has been demonstrated that metabolic alterations are at the core of PCa aggressiveness. Taking this into consideration, it remains of high importance to understand metabolic alterations within PCa epithelial cells and the TME [67].

During the performance of a genetic screen to identify alterations in gene expression associated with poor prognosis and higher capacity of metastasis, the ASPA gene was identified as a possible candidate involved in this process (data not published). The ASPA gene encodes an enzyme that catalyses the conversion of NAA to aspartate and acetate, especially in the brain (Figure 8). Mutations in ASPA cause Canavan disease [68]. NAA is the second most abundant brain metabolite with concentrations around 10 nM [69].

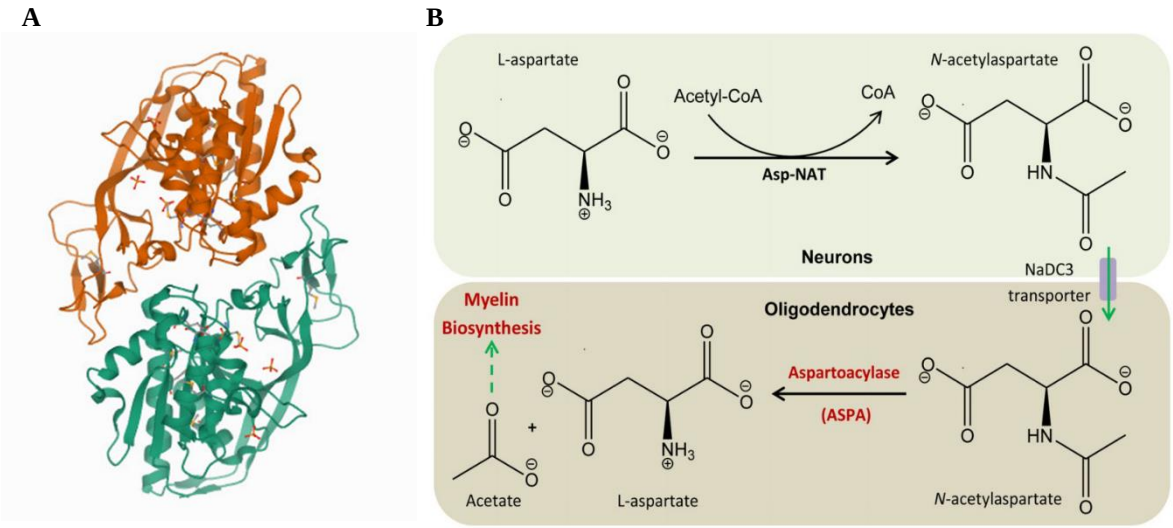

Figure 8: Aspartoacylase enzyme and its biological function. *(A) Crystal Structure of an Aspartoacylase from Homo Sapiens (Protein Data Bank, 2006). (B) Schematic representation of the biological role of ASPA (Wijayasinghe et al., 2014).*

It has been previously demonstrated that ASPA is more expressed in normal volunteers than in individuals with PCa, when analysing mRNAs expression in prostate tissue [70]. Moreover, it has been identified that NAA is more abundant in tumours when compared to non-cancerous tissues, suggesting a critical role of this metabolite in the development of pathological conditions, even outside the brain [69]. These events lead to the hypothesis that ASPA enzyme may suffer a downregulation concomitant with tumour progression and in association with a more aggressive phenotype.

Multiplex Immunofluorescence

It is becoming increasingly important to measure not just the average expression of molecules in homogenised tissue but also their spatial distribution while preserving cellular and tissue architectural features. Such high resolution molecular imaging is technically challenging, especially when signals of interest are co-localized [71].

The unique heterogeneity in the PCa microenvironment highlights a crucial need to employ technologies that can provide a subpopulation-specific analysis. In fact, such technologies would help researchers in thoroughly dissecting the intricate interactions between specific subpopulations and their surrounding microecology [64].

Multiplex Immunohistochemistry/Immunofluorescence (mPlex IHC/IF) technologies, which allow the simultaneous detection of multiple markers on a single tissue section, have been introduced and adopted in both research and clinical settings. The ability to label multiple markers on a single section is of particular significance when studying samples taken from rare donors, where tissues may be of low availability [72]. In particular, mPlex IF has arisen as an important tool for profiling tumour tissues [73]. This is a reliable high-throughput method that allows cell-by-cell identification of multiple markers on tumour cells and tumour-associated immune cells playing an important role in characterizing molecular signalling as well as the TME [74]. Because mPlex IF allows the use of multiple markers in one slide, we can directly observe various biomarkers expressed by a single cell and analyse their spatial relationships in various cell populations, something that cannot be achieved by traditional chromogen based IHC. Thus, with a combination of carefully selected antibodies, many cell subsets can be identified [73].

Stratification of cancer patients based on molecular expression profiles will become crucial in the era of personalised medicine and reliable biomarkers will be pivotal to ensure optimal patient selection and care [75]. During the last decade, many predictive and prognostic biomarkers have entered clinical oncological practice, and many more are expected to do so in the years to come. The use of biomarkers to stratify patients with PCa is limited, although several clinical trials are exploring potential candidates [76]. There were a myriad of PCa biomarker studies focusing on the TME over the last 10-15 years, and many of them have focused on its potential prognostic value. Hence, clinical recurrence (CLR) in PCa was linked to changes in the TME in several studies, including reports on CLR-dependent alterations in expression profiles of CAF markers and vascular markers. Interestingly, most commercially available prognostic biomarker-panels have also several stromal cell markers in their gene panels. However, transversal data on the relation between CLR and different key markers of the TME are often lacking, since most of these studies focus on individual markers and/or single pathway [75].

By adopting a biomarker-driven precision therapy approach and using predictive treatment biomarkers, physicians could more accurately assign patients to the best available standard of care that offers the maximal benefit for each patient. The study of molecular signals associated to disease progression is a valuable strategy to target metastasis before it emerges. Taking this into consideration, it is important to evaluate the genes and programs contained within these signatures as potential metastasis-regulatory cues.

Working hypothesis and Goals

The present project aims to characterize the PCa TME using Multispectral Microscopy to establish a correlation of TME features with disease stages and patients' outcome and ultimately unravel a possible phenotype which could predict metastasis development in the primary tumour samples, before clinical manifestation.

The results from this project could provide the basis for the following future studies:

- Validation of a set of molecular markers and correlation of their abundance and localization with metastatic capacity.
- Exploitation of these markers for the development of an imaging method of disseminated cells and to establish early diagnosis and therapies.
- Evaluation of the involved metabolic programs as potentially regulatory for metastasis development.

Materials and Methods

Human Samples

Ethical approval

This project was submitted and approved by the Champalimaud Foundation's Ethics Committee, since Formalin-Fixed Paraffin Embedded (FFPE) archival blocks with human material were used during the development of the experimental work. A waiver of consent was requested due to the fact this is an observational retrospective study without interfering with clinical management of the patients; furthermore, some patients have already died of the disease. Tissue samples were retrospectively identified from the archives of the Service of Anatomic Pathology of the Champalimaud Clinical Centre and were classified by a pathologist. All human samples and the corresponding necessary clinical data were received in a de-identified manner through the Champalimaud Foundation Biobank. Data of interest included age at diagnosis, PSA at diagnosis, histopathological diagnosis, tumour stage, tumour recurrence/progression, patient status and follow-up time.

FFPE blocks of human prostatic tissue

The 123 tissue blocks came from a cohort of 114 patients, 20 correspond to benign prostatic hyperplasias (BPH), and 103 to different grades and stages of PCa. From the 103 PCa patients, 85 tissues corresponded to primary PCa specimens (22 Grade group (GG) 2, 23 GG3, 20 GG4 and, 20 GG5) and 18 to metastatic PCa. Interestingly, we identified 10 cases with the primary tumour and the corresponding metastasis.

Types of tissues and patients' data are summarized in Table 4. The mean age of disease diagnosis was 67 years and mean time of clinical follow-up was 58.4 months. From the samples analysed, almost all BPH were obtained via Transurethral Resection (TUR) and PCa samples obtained from surgery (prostatectomy) and biopsy samples.

After the initial diagnosis of PCa, the great majority of the patients underwent prostatectomy or Hormone Therapy; being the most used drugs Zoladex, Bicalutamide, Leuprolide, Casodex, Cyproterone, Triptorelin.

Table 4: Clinico-pathological characteristics of the 123 tissue specimens from the 114 patients.

Number of Patients	114
Number of Samples	123
Age at Diagnosis, years	
Mean	67
Range	47-89
Prostate Benign Hyperplasias Samples	20
Prostate Cancer Samples	103
Primary	85
Gleason Score 7 (3+4) – G2	22
Gleason Score 7 (4+3) – G3	21
Gleason Score 8 (4+4) – G4	22
Gleason Score 9-10 – G5	20
Metastasis	18
Clinical follow-up, months (n=102)	
Mean	58.4
Range	0.2-268.0
Type of Tissue	
BPH	
Millin Prostatectomy	19
TUR	1
PCa	
Radical prostatectomy	46
PCa Biopsy	30
Bone Biopsy	6
Colon Biopsy	1
Liver Biopsy	3
Lymph Node biopsy	2
Lung Biopsy	3
Ressection (Ress)	2
TUR	1

Focusing on the PCa patients (briefly described in Table 5), the mean age at diagnosis was 66 years old (range from 47 to 89 years), and the median PSA at diagnosis was 7.4 ng/mL. Notably, the mean PSA at diagnosis was 196..3 ng/mL, since the cohort included patients with very elevated PSA (of note, a patient with 10000 ng/mL was included in the study). This group of patients was also evaluated in terms of biochemical recurrence, development, and site of metastasis. The mean time of clinical follow-up was 64.1 months. The patients without data were not included for statistical purposes and those patients whose clinical follow-up was short (less than 36 months) were considered Lost. A total of 17 patients died during the period of follow-up: 14 of the disease and 3 from other causes. The clinico-pathological features were correlated with patient's outcome and with the immunoexpression of the biomarkers studied.

Table 5: Clinico-pathological characteristics of the 103 PCa patients. iPSA stands for initial PSA and pTNM is the TNM staging of the samples after prostatectomies. AWD-alive with disease; AWOD-alive without disease; DOD-death of disease; DOOC-death of other causes.

Number of patients (PCa)	*103*
Age at Diagnosis, years	
Mean	*66*
Range	*47-89*
iPSA, ng/mL (n=81)	
Median	*7.9*
Mean	*196.3*
Range	*2.3-10000*
D'Amico classification	
<10	*47 (59,5%)*
10 to 20	*13 (16,5%)*
>20	*19 (24%)*
Prognostic WHO Grade Groups at diagnosis (n=88)	
Group 1 (Gleason score ≤ 6)	*3 (3,4%)*
Group 2 (Gleason Score 3+4=7)	*20 (22,7%)*
Group 3 (Gleason Score 4+3=7)	*16 (18,2%)*
Group 4 (Gleason score 8)	*31 (35,2%)*
Group 5 (Gleason score 9-10)	*18 (20,5%)*
Prognostic WHO Grade Groups (prostatectomy) (n=49)	
Group 2 (Gleason Score 3+4=7)	*22 (45%)*
Group 3 (Gleason Score 4+3=7)	*22 (45%)*
Group 4 (Gleason score 8)	*4 (8%)*
Group 5 (Gleason score 9-10)	*1 (2%)*
pTNM (n=49)	
T2	*1 (2%)*
T2a	*2 (4,1%)*
T2b	*2 (4,1%)*
T2c	*19 (38,8%)*
T3a	*18 (36,7%)*
T3b	*7 (14,3%)*
Nx	*13 (26,5%)*
N0	*31 (63,3%)*
N1	*5 (10,2%)*
Biochemical Recurrence (BR) (n=85)	
No	*42 (49,4%)*
Persistence	*17 (20%)*
Yes	*26 (30,6%)*

Average time to BR, months (n=85)	
Mean	*36.1*
Range	*2.6-131.8*
Metastasis (n=85)	
No	*48 (56,5%)*
Yes	*37 (43,5%)*
Time to metastasis, months (n=85)	
Mean	*27.1*
Range	*0-203.3*
Metastatic site	
Bone	*14*
Bone, Lymph Node	*5*
Bone, Lung	*1*
Liver	*1*
Lymph Node	*13*
Lung	*2*
Lung, Lymph Node	*1*
Clinical follow-up, months (n=89)	
Mean	*64.1*
Range	*0.2-268.0*
Status of the follow-up (n=83)	
AWD	*16 (19,3%)*
AWOD	*50 (60,2%)*
DOD	*14 (16,9%)*
DOOD	*3 (3,6%)*

Optimization of antibodies by IF

Optimization of antibodies was performed by IF in FFPE tissue blocks of different tissues (brain metastatic carcinoma, normal fallopian tube, normal lung, and prostate cancer) as positive controls. Tissue sections were cut at a thickness of 5µm using a Leica RM2255 microtome (Leica Microsystems) by the Histology Platform of the Champalimaud Centre for the Unknown. After deparaffinization using xylene, a graded ethanol series (100%, 95% and 70% ethanol) and washing with distilled water, slides were placed in a plastic container filled with antigen retrieval buffer in Tris-EDTA buffer pH = 9.0 (Epitope Retrieval Solution, RE7119, Novocastra, Leica Biosystems) or citrate buffer pH = 6.0 (0,1M Citric Acid and 0,1M Sodium Citrate in deionized water). The liquid was pre-heated for 30 minutes and the sections were immersed for an additional 30 minutes. Slides were allowed to cool down in the buffer at room temperature (RT) and were then rinsed with distilled water and permeabilized for 30 minutes with 0,2% TritonX (Fisher Scientific, Jassen Pharmaceuticalaan, #9002-93-1) in 1X Phosphate Saline Buffer (PBS)

(Mediatech, Corning) at RT. To initiate protein stabilization and background reduction, 0.5mg/mL Bovine Serum Albumin (BSA) containing 0.1% Tween 20 (Fisher Scientific, Jassen Pharmaceuticalaan) in 1X PBS was used for 30 minutes at RT. Slides were then incubated for 2 hours with the primary antibodies against the immune markers at specific dilutions:

- **Anti-ASPA antibody** (clone EPR22072, ab223269, Abcam), dilution 1:100, 1:200, 1:250, 1:500 and 1:1000;
- **Anti-CD31 Alexa Fluor® 647 conjugated antibody** (clone EPR3094, ab218582, Abcam), dilution 1:25, 1:50, 1:100 and 1:200;
- **Anti-CD68 antibody** (clone KP1, ab955, Abcam), dilution 1:25, 1:50, 1:100 and 1:200;
- **Anti-Cytokeratin 18 antibody** (polyclonal, ab219271, Abcam) dilution 1:50, 1:100 and1:200;
- **Anti-Desmin Alexa Fluor® 555 conjugated antibody** (clone Y66, ab203422, Abcam) dilution 1:50, 1:100 and 1:200.

Next, the slides were washed 3 times with 1X PBS and incubated for 1 hour at RT with anti-mouse, anti-rabbit or anti-goat secondary antibodies conjugated with Alexa fluor dyes (Invitrogen) when applicable as described in Table 6 (dilution 1:100).

Table 6: Description of the secondary antibodies used, targeting the corresponding primary antibodies. Alexa Fluor dyes were tested and optimized for the three primary antibodies that are not conjugated with secondary antibodies.

Primary Antibody	***Secondary Antibody***
ASPA	Alexa Fluor® 594 donkey anti-rabbit IgG (A21207, Invitrogen)
CD68	Alexa Fluor® 488 donkey anti-mouse IgG (A21202, Invitrogen)
Cytokeratin 18	Alexa Fluor® 568 donkey anti-goat IgG (A11057, Invitrogen)

After three additional washes in 1X PBS, the slides were counterstained with Prolong™ Diamond Antifade Mountant with DAPI (P36962, Invitrogen) and covered with a coverslip. Slides were placed at -20ºC before visualization under the microscope.

Multiplex IF staining

Once each antibody was optimized for the single staining, the markers were validated by mPlex IF in three different sets. The first set included Cytokeratin 18, followed by set two that was composed of ASPA and CD68, and the last set included CD31 and Desmin. Brain metastatic carcinoma was identified as the final positive control where all markers were expressed with good and clear signal.

For the mPlex IF, BOND Wash Solution 1X (AR 9590, Leica Biosystems) was used instead of 1X PBS solution and an additional step took place in the end of the staining: fixation with 100% Ethanol and 4% Formalin for 10 minutes each. Slides were placed in a dark at RT for 24 hours and in -20ºC for another additional 24 hours before visualization.

After the optimization procedure of the mPlex IF staining, the protocol was applied to all the samples of the cohort.

Multispectral imaging

Image Acquisition

Fluorescence images were acquired using a CRI Nuance Multispectral camera mounted on a Nikon 90i automated fluorescence microscope (at magnification 200x) and controlled by MetaMorph software. The different biomarkers were recorded taking into consideration the different wavelengths of absorption and emission of the biomarkers tested (Table 7 & Figure 9).

Table 7: Wavelengths of absorption and emission of the Alexa Fluor dyes included in the staining protocol. Aiming to distinguish the five biomarkers of interest, five dyes were selected according to their physical properties, avoiding phenomena of cross-talking and spectrum overlapping.

Secondary Antibody	***λ / nm (absorption)***	***λ / nm (emission)***	***Filter***	***Final Colour***
Alexa Fluor 488	495	519	FITC	**Green**
Alexa Fluor 555	555	565	555	**Yellow**
Alexa Fluor 568	578	603	M1	**Orange**
Alexa Fluor 594	590	617	M1	**Red**
Alexa Fluor 647	650	668	M2	**Pink**

Spectral library building

Initially, for each antibody a single-stained section was prepared counterstained with DAPI to build a library containing the emitting spectral peak of each fluorophore. Background signals were eliminated, and a library was created with the peaks of each individual fluorophore plus DAPI.

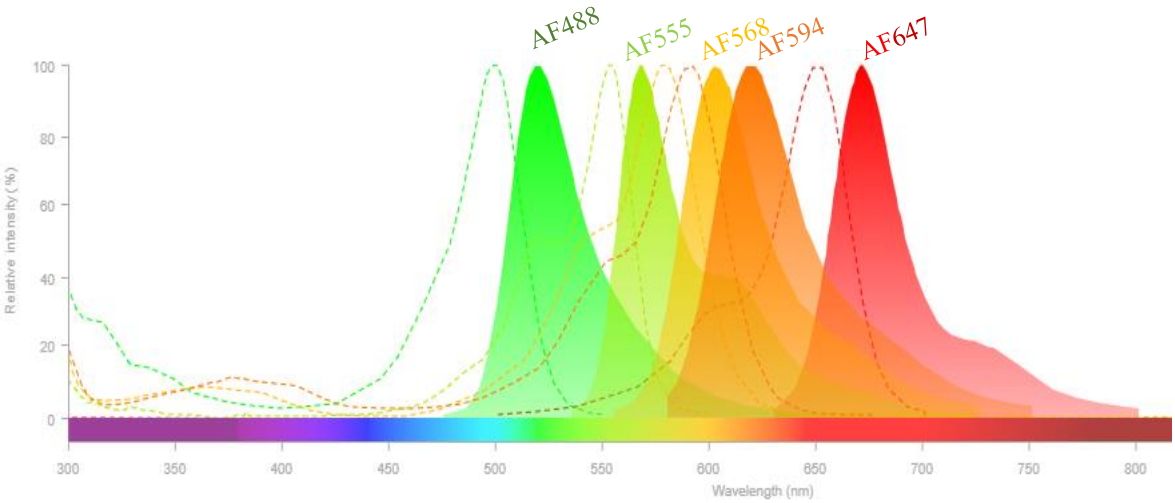

Figure 96: Excitation and Emission Spectrum of the Alexa Fluor dyes. *Alexa Fluor 488 (CD68), Alexa fluor 555 (Desmin), Alexa Fluor 568 (Cytokeratin 18), Alexa Fluor 594 (ASPA), Alexa Fluor 647 (CD31) were used. The overlapping of the excitation and emission wavelengths of the different antibodies did not interfere in the accurate detection of each antibody (Image adapetd from https://www.thermofisher.com/order/fluorescence-spectraviewer#!/).*

Case analyses

Each specimen was analysed in a similar manner, irrespective of tissue type except for metastatic samples as illustrated in Figure 10. Briefly, five representative areas – Regions of Interest (ROIs) - were randomly selected from stroma intermingled with glands – hyperplastic (Str Hyp) or malignant (Str Tum)- and from the stroma located far from the glandular structures (Str Far). For the metastatic samples, only five ROIs in the tumoral area were acquired (Str Met) since these samples consist essentially of tumour tissue.

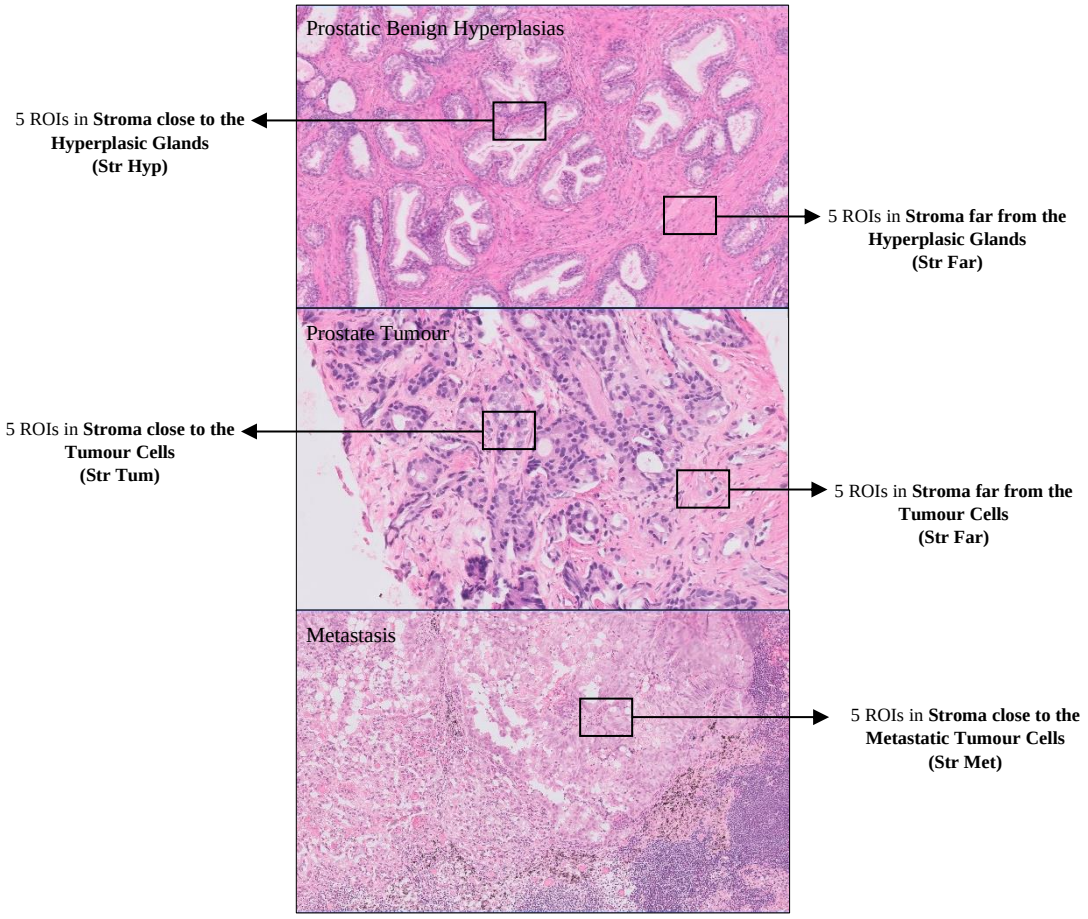

Figure 10: Schematic view of the ROIs selected for the acquisition process, within the type of samples in analysis. *Five regions in the stroma close to benign / malignant prostatic glands and other five regions in the stroma far from the glands were selected in each tissue specimen (magnification 100x).*

Image Collection and Analysis

Image analysis was conducted using Fiji software. During the analysis, 8-bit images were thresholded at the same intensity value for a specific staining and converted to binary format. Each ROI analysed corresponded to 0,347mm^2 of tissue.

The expression of ASPA and Desmin was determined by calculating the pixel intensity of these markers. The co-localization analysis between ASPA and Desmin, as well as ASPA and CD31 was performed by using an appropriate plugin: JACoP. This functionality allows the calculation of Manders' coefficient which can predict the degree of co-localization between two images from different channels. This coefficient ranges from 0 to 1, from no co-localization to 100% co-localization between the two images, respectively. The population of macrophages was counted using the Particles Analysis functionality and the number of CD68 positive cells was assessed in each ROI. Within the tumour samples, the number of peritumoral and intratumoral macrophages was also considered – being the different regions distinguished based on Cytokeratin 18 signal. To evaluate the vascular density of the samples the Vessel Analysis plugin was applied to the images in study that permitted to assess the expression intensity of CD31 (endothelial cells).

Statistical Analysis

Excel was used for data organization, and GraphPad Prism 8.0.2 (GraphPad Software, Inc., La Jolia, California, USA) was used for graph construction and statistical analysis. The data are presented as mean ± standard deviation (SD). Firstly, the normality of the samples was tested by performing the Shapiro-Wilk test. The means of the data obtained were analysed by Student t test when there were two sets, and ANOVA when there were three or more data sets. Whenever samples did not follow normality, non-parametric tests were used: Mann-Whitney test for sets of two and Kruskal-Wallis test when there are three or more sets of samples. A p-value superior to 0.05 was statistically considered as non-significant. A p-value < 0.05 is statistically significant (*), p-value < 0.01(**) is very statistically significant and p-value < 0.001(***) or p-value < 0.0001(****) are extremely statistic significant.

A nonparametric Spearman rank correlation test was used to evaluate the correlation between different qualitative and clinico-pathological variables (two-tailed test, CI 95%). Kaplan-Meier curves representing the percentage of patient survival were performed by stratifying the patient's samples using the median expression for the biomarkers; Log rank test was used for performing statistical analyses of survival.

Results and Discussion

Validation of the cohort

To determine whether our selected cohort was representative of the general PCa, patients were stratified according to PCa Grade Groups and PSA level classification by D'Amico, and metastasis-free, biochemical recurrence-free, disease free and overall survival curves were plotted. Concerning metastasis-free survival (MFS), overall survival (OS), and disease free-survival (DFS), higher Grade and higher levels of PSA significantly correlated with a poorer outcome, whereas for biochemical recurrence-free survival (BRFS) even though there was a similar tendency, it did not reach statistical significance (Figures 11 and 12). Correlation with disease specific-free survival (DSFS) was also assessed, and although the results followed the same tendency, they were not significant (Supplementary Figure 47-A and B).

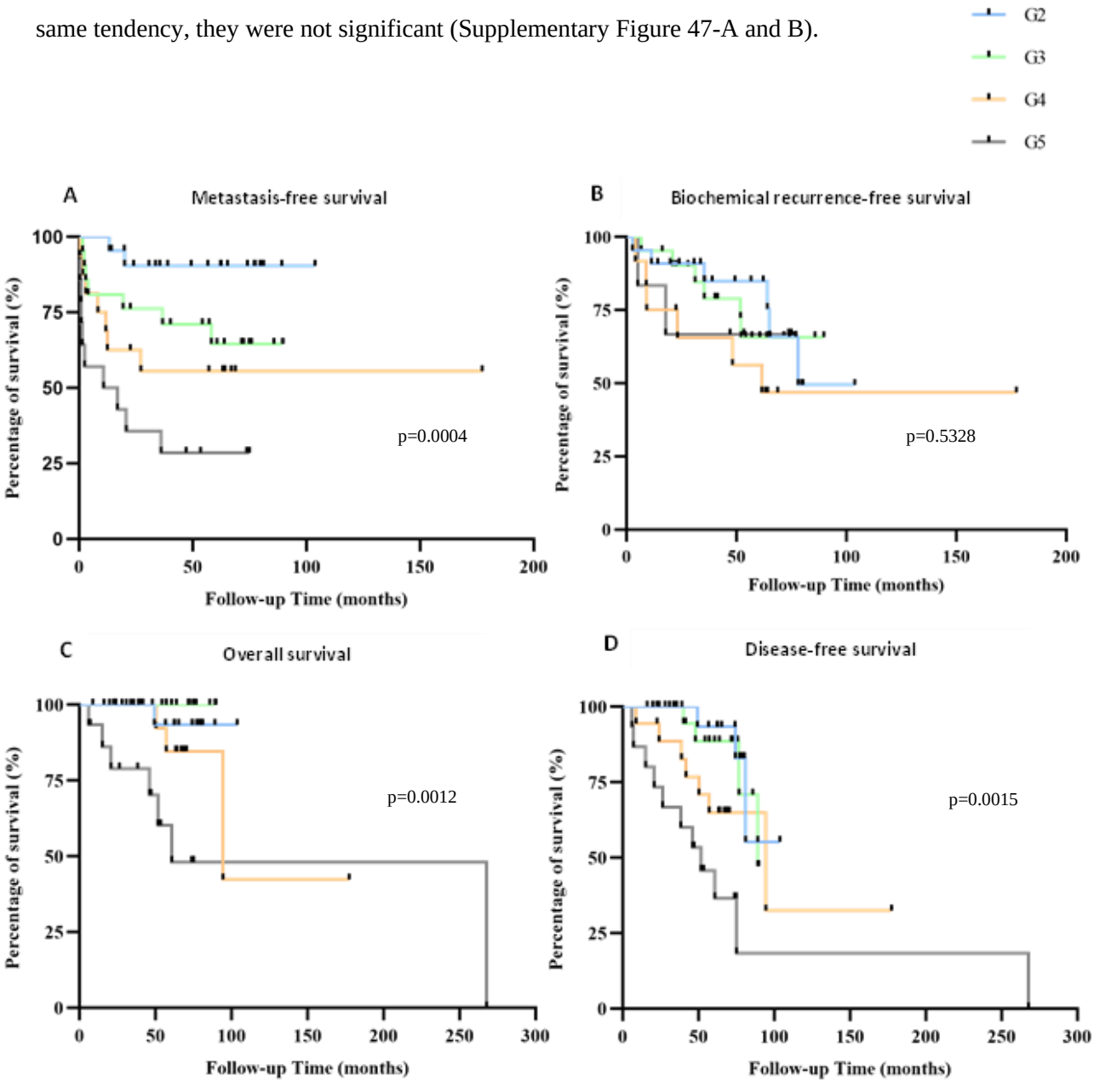

Figure 11: Cohort stratification according to PCa grade groups, *concerning MFS (A), BRFS (B), OS (C) and DFS (D).*

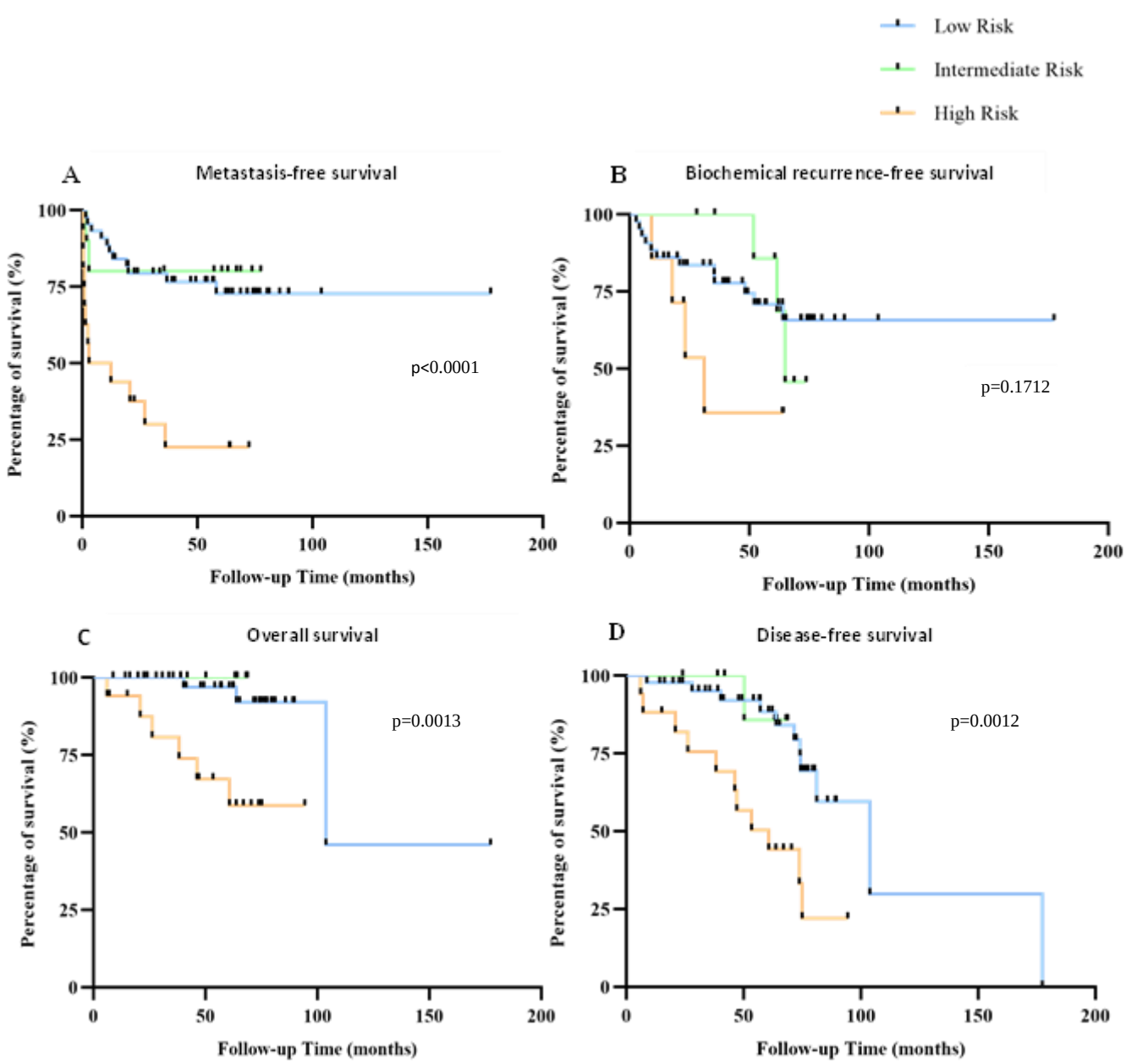

Figure 12: Cohort stratification according to the levels of PSA based on D'Amico classification*, concerning MFS (A), BRFS (B), OS (C) and DFS (D).*

Singleplex IF Validation

In order to study the interaction between the population of macrophages, fibroblasts and ASPA expression, specific markers were selected to elucidate the presence and abundance of these TME populations (briefly explained in Table 8). CD68 is a highly expressed protein in macrophage lineage, including monocytes, histiocytes, giant cells, Kupffer cells, and osteoclasts. In its turn, Desmin is a protein that is a muscle-specific, type III intermediate filament that integrates the sarcolemma, Z disk, and nuclear membrane in sarcomeres and regulates sarcomere architecture; due to its biological function, it was selected to permit the identification of the fibroblasts network of the prostate gland stroma. CD31 marker was chosen aiming the identification of blood vessels. To elucidate the localization of tumour cells, and guide the acquisition of the different ROIs, Cytokeratin 18 was used since it is highly expressed in PCa cells and benign prostate glands. To identify the expression of the five biomarkers, Alexa Fluor dyes were used. Specifically, two antibodies were already conjugated with Alexa Fluor dyes whereas the other three were not conjugated. The labelling with proper secondary antibodies, attributed different and distinguishable colours to the diverse biomarkers.

Table 8: Properties and biological functions of the markers analysed in PCa microenvironment.

BIOMARKER	BIOLOGICAL FUNCTION
ASPA	Enzyme that catalyses the deacetylation of NAA to produce acetate and L-aspartate. NAA occurs in high concentration in brain. Found in the cytoplasm as well as in the nucleus.
CD31	Transmembrane glycoprotein; exists concentrated at the borders of endothelial cells. It has been reported to be detected in pre-existing and newly formed vessels in cancer tissues.
CD68	Highly expressed in the cellular membrane of tissue macrophages. Could play a role in phagocytic activities of tissue macrophages, both in intracellular lysosomal metabolism and extracellular cell-cell and cell-pathogen interactions. Binds to tissue- and organ-specific lectins or selectins, allowing homing of macrophages subsets to particular sites.
CYTOKERATIN 18	Belongs to the intermediate filament family – cytoskeletal protein. The known function of Cytokeratin 18 is to provide a flexible intracellular scaffolding to structure cytoplasm, resist stresses externally applied to the cell, and maintain normal mitochondrial structures. Recognized as an epithelial marker in diagnostic histopathology, it is highly expressed in PCa and benign prostate glands and has an important function in tumour cell behaviour.
DESMIN	Class III intermediate filaments found in muscle cells (cytoplasmatic location). In adult straited muscle they form a fibrous network connecting myofibrils to each other and to the plasma membrane from the periphery of the Z-line structures.

To optimize the staining protocol for each biomarker, different conditions were tested (Table 9) and evaluated under the fluorescence microscope. Antigen Retrieval pH 6.0 and pH 9.0 were tested, and for all the antibodies pH 9 was more successful, achieving a higher intensity and better definition of the signal. Dilution of each antibody was also optimized, taking into consideration the information identified in each antibody's data sheet. Different secondary antibodies were analysed, according to the available colours. The choice of the Alexa Fluor dye aimed to attribute colours to make biomarkers distinguishable between them and avoid cross-reactions, as well as unspecific signals. Lastly, we were able to obtain specific and clear signals. Representative images of the optimized conditions are presented in Figure 13.

Table 9: Optimization procedure for single staining; the different parameters tested included the dilution factor, positive control, and secondary antibody.

Antibody	***Catalog #***	***Dilution Factor***	***Positive Control***	***Secondary Antibody***
ASPA (metabolism marker)	ab223269	100; 200; 250; 500; 1000	Brain; Prostate	Alexa Fluor 488 Alexa Fluor 568 Alexa Fluor 594
*CD31 * (endothelium marker)*	ab218582	25; 50; 100; 200	Fallopian Tube; Kidney	*conjugated with Alexa Fluor 568
CD68 (macrophages marker)	ab955	25; 50; 100; 200	Lung; Spleen	Alexa Fluor 488 Alexa Fluor 568 Alexa Fluor 594
Cytokeratin 18 (intermediate filaments marker)	ab219271	50; 100; 200; 300; 500	Fallopian Tube; Prostate	Alexa Fluor 488 Alexa Fluor 568 Alexa Fluor 594
*Desmin * (fibroblasts marker)*	ab203422	50; 100; 200; 300; 500	Fallopian Tube	*conjugated with Alexa Fluor 555

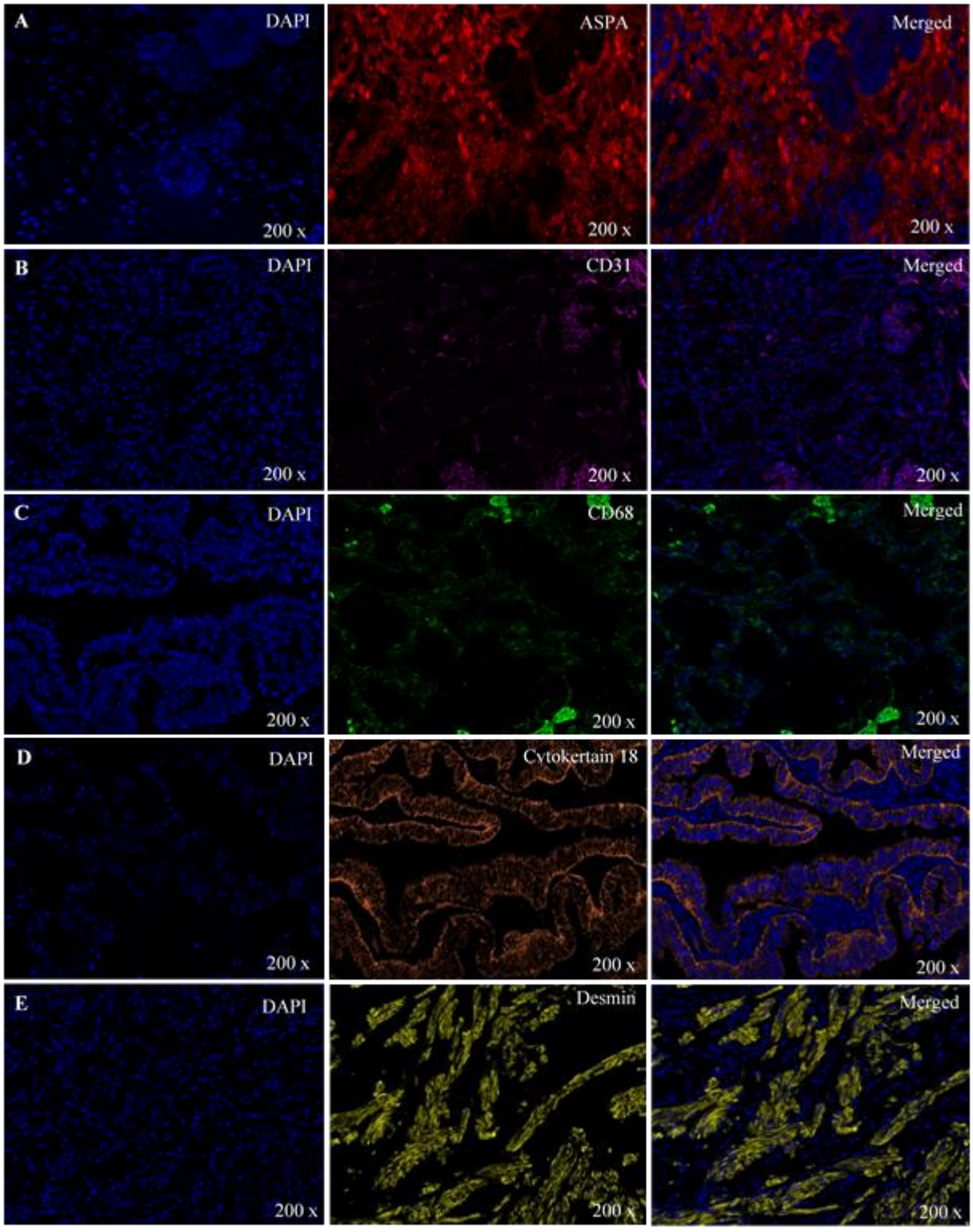

Figure 13: Simgle Staining Optimization. Immunofluorescence expression of biomarkers in the positive controls. *(A) ASPA staining (red) in brain tissue with metastatic carcinoma. (B) CD31 staining (pink) in kidney tissue. (C) CD68 staining (green) in lung tissue. (D) Cytokeratin staining (orange) in fallopian tube. Desmin staining (yellow) in fallopian tube tissue. Nulear DNA is labeled with DAPI (blue). These images were made with Multispectral Microscope with CRI multispectral camera with the 20X objective.*

The final settings to build the mPlex staining are summarized in the table below (Table 10).

Table 10: Optimized parameters for each biomarker, obtained from the Single Staining optimization protocol. The best conditions tested indicated the final dilutions and type of secondary antibody to use to acquire the best signal from each primary antibody.

Antibody	Source	Type of Antibody	Clone Type	Final Dilution	Secondary Antibody
ASPA	Rabbit	Monoclonal	IgG	100	Alexa Fluor 594
CD31 *	Rabbit	Monoclonal	IgG	25	*conjugated with Alexa Fluor 568
CD68	Mouse	Monoclonal	IgG1	25	Alexa Fluor 568
Cytokeratin 18	Goat	Polyclonal	IgG	300	Alexa Fluor 488
Desmin *	Rabbit	Monoclonal	IgG	500	*conjugated with Alexa Fluor 555

Duplex and Triplex IF Validation

After the optimization of the single staining, different sets of antibodies were tested to evaluate possible competition between them (Table 11). Even when individual antibodies have been validated it is necessary to demonstrate that mixtures of antibodies perform as expected. When combined, some antibodies may compete and generate unexpected patterns of staining not observed with individual antibodies, and mixtures of many antibodies can exhibit substantial interference. The first approach aimed to test duplex of biomarkers (Figure 14). When combined, ASPA and Desmin were clearly distinguishable. A good signal was obtained, and it was possible to evaluate the expression on each antibody, although it was possible to observe a co-localization of the expression profiles (Figure 14-A). The second duplex – CD31 and Desmin – was also successful and a good signal from each marker was detected (Figure 14-B). When mixing ASPA, CD68 and Cytokeratin 18 we were not able to observe the Cytokeratin 18 signal, indicating the occurrence of a competition phenomenon. To address this challenge, the 3 markers were divided in different sets. It was found that better signals were obtained when Cytokeratin 18 was added first, followed by a mixture of ASPA and CD68 (Figure 15-A). For the triplex ASPA, CD68 and Desmin, the results demonstrated that there was no competition or loss of signal intensity (Figure 15-B).

Table 11: Summary table of the Multiplex – duplex and triplex approaches tested. In this project we tested different combinations of antibodies to evaluate possible cross-reactions or loss of signal.

Antibody	*Positive Controls*	*Secondary Antibody*
ASPA + Desmin	Brain; Prostate	Alexa Fluor 594 + Conjugated with Alexa Fluor 555
CD31 + Desmin	Fallopian Tube; Prostate	Conjugated with Alexa Fluor 568 + Conjugated with Alexa Fluor 555
ASPA + CD68 + Cytokeratin 18	Brain; Lung; Prostate	Alexa Fluor 594 + Alexa Fluor 488 + Alexa Fluor 568
ASPA + CD68 + Desmin	Brain; Lung; Prostate	Alexa Fluor 594 + Alexa Fluor 488 + Conjugated with Alexa Fluor 555

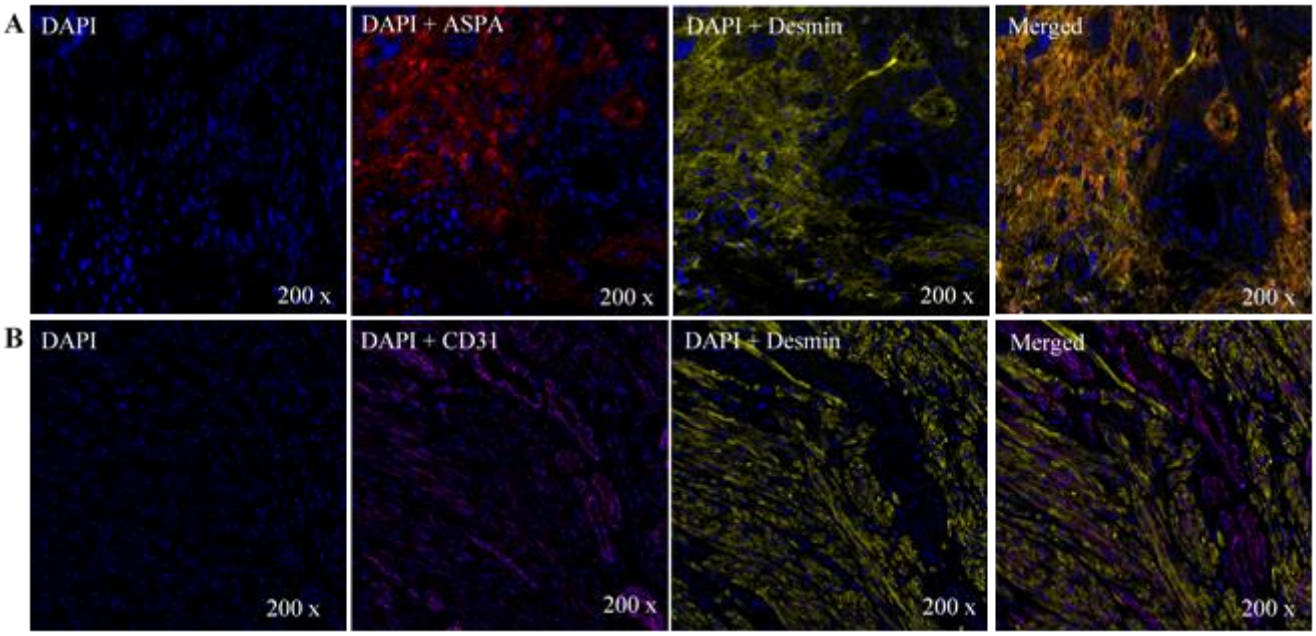

Figure 14: Duplex Staining Optimization. *(A) Immunofluorescence expression of ASPA (red) and Desmin (yellow) in brain tissue with metastatic carcinoma. (B) Immunofluorescence expression of CD31 (pink) and Desmin (yellow) in fallopian tube tissue. Nuclear DNA is labeled with DAPI (blue). These images were made with Multispectral Microscope with CRI multispectral camera with the 20X objective.*

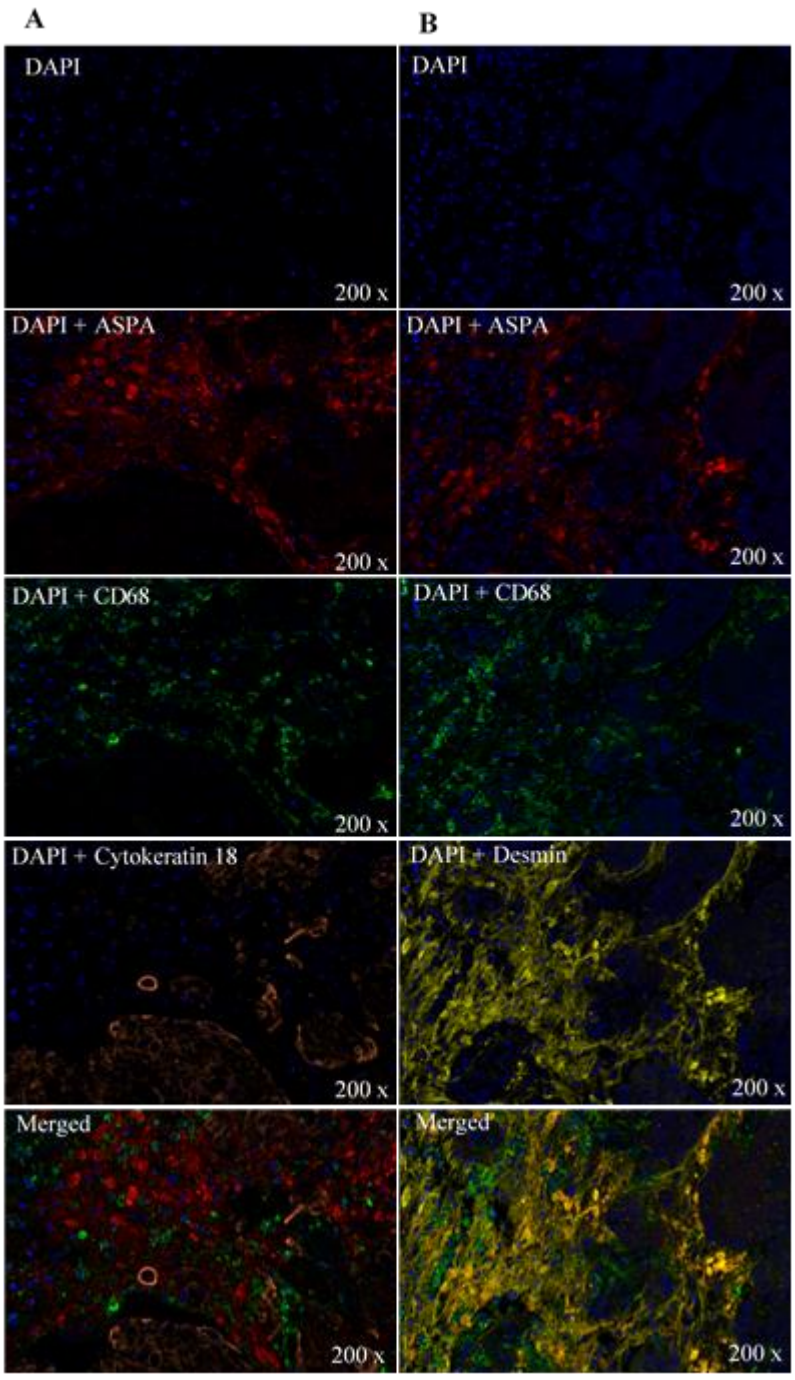

Figure 15: Triplex Staining Optimization. *(A) Immunofluorescence expression of ASPA (red), CD68 (green) and Cytokeratin 18 (orange) in brain tissue with metastatic tissue. (B) Immunofluorescence expression of ASPA (red), CD68 (green) and Desmin (yellow) in brain tissue with metastatic tissue. Nulear DNA is labeled with DAPI (blue). These images were made with Multispectral Microscope with CRI multispectral camera with the 20X objective.*

After this optimization process, it was concluded that to get the finest signal from all the antibodies of interest, the best staining protocol corresponded to the first antibody set including Cytokeratin 18 alone labelled with Alexa568, the second antibody set including ASPA and CD68, labelled with Alexa594 and 488 respectively, and the third and final antibody set including the two primary conjugated antibodies CD31-alexa647 with Desmin-alexa555 (Figure 16).

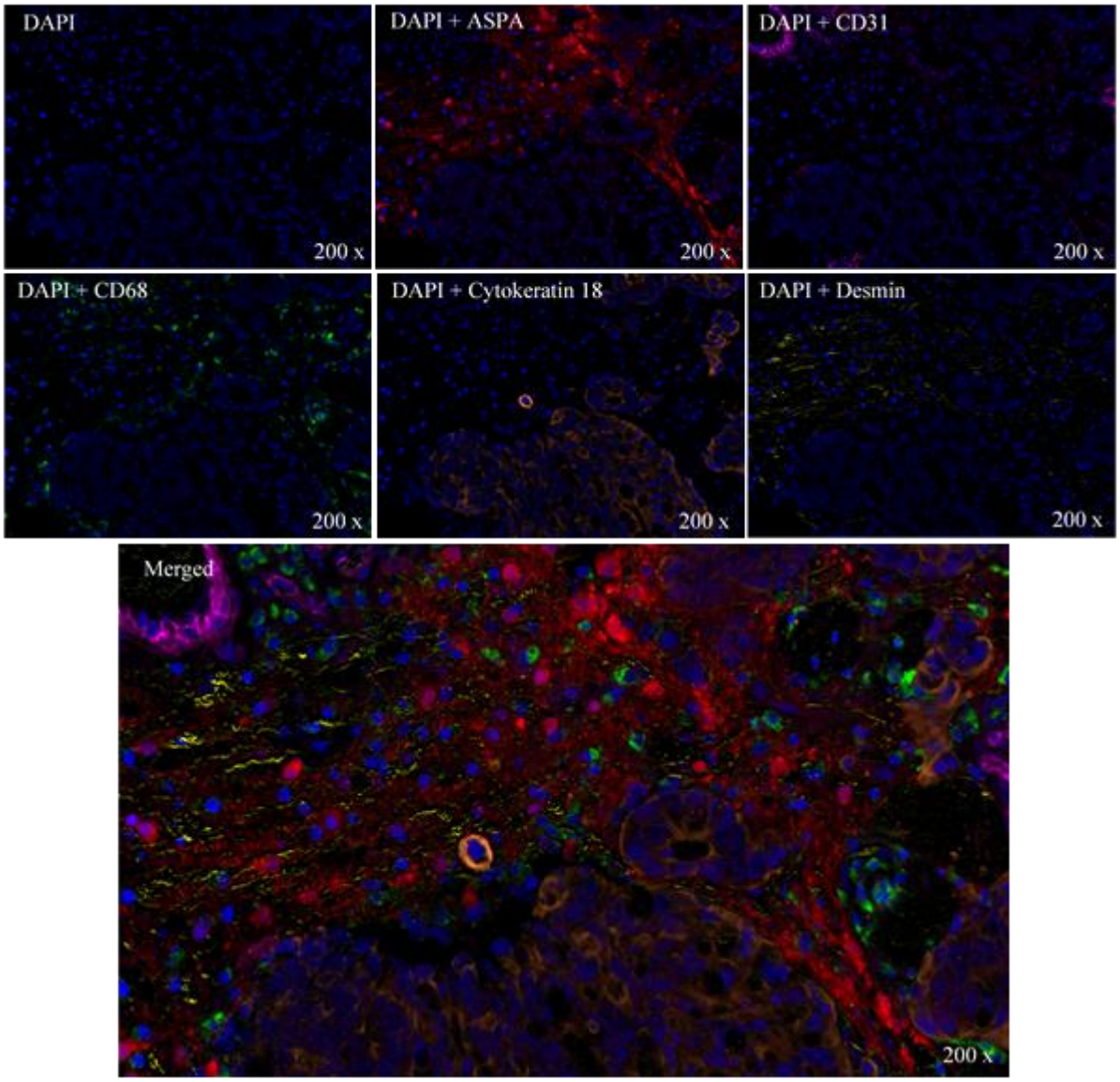

Figure 16: Multiplex Staining Optimization. *FFPE brain tissue with metastatic carcinoma. Nuclear DNA labeled with DAPI (blue), Anti-ASPA staining (red), Anti-CD31 staining (pink), Anti-CD68 staining (green), Anti-Desmin staining (yellow) and tumor cells expressing Cytokeratin 18 (orange). These images were made with Multispectral Microscope with CRI multispectral camera with the 20X objective.*

The last part of the optimization protocol focused on the image acquisition parameters, namely times of exposure considering the wavelengths of emission and excitation of each dye. Different times were assessed to obtain a specific and clear signal from each biomarker (Table 12).

Table 12: Image acquisition parameters in Multispectral Microscope with CRI Multispectral Camera. The acquisition information, especially times of exposure, was determined for the five biomarkers plus DAPI.

Filters	*Colour*	*Wavelengths Range*	*Excitation*	*Emission*	*Peaks*	*Exposure Time*	*Primary Antibody*	*Secondary Antibody*
DAPI	Blue	460-480			470	250		
FITC	Green	510-560	496	519	530; 540	150	CD68	Alexa Fluor 488
M1	Orange	580-650	578	603	610	300	CK18	Alexa Fluor 568
M1	Red	580-650	590	617	620	300	ASPA	Alexa Fluor 594
M2	Pink	640-710	650	665	680	150	CD31	Alexa Fluor 647
555	Yellow	560-630	555	569	580; 610	250	Desmin	Alexa Fluor 555

Multispectral Microscopy and Image Acquisition

Multispectral imaging, through its ability to separate autofluorescence from label fluorescence, can increase sensitivity as much as 300 times compared to conventional approaches, and concomitantly improve quantitative accuracy[77]. Using Multispectral imaging allowed the separation of five fluorophores, with each signal quantitated and visualized separately. This is an approach that optimizes the opportunities for multiplexing while at the same time overcomes the effects of autofluorescence on detectability and reliable quantitation.

FFPE tissue specimens were stained with the 5 biomarkers described above; the samples were analysed under the microscope and 10 ROIs were acquired in each specimen as follows: the selection of the regions was aleatory and aimed to choose 5 regions within the stromal areas in between the tumour glands (Str Tum) and 5 regions in the periphery of the tumour nests (Str Far). Considering the 20 samples from BPH, 5 regions close to the hyperplasic glands were selected (Str Hyp) and 5 regions far from the hyperplasic glands (Str Far). In the case of metastasis samples, only 5 regions were acquired within the stroma close to the tumour cells (Str Tum), since these samples were smaller, being the majority biopsy samples. This selection was guided by the Cytokeratin 18 staining that identifies the tumour cells. The microscope used has 5 long-pass filters, and for each, the spectra observed are captured, so that across all filters, the complete spectral properties of each independent signal can be effectively employed for spectral unmixing. To visualize the raw images, to build the libraries and perform the unmixing of the scanned images the Nuance software was used.

Spectral unmixing can faithfully separate signals that may overlap both spatially and spectrally, without "crosstalk" (signals from one label showing up in a channel ostensibly dedicated to another). The basic mathematical approach is part of the conventional spectroscopic toolbox and is at heart a simple least-squares fit that takes the experimental measured spectrum at each pixel and breaks it up as a linear combination of spectra corresponding to the signals expected to be present [78].

To ensure faithful unmixing results, it is essential to obtain accurate spectra representing each signal in the image. These can be provided to the software via established spectral libraries. Once the unmixing has taken place, the individual component images can be combined in a "composite" image, with control over the pseudo-colour assigned to each plane [77].

The optimization of the Multispectral libraries was performed using the control slides for each biomarker. The importance of the multispectral library relies on the assurance that the spectrum of interest from each specific marker is separately imaged. Afterwards, the library allows the correct merging of all images together in a final composite. Finally, it was possible to build a multispectral library that was used to unmix all scanned images, allowing a good image analysis and antibody quantification (Figure 17).

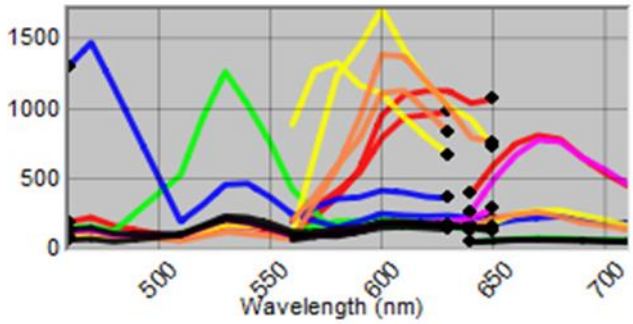

	Name	Color
1	ASPA	Red
2	CD68	Green
3	DAPI	Blue
4	DESMIN	Yellow
5	CK18	Custom
6	CD31	Magenta
7	Background 1	Black
8	Background 2	Black

Figure 17: Multispectral library sprectrum peaks for the biomarkers in analysis and DAPI. *Optimized library was built using Nuance software.*

Application of mPlex IF to PCa specimens

A total of 123 samples were stained according to the optimized protocol and the expression of the biomarkers were analysed accordingly. Representative images are presented to demonstrate the different and progressive disease stages selected for analysis, and the immunostaining obtained after the optimization phase (Figure 18). The desired markers were detected efficiently, with different patterns and abundance of expression.

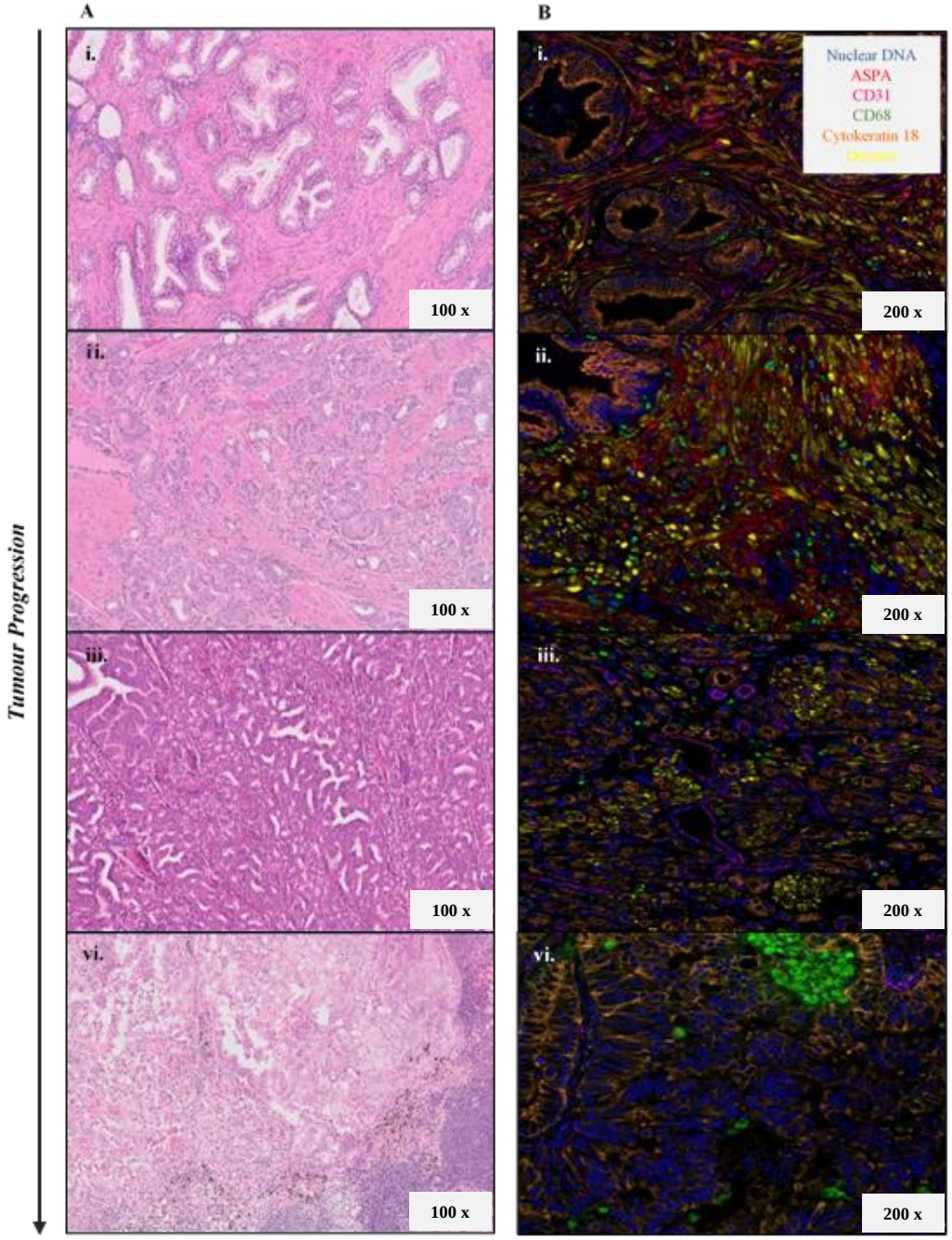

Figure 18: Representative images of the samples from the cohort with Hematoxylin & Eosin (H&E, A) and mPlex IF (B) staining methods. *Images in A display a H&E slide of a BPH (i), PCa with Gleason Score 7 (ii), PCa with Gleason Score 8 (iii) and a Lymph Node metastasis (iv) - this is the current imaging method used for pathologists in PCa diagnosis. Images in B correspond to the multiplex IF staining of the same cases as displayed in image A.*

Biomarker Immunoexpression and Disease progression

All molecular data obtained from the stainings was acquired and treated using extensively the functionalities of Fiji software. A protocol of image analysis according to the aims of the project and the tools available was designed.

The enrichment of each molecular marker was determined according to the spatial localization as well as their prognostic relevance. Biomarkers immunoexpression was associated with PCa recurrence, aggressiveness, and metastasis. The statistical analysis performed aimed to establish a comparison between the 2 compartments analysed and between the different stage groups. The most relevant data is presented in this Section, but all graphs and summary tables are presented in Supplementary Data.

ASPA Expression Intensity decreases with tumour progression

The results obtained from the analysis of ASPA expression indicate that with the progression of the disease less ASPA is detected, especially close to the prostatic glandular cells. When comparing the enzyme expression between the glandular regions (Str Hyp and Str Tum) and the stroma areas far from the glands (Str Far), there are significant differences, with exception of stage G4, suggesting that close to hypertrophic/ tumoral glands there is a possible downregulation of the enzyme, that becomes more evident in higher disease stages (Figure 19).

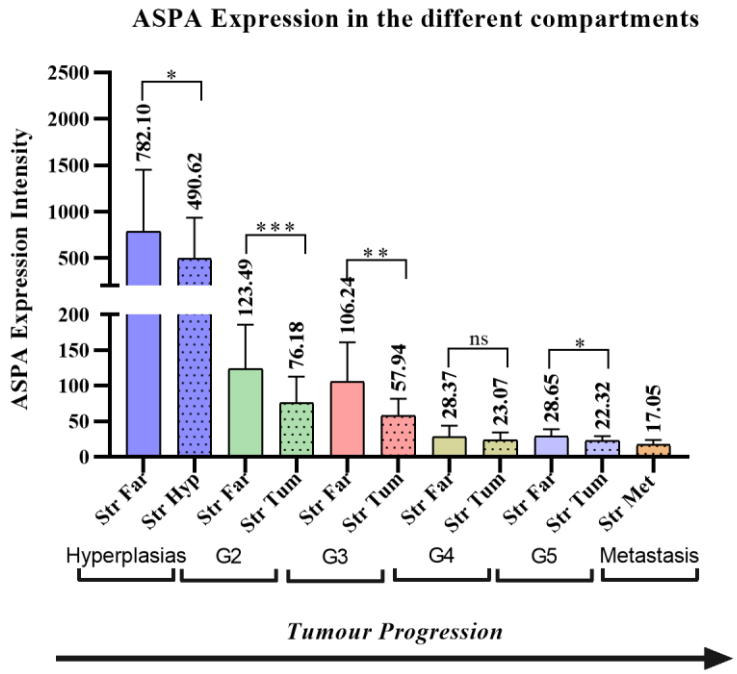

Figure 19: ASPA Expression Intensity in the different stages, in the two types of ROIs analysed.

Focusing on the stromal areas in the periphery of the glands, there are statistically significant differences between the different stages of the disease. Considerable variations between disease stages are also observed in the areas close to the glands, emphasizing the alteration on the ASPA pattern of expression in the TME (Figure 20-A and B).

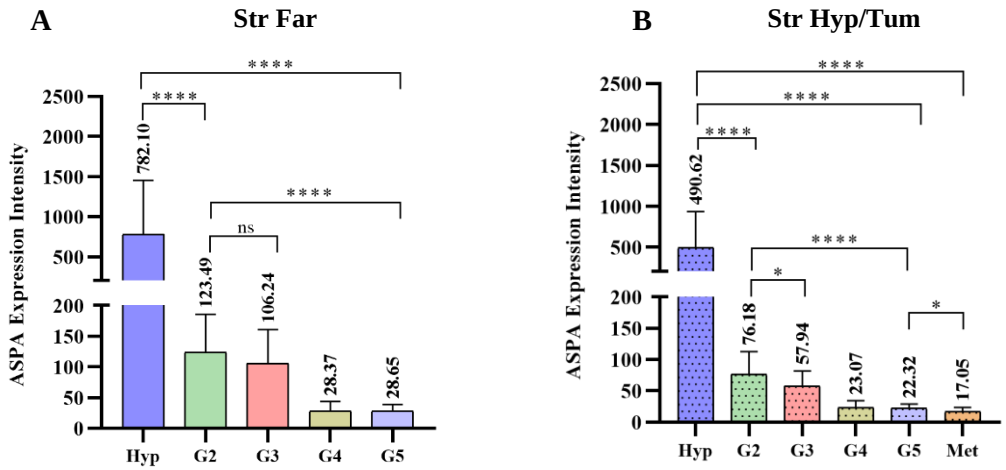

Figure 20: ASPA Expression Intensity in the different stage groups. *(A) Analysis in the stroma far from prostatic glands; (B) Analysis in the areas close to prostatic glands.*

Our results indicate that the decrease in ASPA expression is in association with disease progression. Little is known about its role in PCa since only very recently it was found in association with higher tumour stages [70,79]. There is the hypothesis that this scenario is observed due to the downregulation of ASPA, or it may be attributed to the fact that there is an accumulation of its metabolite: NAA, that may give molecular signals for tumour cells to activate molecular pathways that culminate in a more aggressive phenotype. All in all, the interaction between prostatic epithelial cells and the TME determines complex changes that pilot disease severity and the metastatic potential. Above all, metabolic alterations, namely enzyme profile of expression, seem to drive the tumour expansion. More studies are needed to develop and prove the hypothesis in study, namely targeted transcriptomic analysis to the study the transcriptome, of the complete set of RNA transcripts that are produced by the genome, under specific circumstances, in specific cell types.

Fibroblasts population is highly abundant in PCa microenvironment

The fibroblasts are highly abundant in PCa microenvironment; Desmin expression is elevated in the different stages of the disease, including in BPH. Interestingly, this pattern of expression starts to decrease in higher stages (Figure 21). In the case of metastasis, the biomarker expression is very low as expected, since in this type of tissues the stroma is very scant, and fibroblasts are not present.

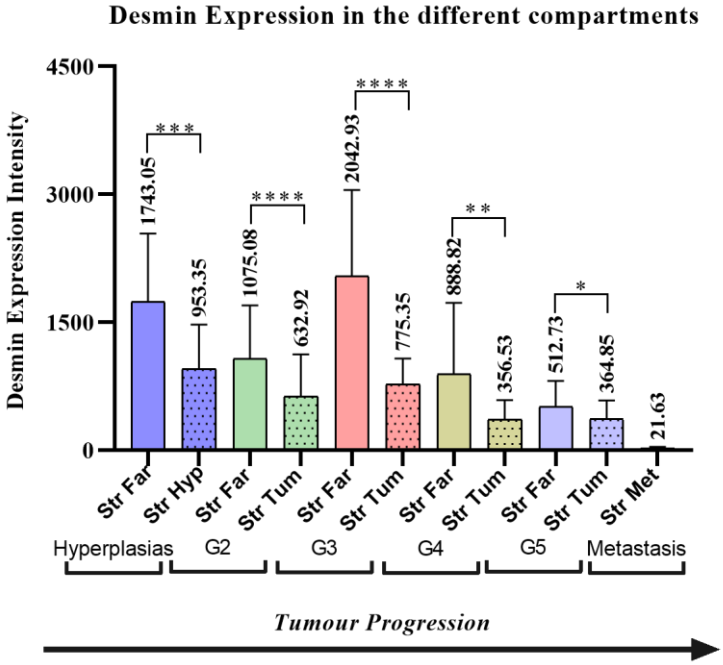

Figure 21: Desmin Expression Intensity in the different stages, in the two types of ROIs analysed.

Important to highlight that fibroblasts network, as expected by the selection of the analysis, are more abundant in the regions far from the hypertrophic and tumoral glands. Comparing the 2 types of compartments analysed, statistically significant differences are found, demonstrating that the nature of the ROIs is distinct (Figure 22-A and B). This proposes that this supportive network is less abundant where there are more hypertrophic / tumoral cells, emphasizing the role of fibroblasts as facilitators of cancer progression, having a supporting role for tumour cells growth as well as extracellular matrix remodelling, promoting angiogenesis, and mediating tumour-promoting inflammation.

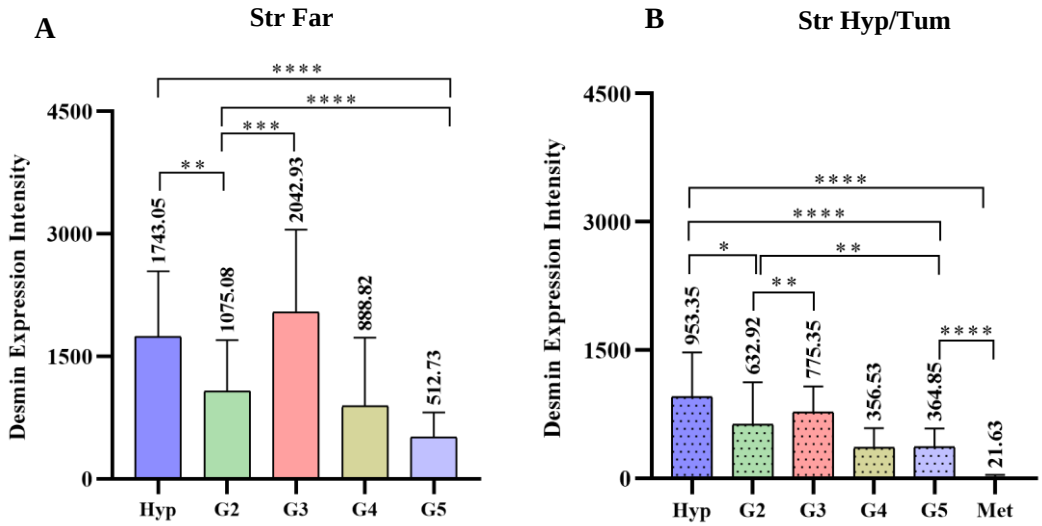

Figure 22: Desmin Expression Intensity in the different stages. *(A) Analysis in the stroma far from prostatic glands; (B) Analysis in the areas close to prostatic glands.*

An increasing bulk of literature demonstrates the relevance of CAFs crosstalk with tumour cells, however many other cell types (such as adaptive and innate immune cells or endothelial cells) populate primary or metastatic sites contributing to a complex network of heterotypic interactions resulting in a global tumour-promoting or inhibiting effect [80].

In the present study, we detected different levels of Desmin expression, and statistical analysis confirmed the differences between stage groups in the distinct areas acquired. Nevertheless, it was not possible to evaluate the activation status of these cells. Detecting fibroblasts having the so-called 'activated' phenotype able to promote cancer progression is still a challenge; although several markers have been proposed and some of them have been largely used across different cancer types (such as α-Smooth Muscle Actin (α-SMA) and Fibroblast Activation Protein (FAP)). Important to highlight that tumour associated stroma is enriched in activated fibroblasts, being of high importance to distinguish the reactive fibroblasts and to characterize its role in TME.

It is determinant to assess the functional role of fibroblasts for ASPA expression and regulation; a valid approach could be the culture of fibroblasts with ASPA knock-out to understand the role of the TME subpopulation in the downregulation of the enzyme.

CAFs have been shown to influence each step of PCa development, growth and metastasis, besides their involvement in development, tissue repair and inflammatory response [81]. Such a complex network of signals and patterns of expression have just started to be unravelled; however, several challenges still need to be overcome due to the lack of functional and metabolic studies to characterize the interplay between fibroblasts and ASPA expression.

Co-localization between ASPA expression and the fibroblasts network

Aiming to evaluate the importance of fibroblasts in ASPA expression, a co-localization analysis between these markers was performed. Manders coefficient was calculated, and we observed that a strong co-localization between ASPA and the population of fibroblasts exists (values for Manders coefficient are close to 1). Particularly, it is observed that almost all the ASPA detected co-localizes with fibroblasts population, but not all fibroblasts co-localize with ASPA, meaning that in the tissue analysed there is more Desmin than ASPA (Figure 23).

Of note, the coefficient is lower in the areas close to the hypertrophic and tumoral glands. These regions have less abundance of Desmin and ASPA expression, justifying the decrease in the value of the coefficient. Concerning the co-localization between ASPA and Desmin, significant statistically differences are detected between the compartments acquired, except for groups G4 and G5. Of note, it is not possible to observe a linear pattern of the co-localization between these biomarkers among the progressive stage groups. Moreover, no differences were detected between the distinct ROIs analysed in the co-localization between Desmin and ASPA. It was only possible to determine that the coefficient values are lower and close to 0.

In the case of metastasis, this analysis was not performed since no significant expression of Desmin was detected.

The colocalization of two or more markers within cellular structures may be defined as an overlap in the physical distribution of the molecular markers within a three-dimensional volume, where this may be complete or partial overlap [82]. By adopting this approach to study, the interplay between fibroblasts and ASPA a statistic analysis of pixel intensity distributions was built, customized to the type of tissues analysed. Calculating the Manders coefficient enables to quantitively characterize the level of co-localization, offering more information than a simplistic qualitative evaluation of overlapping pixels.

Nevertheless, due to the importance of fibroblasts in the TME and their influence on the signalling with other cells in the tumour nest, it would be of great importance to develop more studies to better assess how fibroblasts participate in ASPA regulation and expression in the PCa microenvironment. Interfering in the activation and in the communication pathways of these cells could represent a novel therapeutic approach to target fibroblasts.

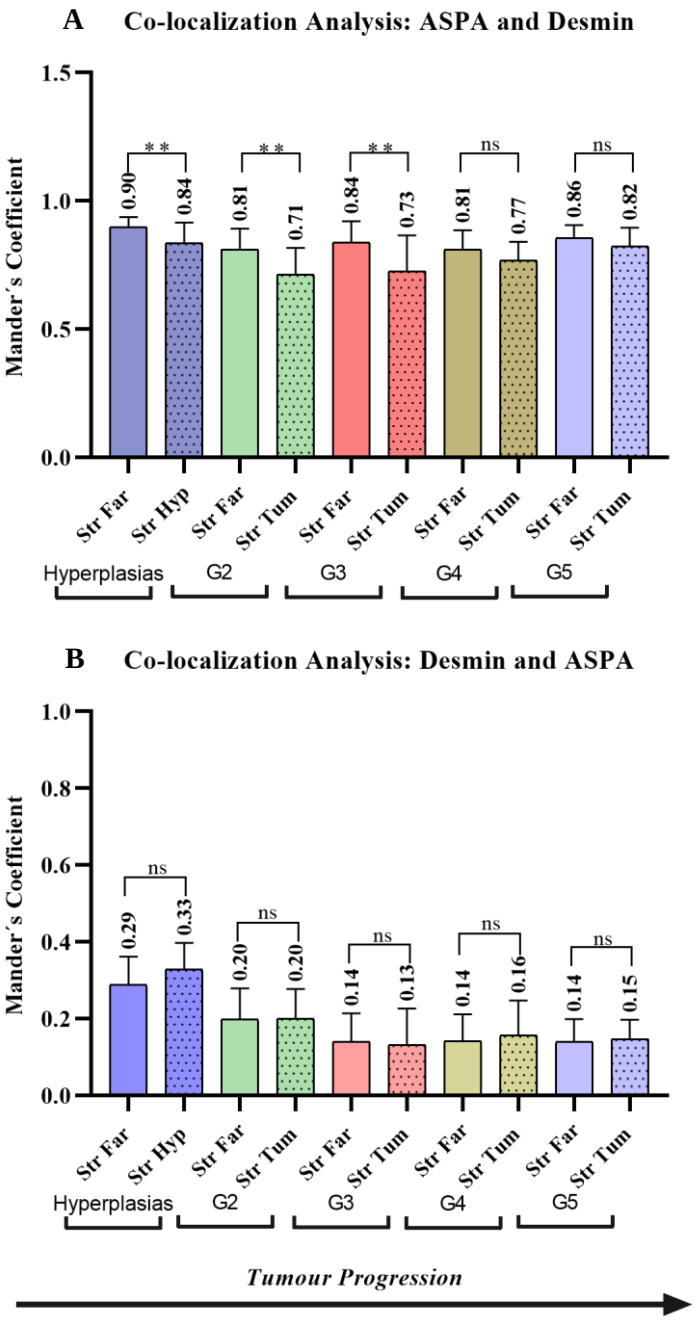

Figure 23: Co-localization Analysis in the different stages, in the two types of ROIs analysed*. (A) Co-localization Analysis between ASPA and Desmin – Manders Coefficient 1. (B) Co-localization Analysis between Desmin and ASPA – Manders coefficient 2.*

Vascular density correlates with proximity to tumour cells and increases in higher stages of the disease

Our results confirmed that CD31 expression increases along with tumour progression, highlighting the importance of vascular density for tumour cells to develop, grow, and eventually spread. Interestingly, CD31 is less expressed in the areas close to the hypertrophic glands. In the case of PCa progression groups the expression is higher close to the tumoral glandular cells, emphasizing the role of endothelial cells in the TME (Figure 24).

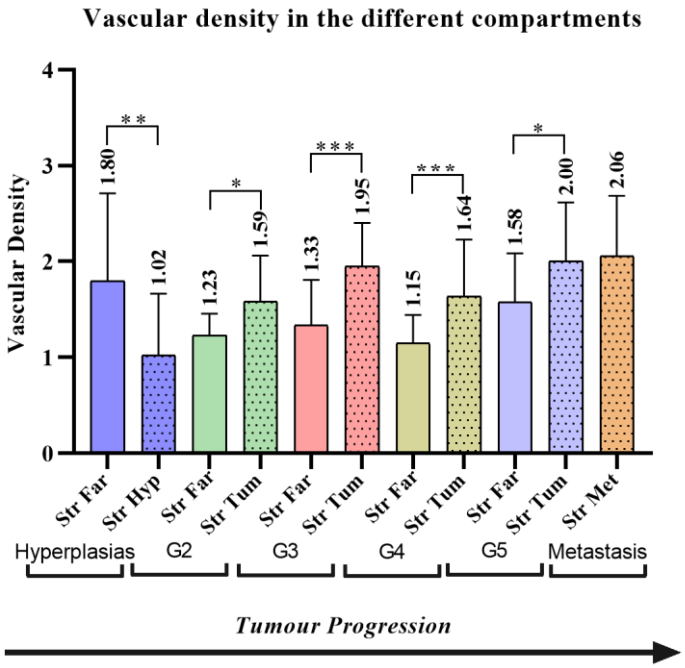

Figure 24: Vascular Density in the different stages, in the two types of ROIs analysed.

Regarding the pattern of expression between the glandular regions and the stroma far from the prostatic glands, statistical differences are detected, leading to the idea that in the different compartments the status of vascularization is different and may be determinant for tumour progression (Figure 25-A and B). Of note, in the group G3 there is a higher increase of vascular density close to the tumoral cells (Figure 25-B).

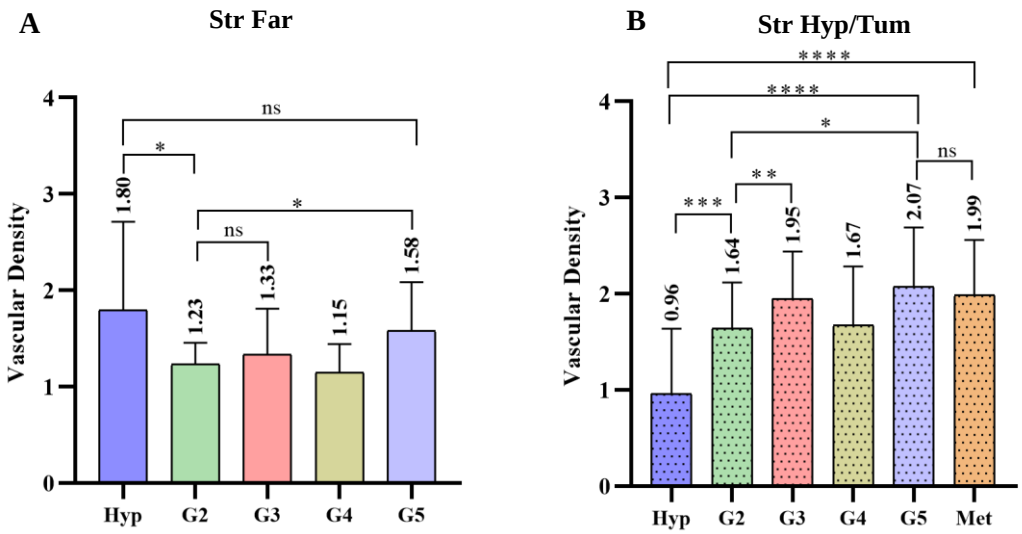

Figure 25: Vascular Density in the different stages. *(A) Analysis in the stroma far from prostatic glands; (B) Analysis in the areas close to prostatic glands.*

In more detail, it was observed that between the stage groups the differences of CD31 expression are more significant in the areas close to the glandular cells, suggesting that the pattern of the biomarker expression is more determinant in these areas between the stage groups, meaning that vascular density is important for tumour progression. Nonetheless, it is not possible to identify a linear pattern of expression that correlates with disease progression.

Moreover, by using CD31 to identify endothelial cells it is not possible to determine the degree of angiogenesis, since we are only able to detect the percentage of the sample area occupied by vessel lumens, following binary reconstruction of images. Afterwards it is also valuable to ascertain a possible involvement of endothelial cells in ASPA expression. Furthermore, it has been shown that the choice of vascular marker and the method of its evaluation are critical for evaluating the angiogenic status [83]. Despite the weaknesses associated to the markers selected, there is a general agreement that angiogenesis plays important roles in tumour growth, progression, and outcome in patients with PCa.

Blood vessels do not correlate with ASPA expression in PCa microenvironment

When analysing the co-localization between ASPA and CD31 there is no correlation between these markers, indicating that blood vessels are not involved in the phenomenon of decreased expression of the enzyme. The Manders coefficient for the different groups ranges from 0,03-0,09, meaning that there is no co-localization (Figure 26). Additionally, it is not possible to identify significant differences between the two compartments analysed or the different stages of the disease.

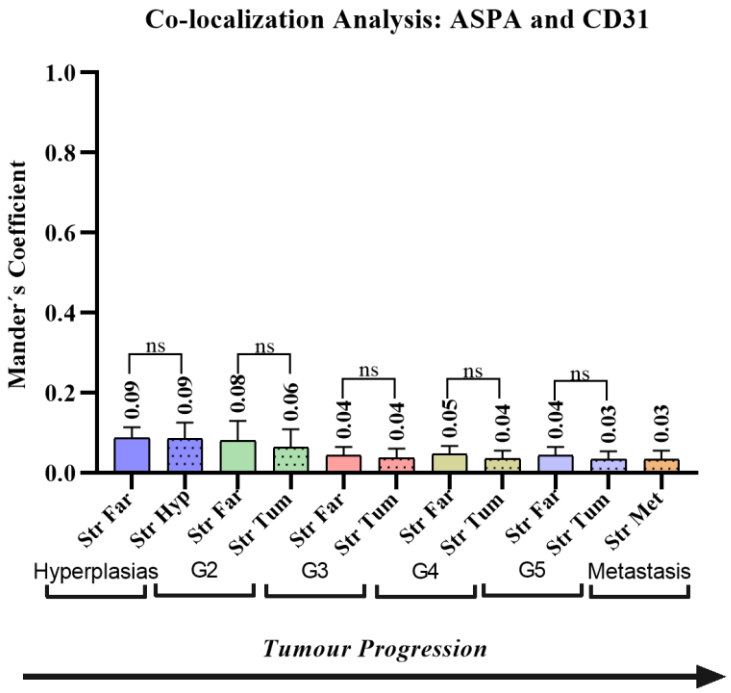

Figure 26: Co-localization Analysis between ASPA and CD31 in the different stages, in the two types of ROIs analysed.

Population of Macrophages increases with tumour progression

Macrophages' infiltrate is evident and increases with tumour progression. In general, there is an increase of this population along with tumour progression (Figure 27). In case of group G3 higher numbers are observed, not coincident with the typical number increase. Interestingly, this group also demonstrated to have higher expression of fibroblasts.

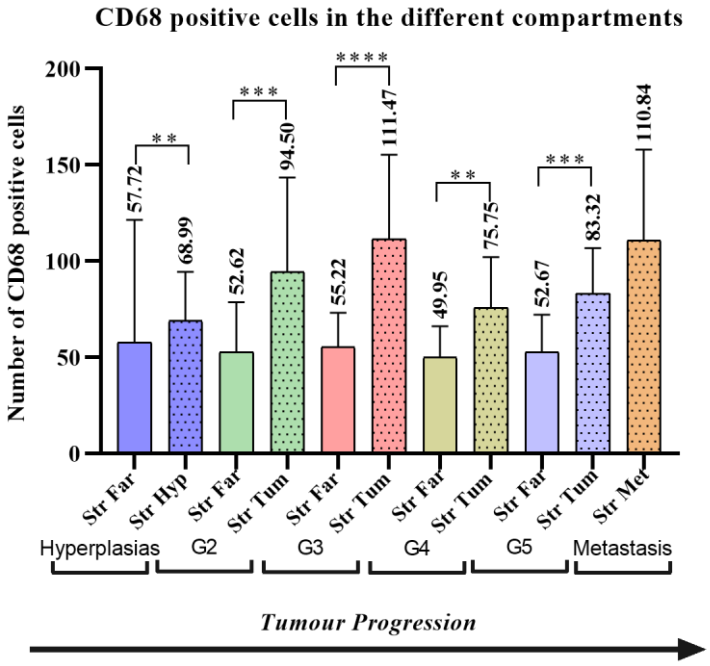

Figure 27: Number of CD68 positive cells in the different stages, in the two types of ROIs analysed.

There are statistically significant differences between the numbers observed in the two types of areas analysed (Figure 27). Curiously, between the different stage groups, in the areas far from the prostatic glands there are no statistically significant differences (Figure 28-A). Nevertheless, when performing the analysis between the groups in the areas close to the prostatic glands, differences are detected (Figure 28-B). This suggests that these numbers may be in correlation with tumour progression and aggressiveness depending on disease stage. Additionally, it indicates that there is a different distribution of cells according to the distinct localization.

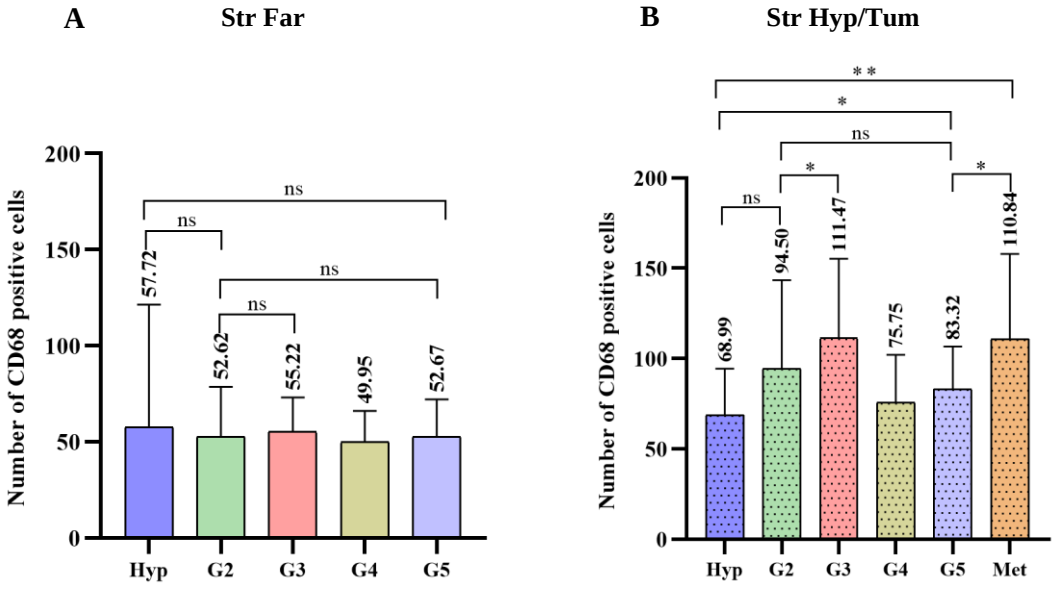

***Figure 28: Number of CD68 positive cells in the different stages**. (A) Analysis in the stroma far from prostatic glands; (B) Analysis in the areas close to prostatic glands.*

A more detailed analysis of the CD68 positive cells distribution was performed to determine the numbers in the Peri- and Intraglandular regions (Figure 29). Higher numbers are detected in the intraglandular regions, especially in PCa samples (Figure 30). These results suggest that macrophages are an important population within TME, and may be in association with tumour progression, playing a role in the establishment of tumour cells.

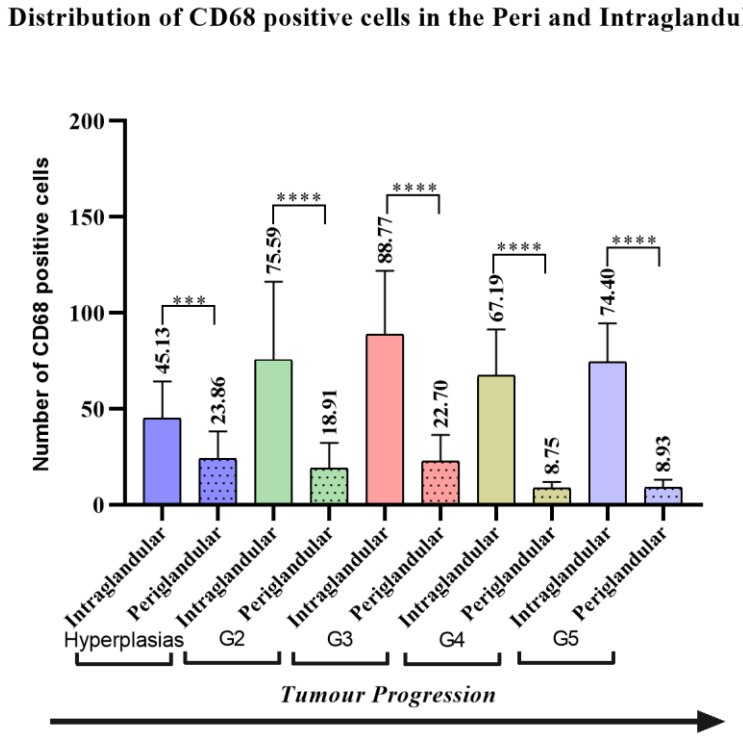

Figure 29: CD68 positive cells in the different stages, in the Intraglandular and Periglandular regions.

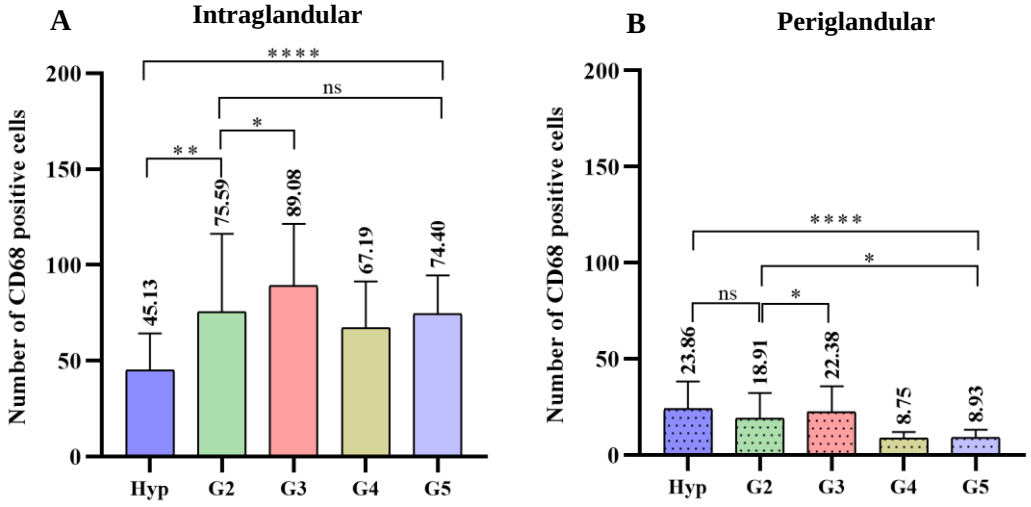

Figure 30: Number of CD68 positive cells in the different stages. *(A) Analysis in the Intraglandular regions; (B) Analysis in the Periglandular regions.*

I also attempted to measure the distances between the population of CD68 to the tumoral cells (guided by the Cytokeratin 18 signal). Since PCa is an adenocarcinoma, composed of many glands invading the stroma, this approach revealed to be irreproducible and with various limitations. A more efficient approach would be using the functionalities of R studio software to determine the distribution of macrophages in relation to tumoral cells.

It is reported that distinct immune cell infiltration patterns in the TME are associated with disease aggressiveness and patient outcome in several cancer types, especially macrophages which are a major component of inflammatory cells. In agreement with a predominant pro-tumorigenic impact, macrophages infiltration is often associated with a poor prognosis and shorter survival. It is now recognised that macrophages exhibit differences in ontogeny, differentiation status and distribution within tumour tissues. Macrophages can be divided into the dual M1-M2 paradigm – being the M1 macrophages anti-tumoral and M2 pro-tumoral. Due to the importance of these distinct subpopulations, as a future experiment we aim to study a possible correlation between the pattern of ASPA expression and macrophages subtypes (M1 and M2). We intend to investigate a potential role of ASPA, or the accumulation of its metabolite, in the process of macrophages differentiation to become pro-tumoral and assess the role of fibroblasts as supporting actors in this scenario.

To study in detail this hypothesis we aim to establish a second mPlex IF, focusing on the activated fibroblasts population (using FAP antibody) and macrophages subtypes. To distinguish these populations CD80 will be used to immunostain M1 macrophages and CD206 to identify M2 macrophages. The future mPlex that we would like to build for this purpose will include the biomarkers summarized in Table 13.

Table 13: Summary table of the optimization parameters to establish a second mPlex IF. Parameters to adjust include antibodies, dilution factors, positive controls, and secondary antibodies.

Primary Antibody	***Dilution***	***Positive Control***	***Secondary Antibody***
Cytokeratin 18 *(goat monoclonal IgG)*	1/300 (optimized)	Fallopian Tube (optimized)	Alexa Fluor **568**
CD80 *(rabbit monoclonal IgG)*	1/500; 1/1000; 1/1500	Lung	Alexa Fluor **647**
FAP *(mouse monoclonal IgG1)*	1/300; 1/400; 1/500	Brain	Alexa Fluor **594**
CD206 *(rabbit monoclonal IgG)*	1/50; 1/100; 1/200	Lung Carcinoma	Conjugated with Alexa Fluor **488**
Desmin *(rabbit monoclonal IgG)*	1/500 (optimized)	Brain (optimized)	Conjugated with Alexa fluor **555**

Comparison between regions close to the prostatic glands and regions far from prostatic glands

Our results demonstrated that there are significant differences on the expression of the biomarkers in the different regions analysed and between the different tumour stages. In summary, it is possible to detect lower levels of ASPA and Desmin expression close to prostatic glands (hyperplasic and tumoral). On its turn, the vascular density, and the numbers of CD68 positive cells are higher in the areas close to the glands. Although, it is not possible to describe a linear pattern of expression, we are able to say that the biomarkers studied have different patterns of expression in the two types of compartments analysed, which can lead to the identification of a signature that can predict metastatic potential. Table 14 summarizes the observed patterns of biomarkers' expression.

Table 14: Biomarkers' expression profile according to the ROIs analysed, and according to disease progression. Summary table describing where the markers are more or less expressed and if their expression profile demonstrates a tendency to increase or decrease for more advanced stages of the disease.

Biomarkers	*Stoma close to the glands*	*Stroma far from the glands*	*Expression with disease progression*
ASPA	+	-	↓
Desmin	+	-	↓
CD31	-	+	↑
CD68	-	+	↑

TME features in correlation with Clinicopathological Data

To analyse the influence of the biomarker's expression on the overall survival, the patients were stratified in groups according to the median of the biomarkers' expression as a cut-off (Supplementary Figure 46). This resulted in a division of high and low expression groups for all markers, and the following analysis of the percentage of survival with the construction of Kaplan-Meier survival curves.

Parameters analysed included MFS, BRFS, OS, DSFS, and DFS according to the expression of the different biomarkers in the stromal areas in between the tumour glands and in the periphery of the tumour nests. For this analysis only patients with the PCa were considered. The results obtained were quite consistent, for this reason only 4 representative graphs are presented for each biomarker. All other graphs are presented in Supplementary data.

Low ASPA is a biomarker of poor clinical outcome

Based on Mantel-Cox test it is possible to detect that those patients with lower levels of ASPA expression have more tendency to develop metastasis and to face biochemical recurrence (Figure 31-A and B). In what concerns OS and DFS, the biomarker showed statistical association with these variables; patients with lower expression of ASPA were more prone to experience poor disease outcome (Figure 31-C and D). In terms of the patient's outcome, comparing the expression in Str Far and Str Tum, we can detect that the survival profiles are similar. Additionally, the median MFS for patients with low ASPA expression in Str Far is 36 months whereas median survival was not reach in high ASPA tumours.

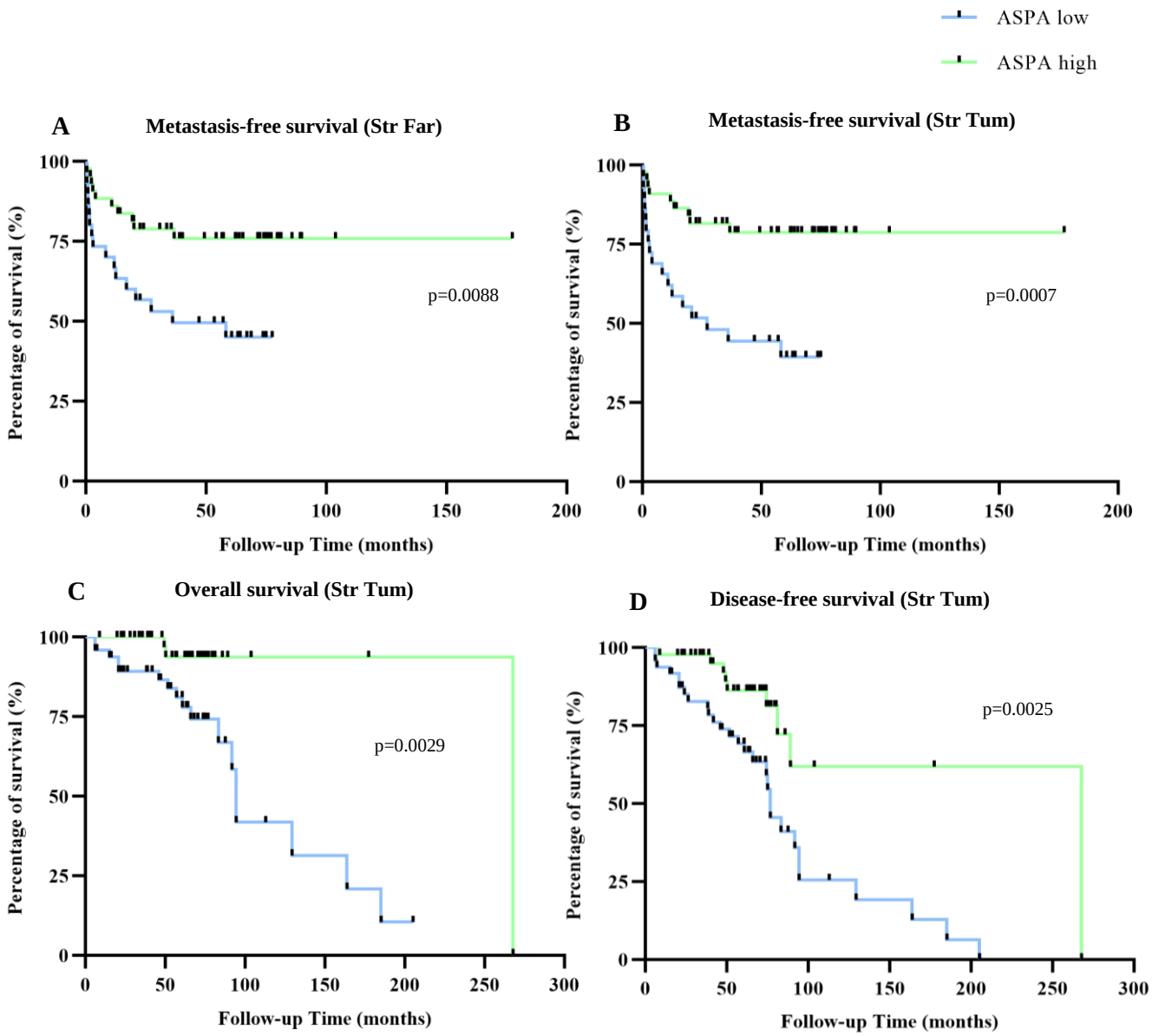

Figure 31: Correlation of ASPA expression with clinico-pathological data*. MFS (A, B), OS (C) and DFS (D) according to ASPA expresion. Two regions considered: Str Far-far from the tumoral glandular cells and Str Tum-close to the tumoral cells.*

Low Desmin levels are associated with poor clinical outcomes

Concerning patients' stratification according to Desmin expression, we can identify that there are statistically significant differences between the two groups (low and high Desmin expression). Concerning MFS, the median survival is 58 months for the patients with low desmin in the regions far from glandular cells, whereas median was not reached in high Desmin tumours (Figure 32-A and B). In terms of OS and DFS, statistically significant differences were found (p value of 0.0060 and 0.0110, respectively, Figure 31 C and D)).

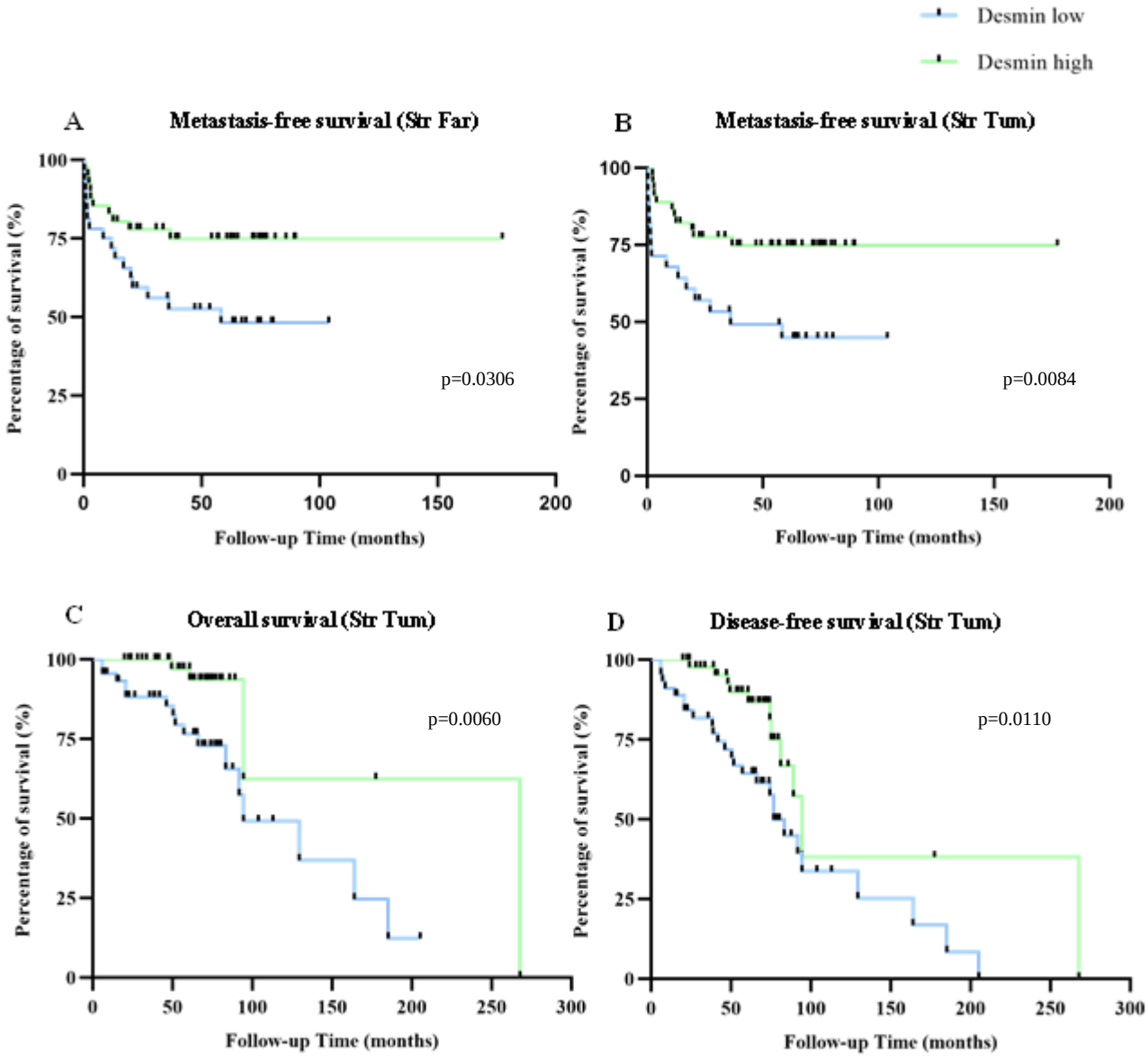

Figure 32: Correlation of Desmin expression with clinico-pathological data. *MFS (A, B), OS (C) and DFS (D) according to Desmin expresion. Two regions considered: Str Far-far from the tumoral glandular cells and Str Tum-close to the tumoral cells.*

Vessel density (determined by CD31 expression) does not correlate with clinical outcome

When analysing the impact of CD31 expression for the patient's outcome, we are not able to identify statistically significant differences between the two groups. Nonetheless, we observe a tendency that those patients with higher vascular density are more prone to develop metastasis, especially those patients that exhibit a higher vascular density in the periphery of the tumour cells (Figure 33-A and B). Regarding OS and DFS, it seems that there may be a tendency for a poor prognosis associated with higher expression of CD31, although not statistically significant (Figure 33-C and D).

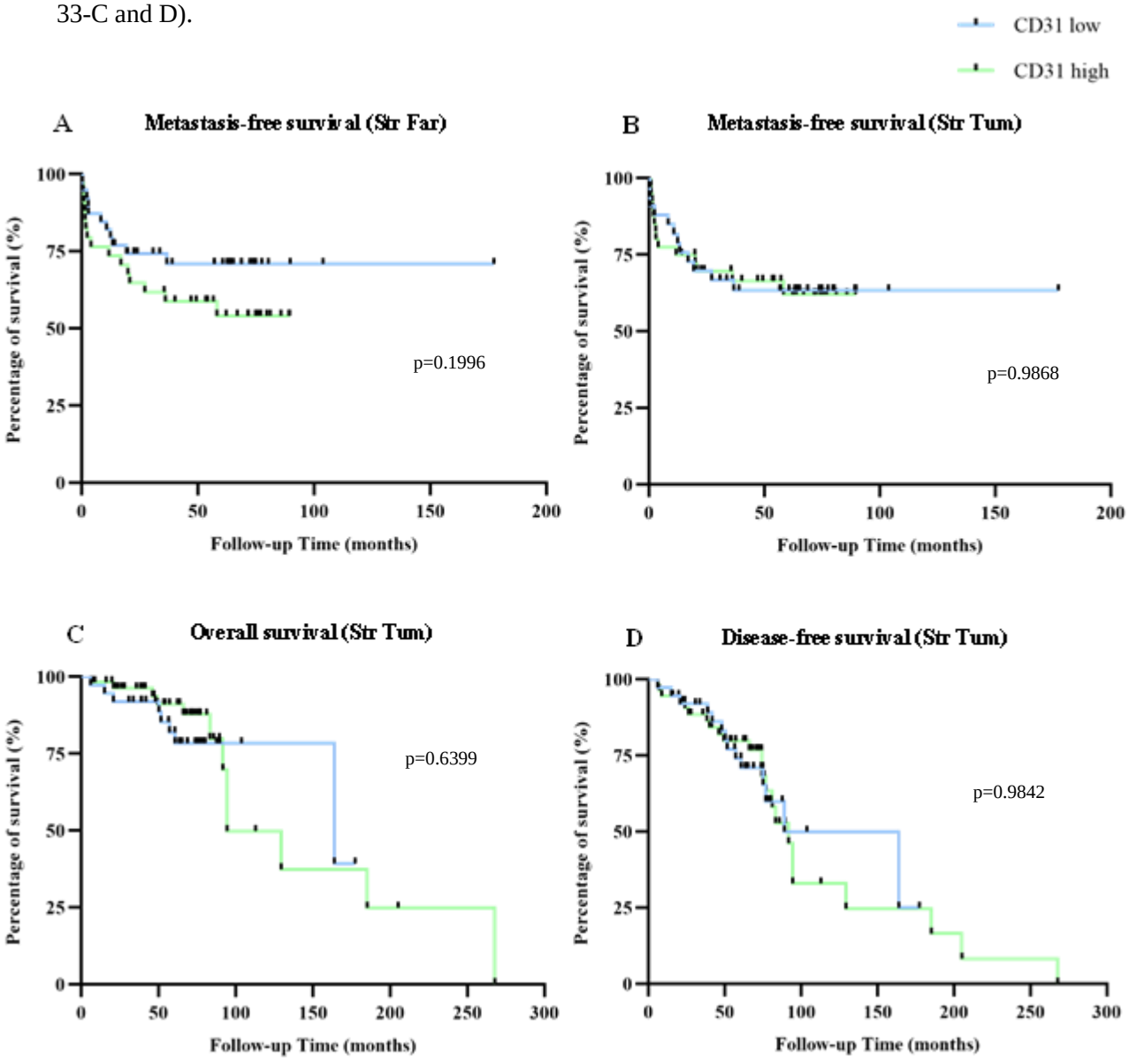

Figure 33: Correlation of CD31 expression with clinico-pathological data. *MFS (A, B), OS (C) and DFS (D) according to Vascular Density. Two regions considered: Str Far-far from the tumoral glandular cells and Str Tum-close to the tumoral cells.*

High numbers of macrophages are associated with metastatic potential

Survival curves were created to evaluate the impact of the number of CD68 positive cells. Higher levels of macrophages in the areas far from the tumour are associated with poor prognosis in terms of MFS (Figure 34-A), although the same tendency is not observed for the tumoral areas, where the differences between the two groups are not statistically significant (p=0.8344 (Figure 34-B)). Patients' outcomes seem to be affected by the number of macrophages identified in the TME, and higher numbers seem to entail poor prognosis, although not statistically significant (Figure 34-C and D).

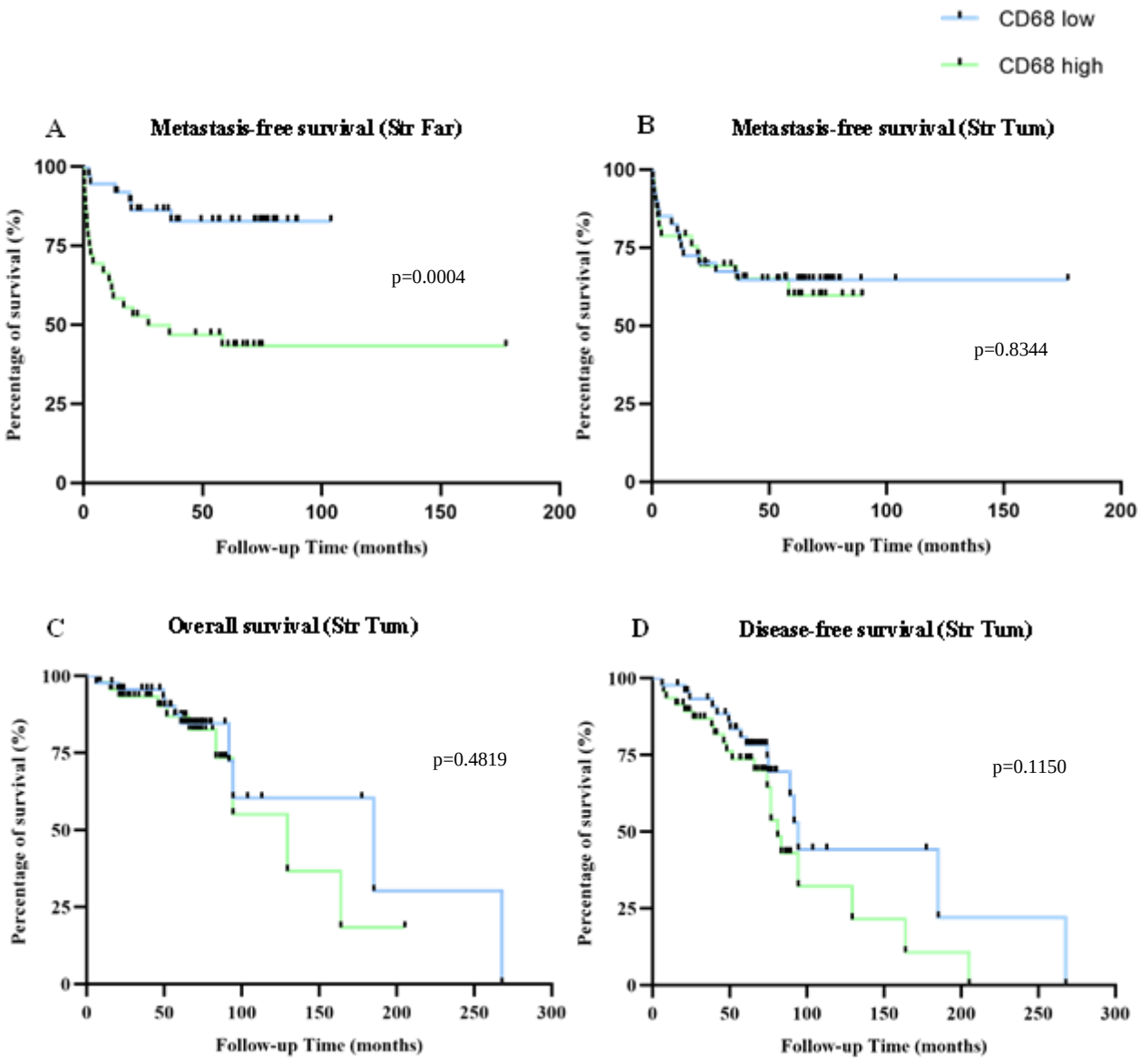

Figure 34: Correlation of CD68 expression with clinico-pathological data. *MFS (A, B), OS (C) and DFS (D) according to CD68 positive cells. Two regions considered: Str Far-far from the tumoral glandular cells and Str Tum-close to the tumoral cells.*

Prognostic Value of the Biomarkers studied

The investigation of these intratumoral-reactive stromal cells in PCa permitted to assess their predictive value on survival of patients and if the biomarkers studied have a relevant prognostic role in stratifying patients, distinguishing aggressive phenotypes from indolent ones.

The survival curves obtained revealed that ASPA may be a marker of poor prognosis in PCa patients, once there is a clear and evident difference in the patients whose expression of ASPA is lower comparing with the patients whose expression is not downregulated. Little is known about the influence of this metabolic microenvironment created by the lower levels of ASPA. Still, it influences the outcome of the patients. At this point it was important to determine if the expression of ASPA influences the clinical outcome in a dependent manner of Gleason Score and iPSA, once these patients that have lower levels of the enzyme have higher grade of the disease.

On its turn, Desmin expression was also associated with a poorer outcome. Other investigations have also suggested that a fundamental alteration in stromal cell biology is associated with PCa progression and that this reactive stroma is likely to regulate the rate of tumour progression and ultimately determine patient outcome [46]. Reduced Desmin has been identified previously as a hallmark of cancer-associated reactive stroma and quantitative analysis showed both to be significant and independent predictor of recurrence-free survival in a study performed by Ayala and colleagues [46]. It stands to reason that markers of stromal biology may be suitable diagnostic and prognostic markers in the assessment of clinical PCa.

Statistical analysis of the survival data set concerning CD31 expression showed that this marker is not a relevant prognostic biomarker, although there is an increase in vascular density with tumour progression. This is also in accordance with the study from Miyata and colleagues, where it was recognised the importance of microvasculature in tumour development and progression, yet CD31 has no pathological significance or prognostic role *per si* [83]. The importance of vascular density is well recognised, still it is a challenge to find appropriate biomarkers that can reflect prognostic outcome and correlate with poor-prognosis features of the disease.

It has been previously reported that highly invasive PCa exhibited an increased CD68 positive cells when compared with benign prostatic hyperplasia. In the same cohort, increased density and cell profile area of CD68+ TAMs were recognized as predictors of shorter cancer-specific survival [84]. Our data indicates that higher numbers of positive CD68 cells in Str Far correlates with poor outcome of patients. Nevertheless, in the areas close to the tumoral nests it was not possible to establish such a significant difference. Such results may reflect the heterogeneous distribution of TAMs in the tissue samples and highlights the importance of the compartment specific macrophages in prostate tumorigenesis. Not only total macrophage amount but also specific macrophage subtypes were found to be correlated with clinical and pathological characteristics

of PCa patients [85]. Due to this fact, it is of high importance to determine the subtypes of macrophages present in the regions analysed, to verify a possible stratification pattern of the patients.

Combinatory Analysis of the Biomarkers and its impact on Metastasis-free survival

A combinatory analysis of the biomarkers studied was performed to understand the possible combined influence of these molecular signatures in patient's outcome. Patients were divided in four groups and the analysis was completed using the information from the areas far from the tumoral cells and from the stroma within the tumour. Generally, we confirmed the results observed previously, supporting the general evidence that there is a cumulative effect of what is observed in the single analysis. As expected, the group with the shortest MFS corresponds to the ASPA low/CD31 high tumours.

Particularly, patients with low ASPA and high levels of vascular density are more prone to experience poor outcome, developing more frequently metastatic disease (Figure 35). Comparing the two different compartments evaluated, it is possible to denotate a similar behaviour of the four groups, both statistically significant (p-value of 0.0001 in Str Far and p-value of 0.0011 in Str Tum, respectively) (Figure 35-A and B).

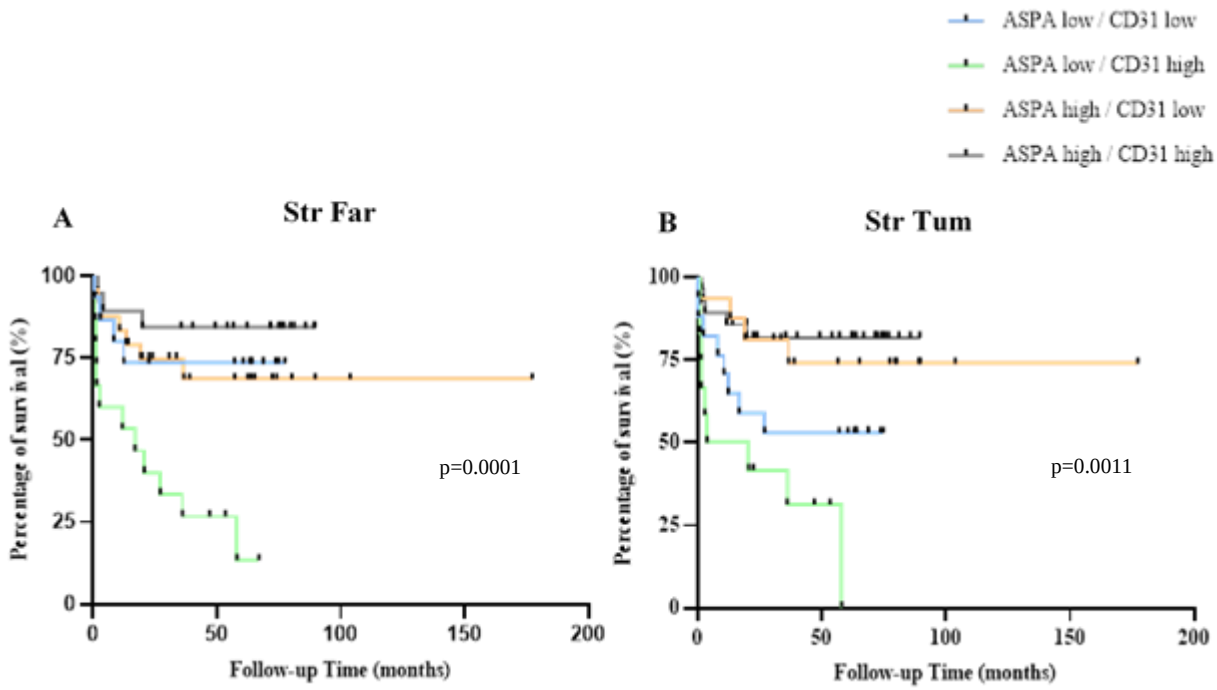

Figure 35: MFS in Str Far (A) and in Str Tum (B) according to ASPA and CD31 expression profile.

Considering the analysis performed with ASPA and the number of CD68 positive cells, patients with low levels of ASPA and higher numbers of macrophages in the stroma have more tendency to develop metastasis. Remarkably, this tendency is more evident in the analysis performed in the areas close to the tumour cells (Figure 36-A and B), highlighting the crucial role of macrophages in the tumoral niche as well as the possible downregulation of ASPA in this scenario. Again, the results obtained confirmed that ASPA is a biomarker of poor clinical outcome and that higher levels of macrophages are in association with disease aggressiveness.

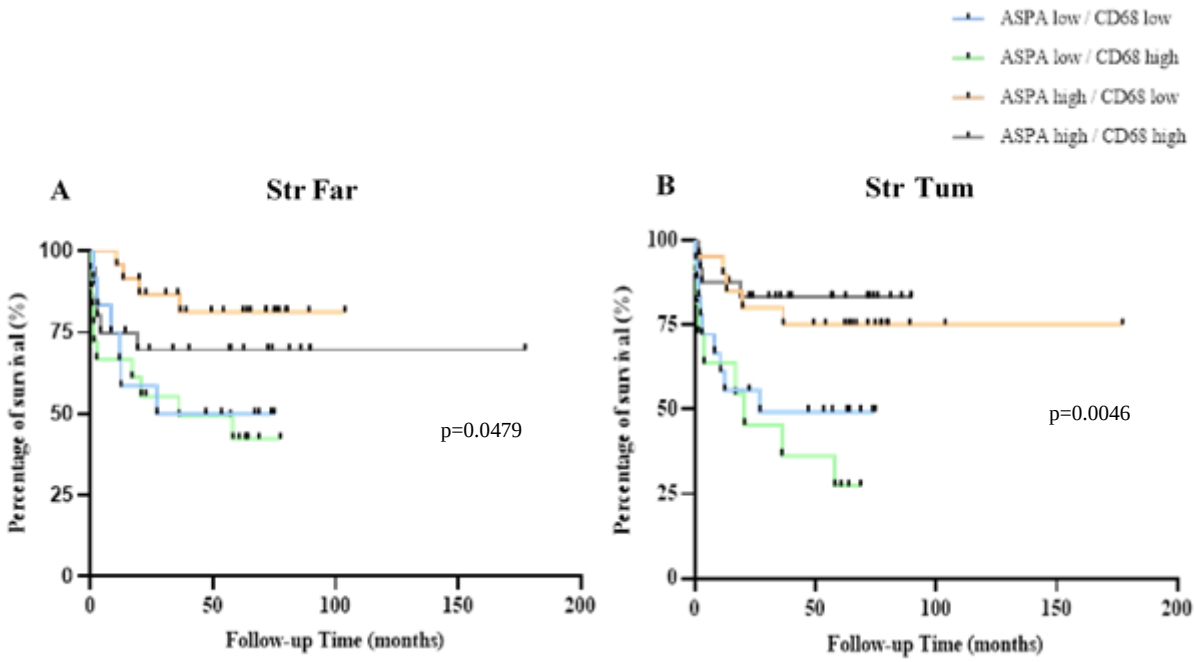

Figure 36: MFS in Str Far (A) and in Str Tum (B) according to ASPA and CD68 expression profile.

The results of the combined analysis between ASPA and Desmin confirmed that in PCa TME when ASPA expression levels are low, the population of fibroblasts is also reduced (Figure 37). Interestingly, these patterns of expression are in association and determine a poor clinical outcome of the patients in what concerns MFS. Both in Str Far and in Str Tum we observe a higher tendency to develop metastasis in individuals with low levels of ASPA and low levels of Desmin (Figure 37-A and B).

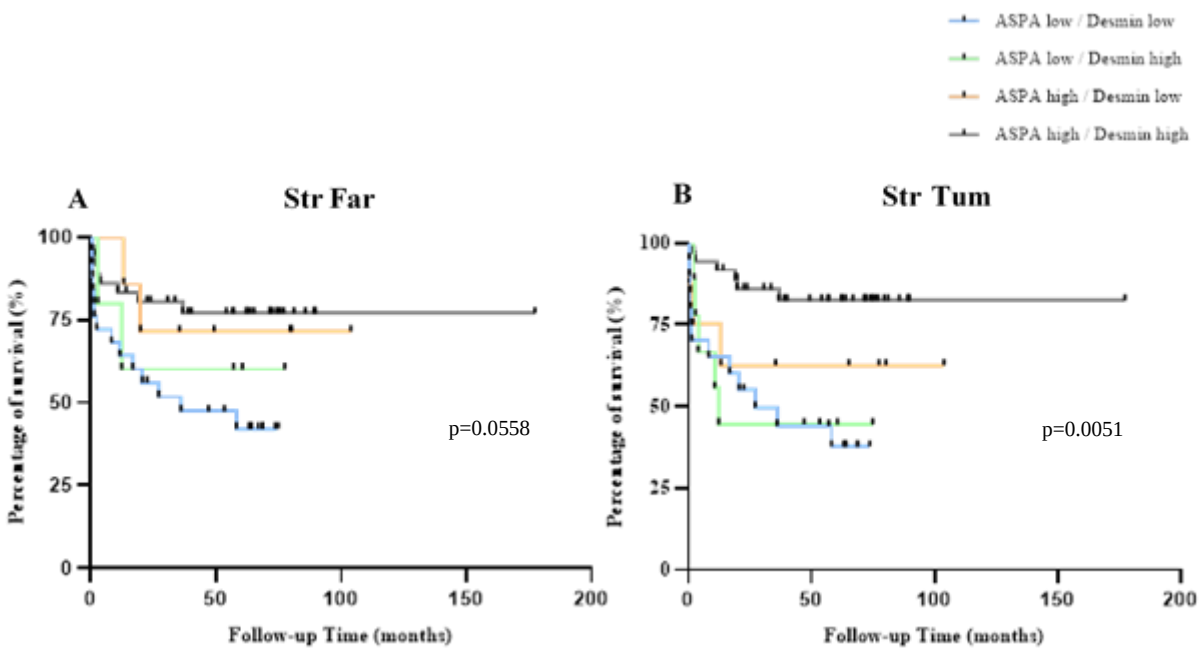

Figure 37: MFS in Str Far (A) and in Str Tum (B) according to ASPA and Desmin expression profile.

All in all, the analysis conducted allowed to understand that when joining the expression patterns of the molecular markers a cumulative effect is observed.

Aiming to determine the strength of the link between the quantitative and qualitative variables analysed a Spearman rank correlation was conducted. This nonparametric analysis permitted to observe the positive or negative correlation between the pairs of variables. Table 15 summarizes the results obtained for the correlation between the values of the biomarkers expression in Str Far and the values of iPSA, Gleason Scores, development of metastasis and Overall Survival. In table 16 it is summarized the values for Str Tum.

The value of Spearman coefficient ranges from -1 to 1: negative to positive correlation, respectively. It was found that there is a positive correlation between ASPA and Desmin, as well as with ASPA and CD68, both in Str Far and Str Tum. In the Str Far, the number of CD68 positive cells positively correlates with iPSA and with Gleason Score (r=0.1956 and r=0.0186, respectively), meaning that there was a pattern where whenever the iPSA level was low, the percentage of CD68 positive cells is also low. Furthermore, the levels of PSA correlate positively with the Gleason Groups, as expected. This means that higher levels of PSA are detected in higher Gleason Groups.

Most importantly, this analysis enabled the confirmation that ASPA expression is independently determinant for metastasis development and overall survival, not depending on initial levels of PSA or on the Gleason Scores. The same is verified for Desmin and CD68. This highly strengths our hypothesis of ASPA being a marker of poor clinical outcome.

Table 15: Spearman rank correlation using qualitative (iPSA, Gleason Score, Metastasis and Overall Survival) and quantitative variables (ASPA, Desmin and CD68) in the Str Far. Spearman correlation rank coefficient (rho, r) and p-value are presented.

Str Far	ASPA	Desmin	CD68	iPSA	Gleason Score	Metastasis	Overall Survival
ASPA							
r	1	0.6238	-0.0027	-0.4237	-0.7528	-0.2893	-0.2778
p-value		**$1.8x10^{-10}$**	0.9804	**0.0002**	**$4.9x10^{-17}$**	**0.0073**	**0.0162**
Desmin							
r		1	0.0561	-0.3864	-0.4941	-0.2316	-0.2342
p-value			0.6098	**0.0007**	**$1.5x10^{-6}$**	**0.0337**	**0.0432**
CD68							
r			1	0.1956	0.0186	0.1295	0.0419
p-value				0.0949	0.8656	0.2376	0.7274
iPSA							
r				1	0.5208	0.4005	0.2913
p-value					**$1.9x10^{-6}$**	**0.0004**	**0.0137**
Gleason Score							
r					1	0.3436	0.4035
p-value						**0.0013**	**0.0003**
Metastasis							
r						1	0.3034
p-value							**0.0082**
Overall Survival							
r							1
p-value							

Table 16: Spearman rank correlation using qualitative (iPSA, Gleason Score, Metastasis and Overall Survival) and quantitative variables (ASPA, Desmin and CD68) in the Str Tum. Spearman correlation rank coefficient (rho, r) and p-value are presented.

Str Tum	ASPA	Desmin	CD68	iPSA	Gleason Score	Metastasis	Overall Survival
ASPA							
r	1	0.5547	0.1658	-0.3992	-0.7586	-0.3145	-0.2646
p-value		**3.6x10-8**	0.1294	**0.0004**	**2.1x10-17**	**0.0034**	**0.0218**
Desmin							
r		1	0.2550	-0.4120	-0.4030	-0.2498	-0.2690
p-value			**0.0185**	**0.0003**	**0.0001**	**0.0211**	**0.0196**
CD68							
r			1	-0.1057	-0.1425	-0.0450	-0.1036
p-value				0.3699	0.1933	0.6825	0.3765
iPSA							
r				1	0.5208	**0**.4005	0.2913
p-value					**1.9x10^{-6}**	**0.0004**	**0.0137**
Gleason Score							
r					1	0.3426	0.4025
p-value						**0.0013**	**0.0003**
Metastasis							
r						1	0.3034
p-value							**0.0082**
Overall Survival							
r							1
p-value							

Challenges associated with mPlex IF and Correlation Data

mPlex IF was extensively used in this project to immunophenotypically characterize PCa microenvironment. Although, this is a powerful tool, giving high contrast, high specificity and allowing a quantitative analysis, there are some weaknesses associated. Protocol optimization was critical for reducing autofluorescence in the tissue, permitting a good staining, when analysing the molecular markers of interest. Moreover, different tissues analysed implied adjustments in the spectral library built at the optimization process.

Besides, during the process of image analysis, finding an appropriate and capable software that allows the use of all the molecular data that the mPlex images hold was a challenge and resulted in a deep search for a software that could perform the analysis needed, as well as protocol design adapted to the aims of the study.

It is important to highlight that we lacked clinico-pathological data from some patients (some of the patients were lost of follow-up for different reasons). This makes it harder to compare and establish a correlation between all the molecular data obtained from the stainings and the clinical information. We believe that a bigger cohort could help to draw more conclusions, strengthening the observed results.

Of note, sparse literature in this field made it difficult to comparatively evaluate the results obtained.

Conclusion and Future Perspectives

Currently, choice of treatment for localized PCa is based on clinical parameters (stage, grade, and PSA level) that lack complete prognostic accuracy, leading to overtreatment of indolent PCa and undertreatment of aggressive PCa. Thus, novel biomarkers are needed to improve risk stratification, guide more personalized treatment decisions and above all distinguish indolent from aggressive PCa.

With mPlex IF, individual cell phenotypes, as well as different cell subpopulations and even rare cell populations, can be identified with extraordinary fidelity according to the expression of antibodies in an mPlex IF panel. This technology therefore has an important role in translational oncology studies. Additionally, the expression of different biomarkers of interest can be examined at the tissue or individual cell level, providing information about cell phenotypes, distribution of cells, and cell biological processes in tumour samples [73]. In the present study we explored if immunoexpression assessment assisted by digital imaging analysis, might provide prognostically relevant information for PCa patients. The results observed suggest that might be a prognostic potential of the multi-layered panel of the biomarkers explored. We also thought and believe that metabolic alterations, namely ASPA expression, are linked to PCa development and progression to a more aggressive phenotype.

Our study demonstrated the potential of ASPA and Desmin as prognostic indicators, adding to the concept that tumours are not purely epithelial, and the tumour-reactive stroma must be considered an important biological component of the cancer. Population of macrophages are also very important in PCa. The data collected and analysed confirmed the relevance to assess the subpopulation of TAM's, namely M1 and M2, in the TME and assess their infiltration status both in tumour nests and in the surrounding areas.

A step forward is the validation of these markers to a different cohort from another institution and verify the patterns of expression and the correlation with clinical data. Of great importance is the establishment of a second mPlex analysis including the populations of macrophages to assess how this metabolic microenvironment created by the downregulation off ASPA influences the polarization of the TAM's and the pattern of infiltration.

Although functional conclusions cannot be drawn based on the present study design, we may assume that we open a path to further studies on the correlation between ASPA expression and PCa microenvironment cell populations

The identification of patients at risk of metastasis, the detection of early metastatic seeding, and the implementation of clinical guidelines to subject these patients to therapies is a promising way to better diagnose and treat PCa patients.

References

1. Sung, H. *et al.* Global Cancer Statistics 2020 : GLOBOCAN Estimates of Incidence and Mortality Worldwide for 36 Cancers in 185 Countries. **71**, 209–249 (2021).
2. Shen, M. & Abate-Shen, C. Molecular genetics of prostate cancer: new prospects for old challenges. *Genes Dev.* **24**, 1967–2000 (2010).
3. Siegel, R. L., Miller, K. D., Fuchs, H. E. & Jemal, A. Cancer Statistics, 2021. *CA. Cancer J. Clin.* **71**, 7–33 (2021).
4. Martin, N. E., Mucci, L. A., Loda, M. & DePinho, R. A. Prognostic determinants in prostate cancer. *Cancer J.* **17**, 429–437 (2011).
5. Patel, S. A. & Vanharanta, S. Epigenetic determinants of metastasis. *Mol. Oncol.* **11**, 79–96 (2016).
6. Linxweiler, J. *et al.* Cancer - associated fibroblasts stimulate primary tumor growth and metastatic spread in an orthotopic prostate cancer xenograft model. *Sci. Rep.* **10**, 1–13 (2020).
7. Packer, J. R. & Maitland, N. J. The molecular and cellular origin of human prostate cancer. *Biochim. Biophys. Acta - Mol. Cell Res.* **1863**, 1238–1260 (2016).
8. Wang, G., Zhao, D., Spring, D. J. & Depinho, R. A. Genetics and biology of prostate cancer. *Genes Dev.* **32**, 1105–1140 (2018).
9. Demarzo, A. M., Nelson, W. G., Isaacs, W. B. & Epstein, J. I. Prostate cancer II Pathological and molecular aspects of prostate cancer. **361**, 955–964 (2003).
10. Robinson, D. *et al.* Integrative Clinical Genomics of Advanced Prostate Resource Integrative Clinical Genomics of Advanced Prostate Cancer. *Cell* **161**, 1215–1228 (2015).
11. Loblaw, D. A. *et al.* Initial hormonal management of Androgen-sensitive metastatic, recurrent, or progressive prostate cancer: 2006 Update of an American society of clinical oncology practice guideline. *J. Clin. Oncol.* **25**, 1596–1605 (2007).
12. Arora, K. & Barbieri, C. E. Molecular Subtypes of Prostate Cancer. *Curr. Oncol. Rep.* **20**, (2018).
13. Perdomo, H. A. G., Zapata-copete, J. A. & Sanchez, A. Molecular alterations associated with prostate cancer. *Cent. Eur. J. Urol.* **71**, 168–176 (2018).
14. Robinson, D. Integrative clinical genomics of advanced prostate cancer. *Cell* **161**, 1215–1228 (2015).
15. Daniel E. Spratt, Zachary S. Zumsteg, Felix Y. Feng, and S. A. T. Translational and clinical implications of the genetic landscape of prostate cancer. *Nat Rev Clin Oncol.* **13**, 597–610 (2016).
16. Chan, J. M., Gann, P. H. & Giovannucci, E. L. Role of Diet in Prostate Cancer Development and Progression. **23**, (2005).
17. Giovannucci, E. *et al.* A Prospective Study of Dietary Fat and. **85**, 1571–1579 (1993).
18. Rawla, P. Epidemiology of Prostate Cancer. *World J Oncol.* **10**, 63–89 (2019).
19. J. Ferlay 1, M. Colombet1, I. Soerjomataram1, C. Mathers3, D.M. Parkin 2, M. Piñeros1, A. Z. 1 and F. B. Estimating the global cancer incidence and mortality in 2018 : GLOBOCAN sources and methods. *Int. J. Cancer* 1941–1953 (2019) doi:10.1002/ijc.31937.

20. Bavik, C. *et al.* The Gene Expression Program of Prostate Fibroblast Senescence Modulates Neoplastic Epithelial Cell Proliferation through Paracrine Mechanisms. 794–803 (2006) doi:10.1158/0008-5472.CAN-05-1716.

21. Begley, L., Monteleon, C., Shah, R. B., Macdonald, J. W. & Macoska, J. A. CXCL12 overexpression and secretion by aging fibroblasts enhance human prostate epithelial proliferation in vitro. 291–298 (2005) doi:10.1111/j.1474-9726.2005.00173.x.

22. Carlise R. Bethel, Jaideep Chaudhary, Matthew D. Anway, and T. R. B. Gene Expression Changes are Age-Dependent and Lobe-Specific in the Brown Norway Rat Model of Prostatic Hyperplasia. **69**, 838–850 (2009).

23. Merriel, S. W. D., Funston, G. & Hamilton, W. Prostate Cancer in Primary Care. *Adv. Ther.* **35**, 1285–1294 (2018).

24. Epstein, J. I. *et al.* The 2014 international society of urological pathology (ISUP) consensus conference on gleason grading of prostatic carcinoma definition of grading patterns and proposal for a new grading system. *Am. J. Surg. Pathol.* **40**, 244–252 (2016).

25. Taneja, S. S. Imaging in the diagnosis and management of prostate cancer. *Rev. Urol.* **6**, 101–13 (2004).

26. Pierorazio, P. M., Walsh, P. C., Partin, A. W. & Epstein, J. I. Prognostic Gleason grade grouping: Data based on the modified Gleason scoring system. *BJU Int.* **111**, 753–760 (2013).

27. Mellinger, G. T., Gleason, D. & Bailar, J. The histology and prognosis of prostatic cancer. *J. Urol.* **97**, 331–337 (1967).

28. Epstein, J. I. An Update of the Gleason Grading System. *J. Urol.* **183**, 433–440 (2010).

29. Gleason, D. F., Mellinger, G. T. & Ardving, L. J. Prediction of prognosis for prostatic adenocarcinoma by combined histological grading and clinical staging. *J. Urol.* **111**, 58–64 (1974).

30. Buyyounouski, M. K. *et al.* Prostate cancer - major changes in the American Joint Committee on Cancer eighth edition cancer staging manual. *CA. Cancer J. Clin.* **67**, 245–253 (2017).

31. Ohori, M., Wheeler, T. M. & Scardino, P. T. The new american joint committee on cancer and international union against cancer tnm classification of prostate cancer. *Cancer* **74**, 104–114 (1994).

32. Gabriele, D. *et al.* Beyond D'Amico risk classes for predicting recurrence after external beam radiotherapy for prostate cancer: The Candiolo classifier. *Radiat. Oncol.* **11**, 1–10 (2016).

33. Miller, K. D. *et al.* Cancer treatment and survivorship statistics, 2016. *CA. Cancer J. Clin.* **66**, 271–289 (2016).

34. Marques, R. B., Dits, N. F., Erkens-Schulze, S., Weerden, W. M. & Jenster, G. Bypass mechanisms of the androgen receptor pathway in therapy-resistant prostate cancer cell models. *PLoS One* **5**, (2010).

35. Kessel, A., Kohli, M. & Swami, U. Cancer Treatment and Research Communications Current management of metastatic castration-sensitive prostate cancer. *Cancer Treat. Res. Commun.* **28**, 100384 (2021).

36. Litwin, M. S. & Tan, H. J. The diagnosis and treatment of prostate cancer: A review. *JAMA - J. Am. Med. Assoc.* **317**, 2532–2542 (2017).

37. Teo, M. Y., Rathkopf, D. E. & Kantoff, P. Treatment of advanced prostate cancer. *Annu. Rev. Med.* **70**, 479–499 (2019).

38. Hanahan, D. & Weinberg, R. A. Hallmarks of cancer: The next generation. *Cell* **144**, 646–674 (2011).

39. Hanahan, D. & Coussens, L. M. Accessories to the Crime: Functions of Cells Recruited to the Tumor Microenvironment. *Cancer Cell* **21**, 309–322 (2012).

40. Balkwill, F. R., Capasso, M. & Hagemann, T. The tumor microenvironment at a glance. *J. Cell Sci.* **125**, 5591–5596 (2012).

41. Stephen L. Shiao1, Gina Chia-Yi Chu2, and L. W. K. C. Regulation of Prostate Cancer Progression by the Tumor Microenvironment. *Cancer Lett.* **380**, 340–348 (2016).

42. DF Quail and JA Joyce. Microenvironmental regulation of tumor progression and metastasis. *Comput. Sci.* **Doctor**, 1423–1437 (2013).

43. Karlou, M., Tzelepi, V. & Efstathiou, E. Therapeutic targeting of the prostate cancer microenvironment. *Nat. Rev. Urol.* **7**, 494–509 (2010).

44. Junttila, M. R. & De Sauvage, F. J. Influence of tumour micro-environment heterogeneity on therapeutic response. *Nature* **501**, 346–354 (2013).

45. Mikala Egeblad, Elizabeth S. Nakasone, and Z. W. Tumors as organs. **18**, 884–901 (2010).

46. Ayala, G. *et al.* Reactive Stroma as a Predictor of Biochemical-Free Recurrence in Prostate Cancer. *Clin. Cancer Res.* **9**, 4792–4801 (2003).

47. Tuxhorn, J. A., Ayala, G. E. & Rowley, D. R. Reactive stroma in prostate cancer progression. *J. Urol.* **166**, 2472–2483 (2001).

48. Gabbiani, G. The myofibroblast in wound healing and fibrocontractive diseases. *J. Pathol.* **200**, 500–503 (2003).

49. Sahai, E. *et al.* A framework for advancing our understanding of cancer-associated fibroblasts. *Nat. Rev. Cancer* **20**, 174–186 (2020).

50. Hussein, M. R. A., AL-Assiri, M. & Musalam, A. O. Phenotypic characterization of the infiltrating immune cells in normal prostate, benign nodular prostatic hyperplasia and prostatic adenocarcinoma. *Exp. Mol. Pathol.* **86**, 108–113 (2009).

51. Bora Gurel, M. et al. Chronic inflammation in benign prostate tissue is associated with high-grade prostate cancer in the placebo arm of the Prostate Cancer Prevention Trial. *Cancer Epidemiol Biomarkers* **23**, 847–856 (2014).

52. Tsukamoto, H., Komohara, Y. & Oshiumi, H. The role of macrophages in anti-tumor immune responses: pathological significance and potential as therapeutic targets. *Hum. Cell* **34**, 1031–1039 (2021).

53. Komohara, Y., Jinushi, M. & Takeya, M. Clinical significance of macrophage heterogeneity in human malignant tumors. *Cancer Sci.* **105**, 1–8 (2014).

54. Xue, J. *et al.* Transcriptome-Based Network Analysis Reveals a Spectrum Model of Human Macrophage Activation. *Immunity* **40**, 274–288 (2014).

55. Gordon, S. & Martinez, F. O. Alternative activation of macrophages: Mechanism and functions. *Immunity* **32**, 593–604 (2010).

56. Martinez, F. O. & Gordon, S. The M1 and M2 paradigm of macrophage activation: Time for reassessment. *F1000Prime Rep.* **6**, 1–13 (2014).

57. Mantovani, A., Marchesi, F., Malesci, A. & Laghi, L. Tumor-Associated Macrophages as Treatment Targets in Oncology. *Nat Rev Clin Oncol.* **14**, 399–416 (2018).

58. de Groot, A. E. *et al.* Characterization of tumor-associated macrophages in prostate cancer transgenic mouse models. *Prostate* **81**, 629–647 (2021).

59. Bates, M., Kovalenko, B., Wilson, E. L. & Moscatelli, D. Endothelial cells support the growth of prostate tissue in vivo. *Prostate* **68**, 893–901 (2008).

60. Bergers, G. & Benjamin, L. E. Tumorigenesis and the angiogenic switch. *Nat. Rev. Cancer* **3**, 401–410 (2003).

61. Zhao, R. *et al.* Endothelial cells promote metastasis of prostate cancer by enhancing autophagy. *J. Exp. Clin. Cancer Res.* **37**, 1–12 (2018).

62. Oshi, M. *et al.* Angiogenesis is associated with an attenuated tumor microenvironment, aggressive biology, and worse survival in gastric cancer patients. *Am. J. Cancer Res.* **11**, 1659–1671 (2021).

63. Filella, X., Fernández-Galan, E., Bonifacio, R. F. & Foj, L. Emerging biomarkers in the diagnosis of prostate cancer. *Pharmgenomics. Pers. Med.* **11**, 83–94 (2018).

64. Bahmad, H. F. *et al.* Tumor Microenvironment in Prostate Cancer: Toward Identification of Novel Molecular Biomarkers for Diagnosis, Prognosis, and Therapy Development. *Front. Genet.* **12**, (2021).

65. Bejarano, L., Jordão, M. J. C. & Joyce, J. A. Therapeutic targeting of the tumor microenvironment. *Cancer Discov.* **11**, 933–959 (2021).

66. Yoshida, G. J. Metabolic reprogramming: The emerging concept and associated therapeutic strategies. *J. Exp. Clin. Cancer Res.* **34**, 1–10 (2015).

67. Martín-Martín, N., Carracedo, A. & Torrano, V. Metabolism and transcription in cancer: Merging two classic tales. *Front. Cell Dev. Biol.* **5**, 1–8 (2018).

68. Sommer, A. & Sass, J. O. Expression of aspartoacylase (ASPA) and Canavan disease. *Gene* **505**, 206–210 (2012).

69. Bogner-Strauss, J. G. N-acetylaspartate metabolism outside the brain: Lipogenesis, histone acetylation, and cancer. *Front. Endocrinol. (Lausanne).* **8**, 1–5 (2017).

70. Kheirkhah, S. *et al.* Monitoring prostate cancer (PCa) with appraise the gene expression of PRUNE2, NCAPD3 and ASPA and their connection with age, family history and tumor stage. *Gene Reports* **21**, 1008–1040 (2020).

71. Mansfield, J. R. Multispectral Imaging: A Review of Its Technical Aspects and Applications in Anatomic Pathology. *Vet. Pathol.* **51**, 185–210 (2014).

72. Chang, W. *et al.* Overview of multiplex immunohistochemistry / immunofluorescence techniques in the era of cancer immunotherapy. *Cancer Commun.* **40**, 135–153 (2020).

73. Parra, E. R. *et al.* Immuno-profiling and cellular spatial analysis using five immune oncology multiplex immunofluorescence panels for paraffin tumor tissue. *Sci. Rep.* **11**, 1–15 (2021).

74. Baker, J. K. and J. Multiplex Immunohistochemistry for Mapping the Tumor Microenvironment. *Signal Transduct. Immunohistochem.* **1554**, 127–141 (2017).

75. Gevaert, T. The potential of tumour microenvironment markers to stratify the risk of recurrence in prostate cancer patients. *PLoS One* **15**, 1–15 (2020).

76. Mccrea, E. M., Lee, D. K., Sissung, T. M. & Figg, W. D. Precision medicine applications

in prostate cancer. *Ther. Adv. Med. Oncol.* **10**, 1–13 (2018).

77. Levenson, R. M., Lynch, D. T., Kobayashi, H., Backer, J. M. & Backer, M. V. Multiplexing with Multispectral Imaging: From Mice to Microscopy. (2008).

78. Farkas, D. L. *et al.* Non-invasive image acquisition and advanced processing in optical bioimaging. **11**, (1998).

79. Sun, C., Gu, Y., Chen, G. & Du, Y. Bioinformatics Analysis of Stromal Molecular Signatures Associated with Breast and Prostate Cancer. *J. Comput. Biol.* **26**, 1130–1139 (2019).

80. Gandellini, P. *et al.* Complexity in the tumour microenvironment: Cancer associated fibroblast gene expression patterns identify both common and unique features of tumour-stroma crosstalk across cancer types. *Semin. Cancer Biol.* **35**, 96–106 (2015).

81. Taddei, M. L., Giannoni, E., Comito, G. & Chiarugi, P. Microenvironment and tumor cell plasticity: An easy way out. *Cancer Lett.* **341**, 80–96 (2013).

82. S. Bolte, F. P. C. A guided tour into subcellular colocalization analysis in light microscopy. *J. Microsc.* **224**, (2006).

83. Miyata, Y. *et al.* Pathological Significance and prognostic role of microvessel density, evaluated Using CD31, CD34, and CD105 in prostate cancer patients after radical prostatectomy with neoadjuvant therapy. *Prostate* **75**, 84–91 (2015).

84. Lindholm, P. F. *et al.* Role of Monocyte-Lineage Cells in Prostate Cancer Cell Invasion and Tissue Factor Expression. **1682**, 1672–1682 (2010).

85. Larionova, I. *et al.* Tumor-Associated Macrophages in Human Breast , Colorectal , Lung , Ovarian and Prostate Cancers. **10**, 1–34 (2020).

Supplementary Data

ASPA Expression in the different disease groups, according to the different compartments analysed

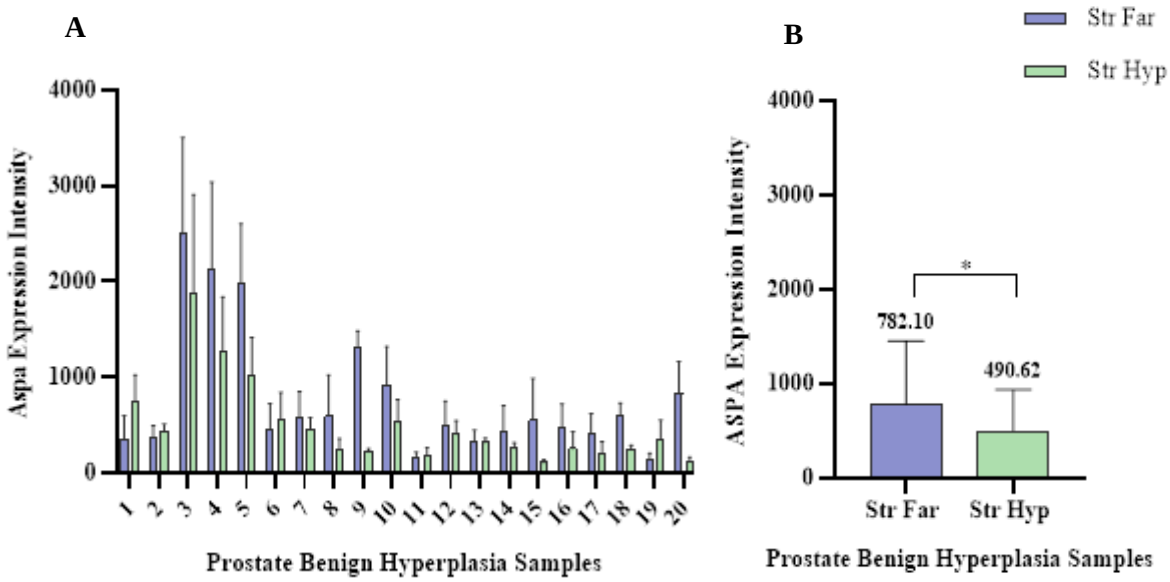

Figure 1: ASPA Expression Intensity in PBH Samples. *(A) Expression Intensity in the 20 samples analysed, in the two compartiments; (B) Expression Intensity in the two types of ROIs analysed.*

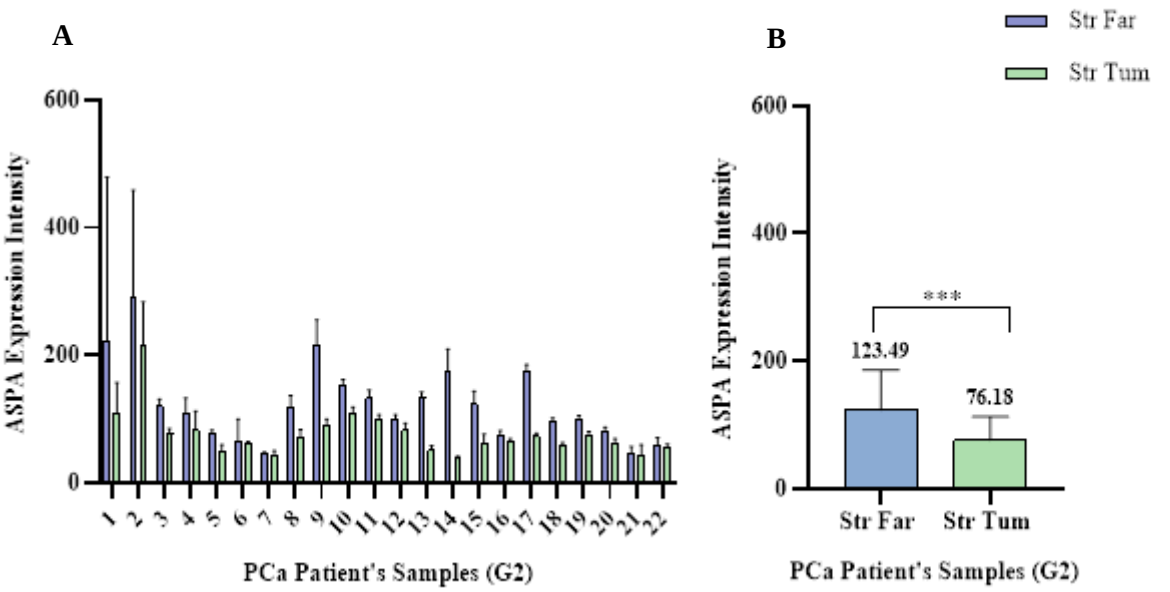

Figure 2: ASPA Expression Intensity in PCa Patient's Samples with Gleason Score 2. *(A) Expression Intensity in the 22 samples analysed, in the two compartiments; (B) Expression Intensity in the two types of ROIs analysed.*

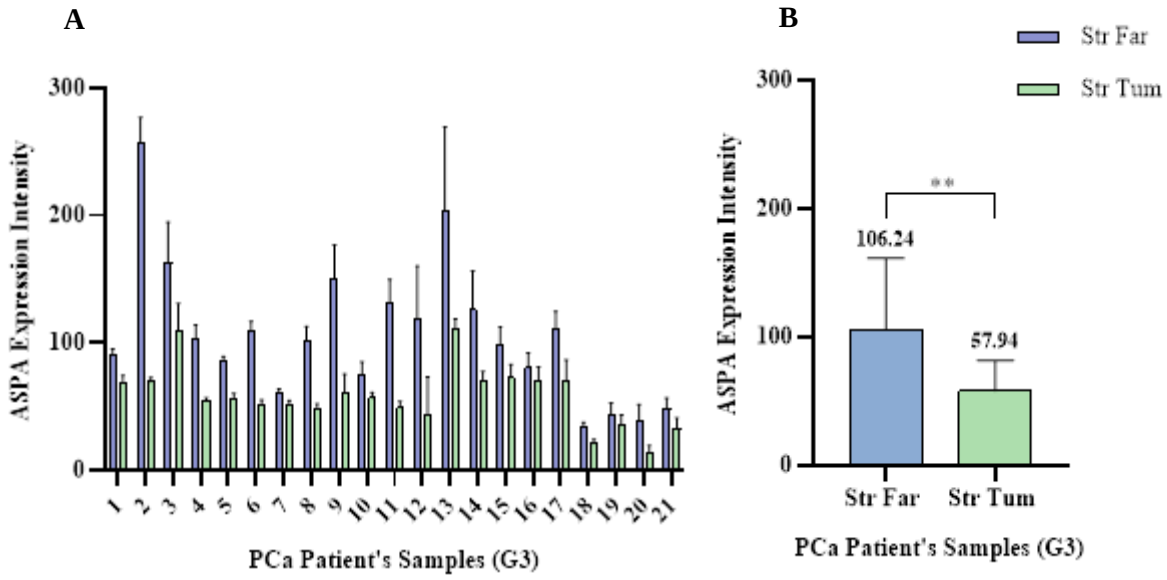

Figure 3: ASPA Expression Intensity in PCa Patient's Samples with Gleason Score 3. *(A) Expression Intensity in the 21 samples analysed, in the two compartiments; (B) Expression Intensity in the two types of ROIs analysed.*

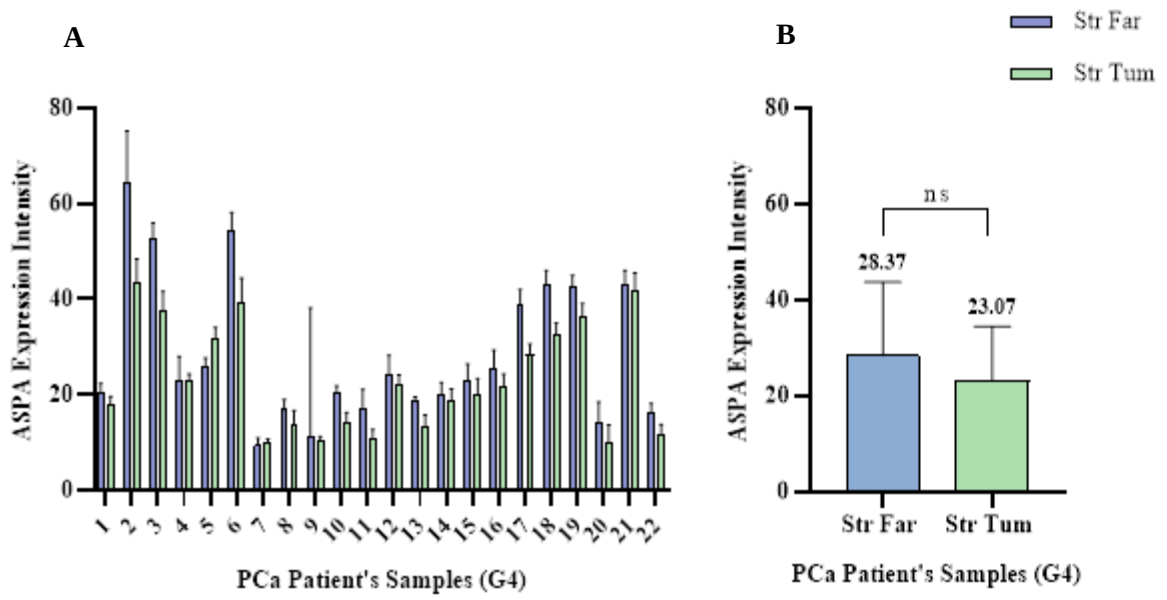

Figure 4: ASPA Expression Intensity in PCa Patient's Samples with Gleason Score 4. *(A) Expression Intensity in the 22 samples analysed, in the two compartiments; (B) Expression Intensity in the two types of ROIs analysed.*

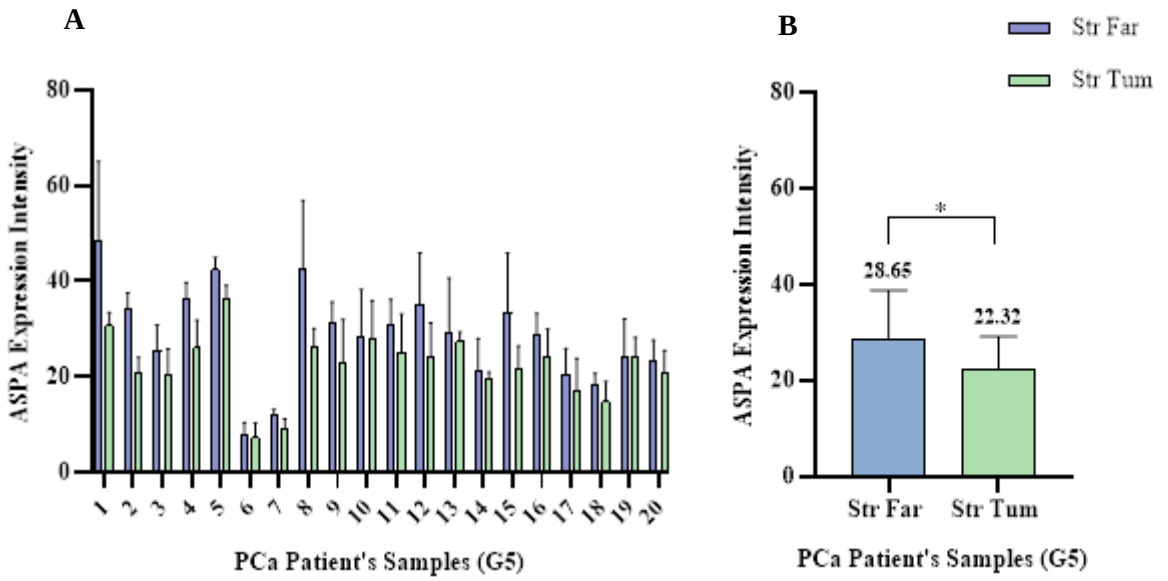

Figure 5: ASPA Expression Intensity in PCa Patient's Samples with Gleason Score 5. *(A) Expression Intensity in the 20 samples analysed, in the two compartiments; (B) Expression Intensity in the two types of ROIs analysed.*

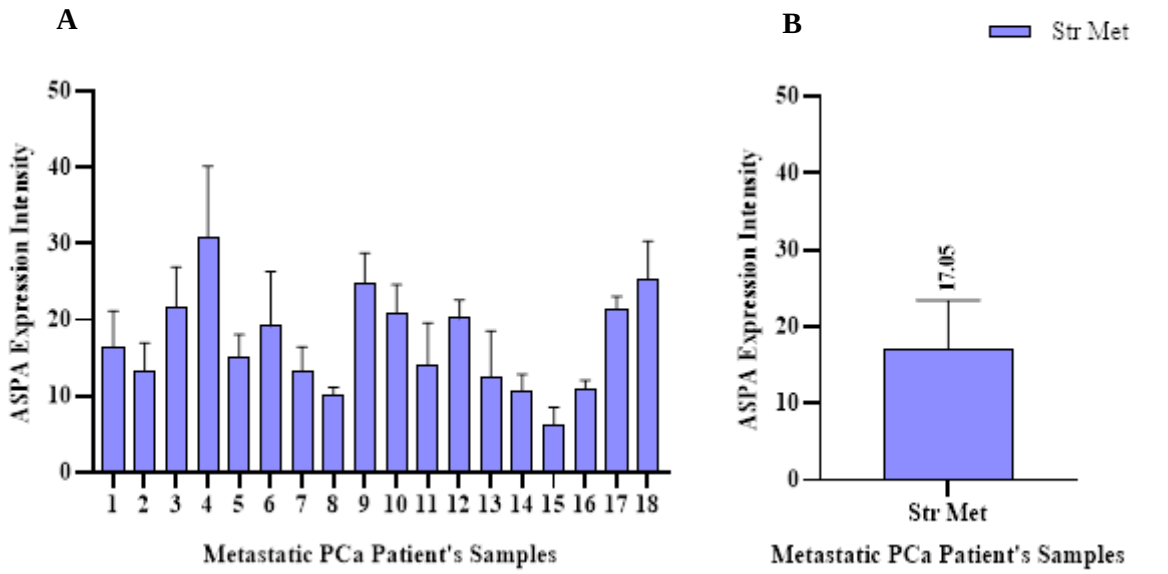

Figure 6: ASPA Expression Intensity in Metastatic PCa atient's Samples. *(A) Expression Intensity in the 18 samples analysed, in the areas close to metastatic cells; (B) Expression Intensity in the Str Met.*

Desmin Expression in the different disease groups, according to the different compartments analysed

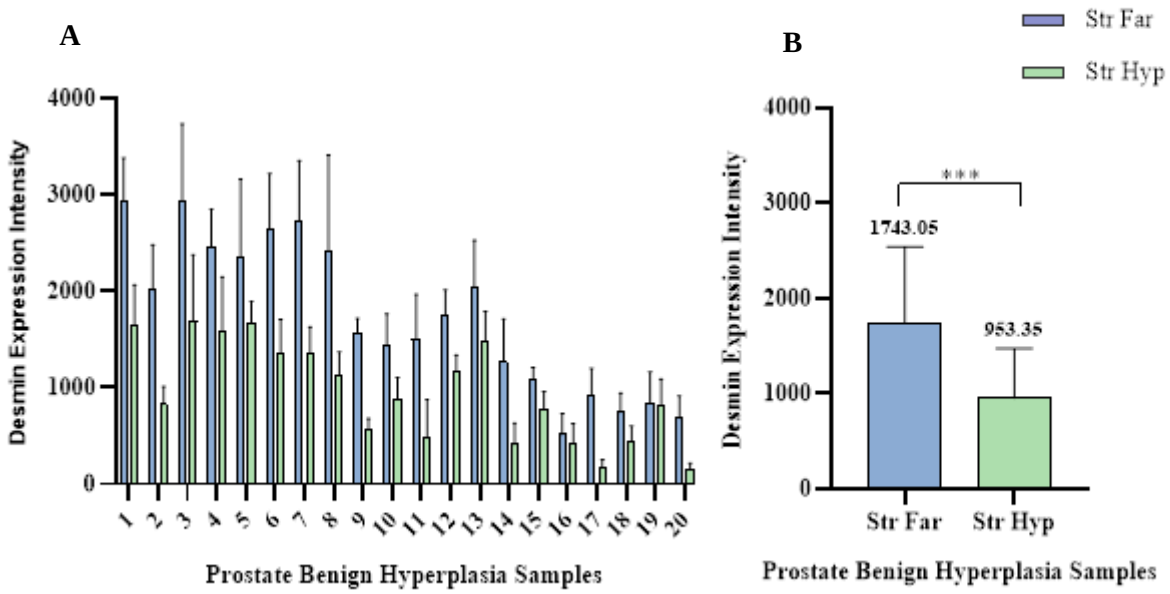

Figure 7: Desmin Expression Intensity in PBH Samples. *(A) Expression Intensity in the 20 samples analysed, in the two compartiments; (B) Expression Intensity in the two types of ROIs analysed.*

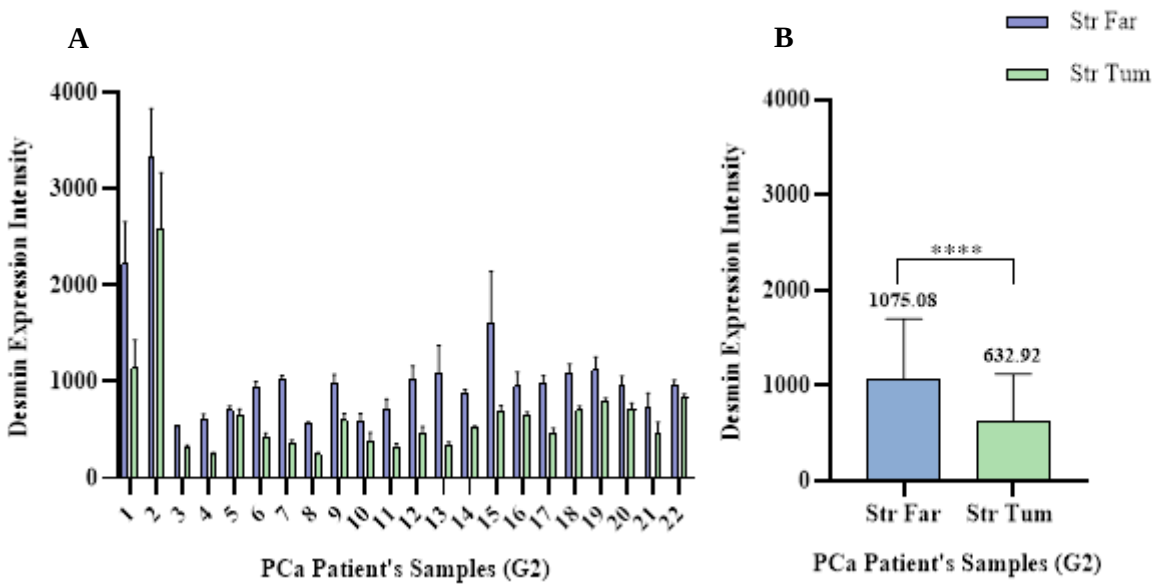

Figure 8: Desmin Expression Intensity in PCa Patient's Samples with Gleason Score 2. *(A) Expression Intensity in the 22 samples analysed, in the two compartiments; (B) Expression Intensity in the two types of ROIs analysed.*

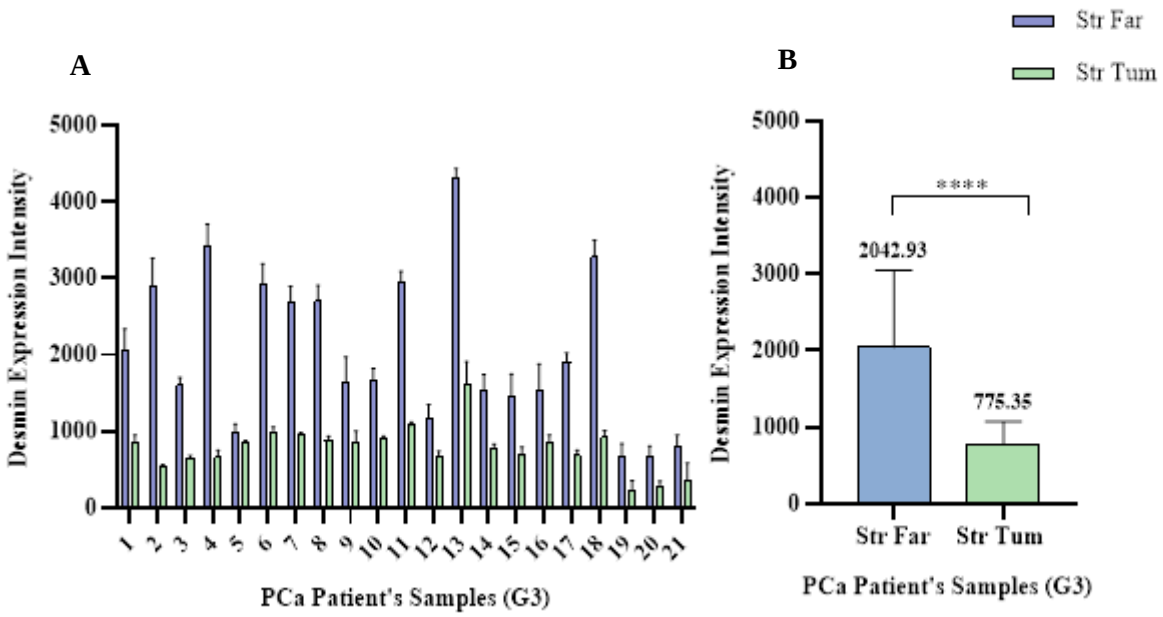

Figure 9: Desmin Expression Intensity in PCa Patient's Samples with Gleason Score 3. *(A) Expression Intensity in the 21 samples analysed, in the two compartiments; (B) Expression Intensity in the two types of ROIs analysed.*

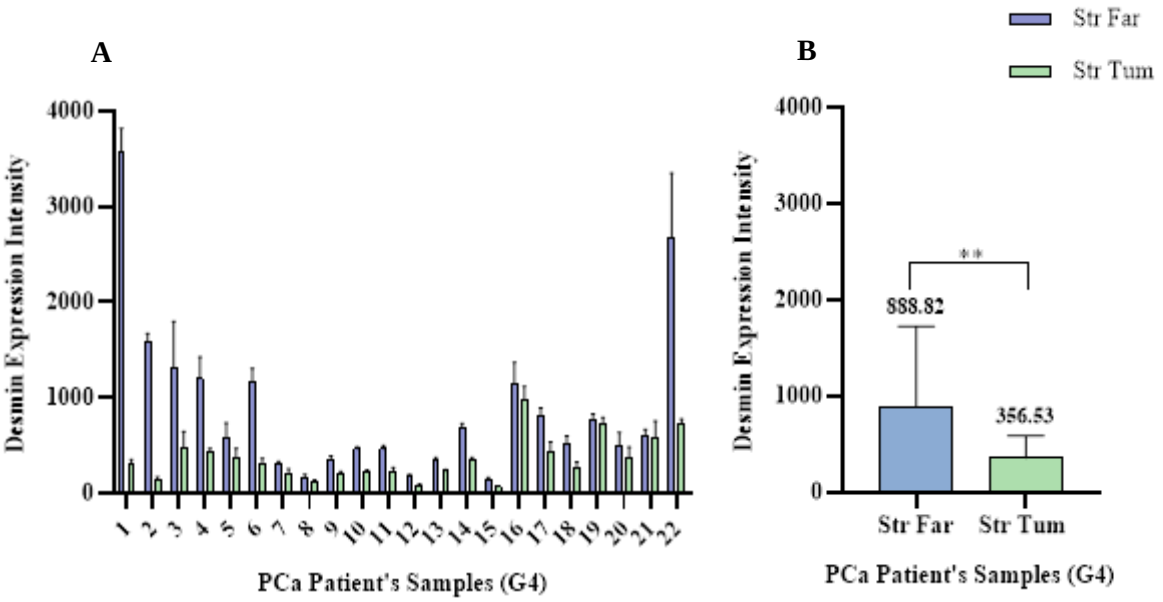

Figure 10: Desmin Expression Intensity in PCa Patient's Samples with Gleason Score 4. *(A) Expression Intensity in the 22 samples analysed, in the two compartiments; (B) Expression Intensity in the two types of ROIs analysed.*

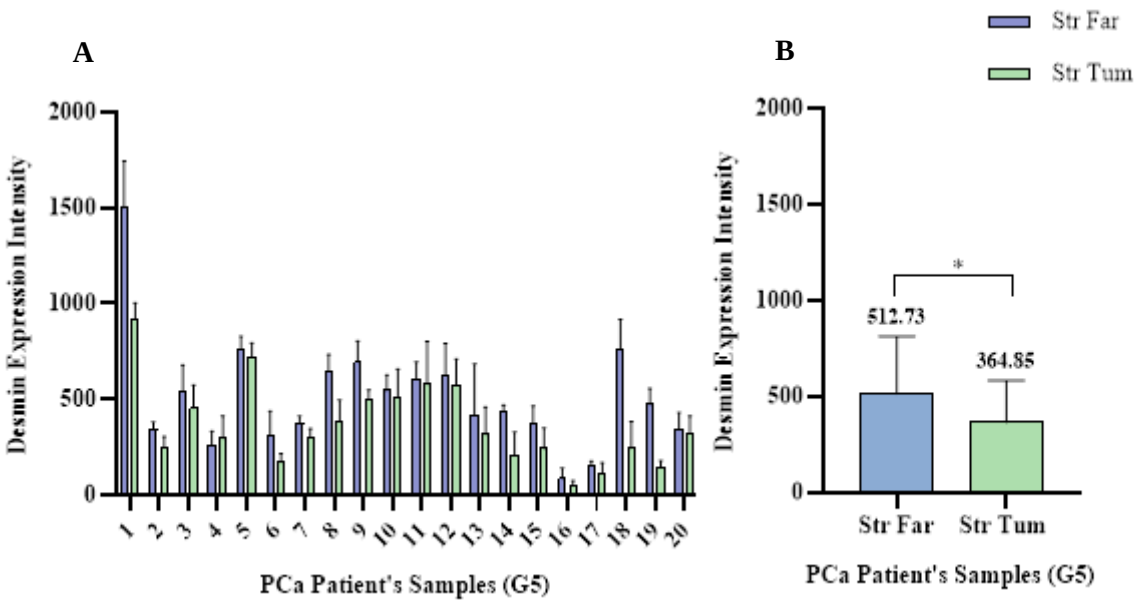

Figure 11: Desmin Expression Intensity in PCa Patient's Samples with Gleason Score 5. *(A) Expression Intensity in the 20 samples analysed, in the two compartiments; (B) Expression Intensity in the two types of ROIs analysed.*

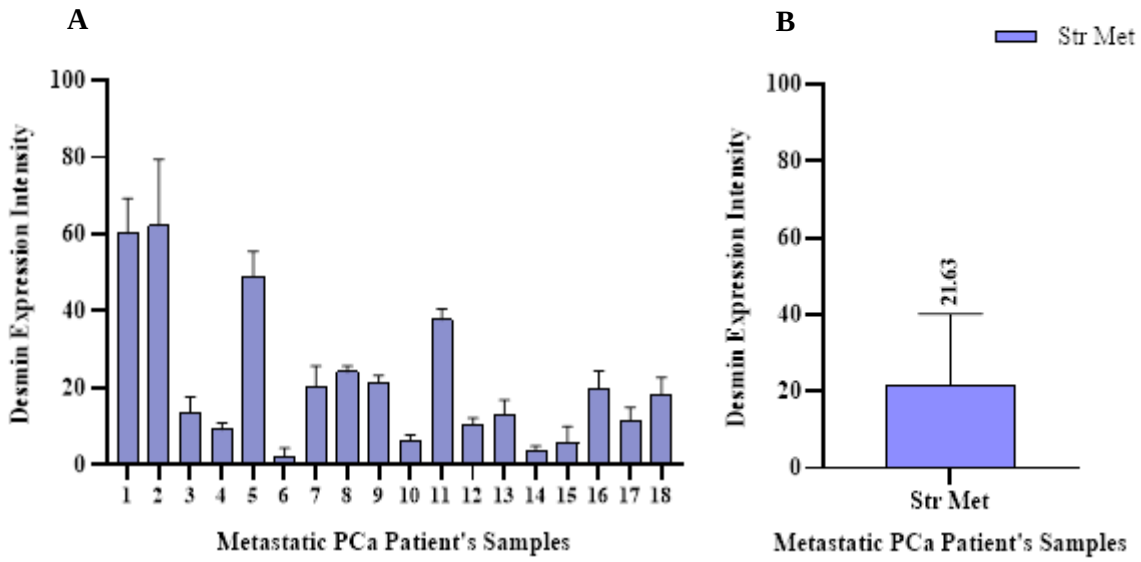

Figure 12: Desmin Expression Intensity in Metastatic PCa Patient's Samples. *(A) Expression Intensity in the 18 samples analysed, in the areas close to metastatic cells; (B) Expression Intensity in the Str Met.*

Co-localization Analysis between ASPA and Desmin in the different disease groups, according to the different compartments analysed

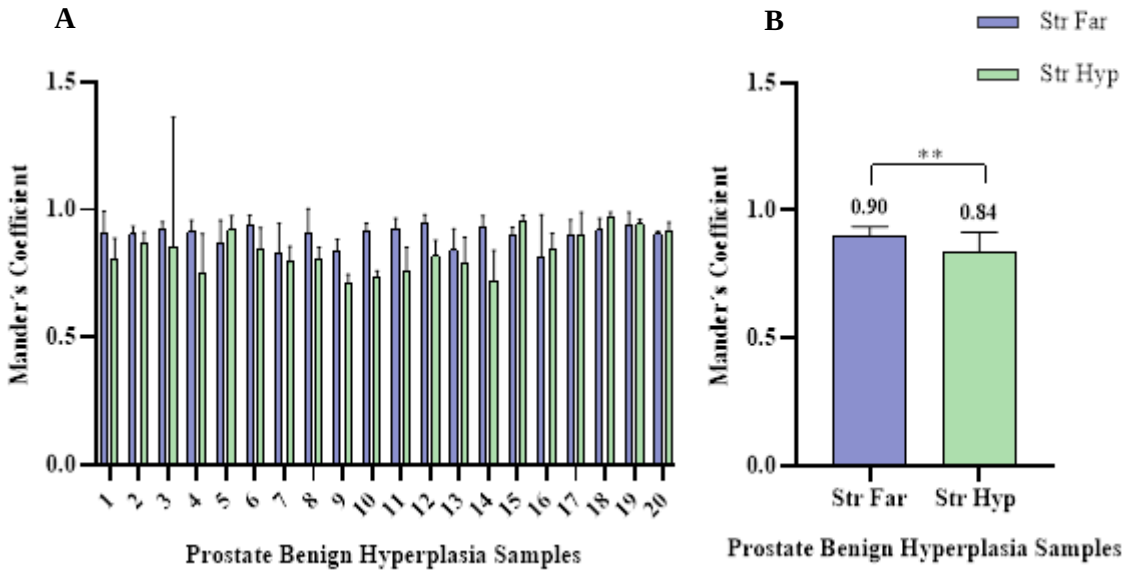

Figure 13: Co-localization Analysis between ASPA and Desmin in PBH. *(A) Manders Coefficient obtained in the 20 samples analysed, in the two compartiments; (B) Manders Coefficient obtained in the two types of ROIs analysed.*

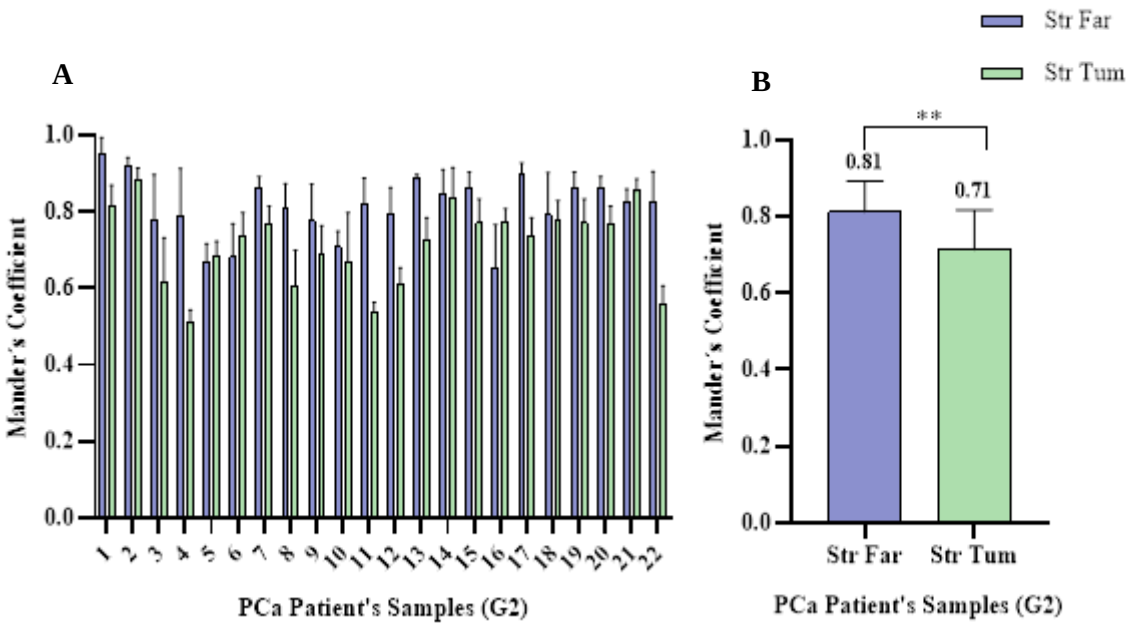

Figure 14: Co-localization Analysis between ASPA and Desmin in PCa Patient's Samples with Gleason Score 2. *(A) Manders Coefficient obtained in the 22 samples analysed, in the two compartiments; (B) Manders Coefficient obtained in the two types of ROIs analysed.*

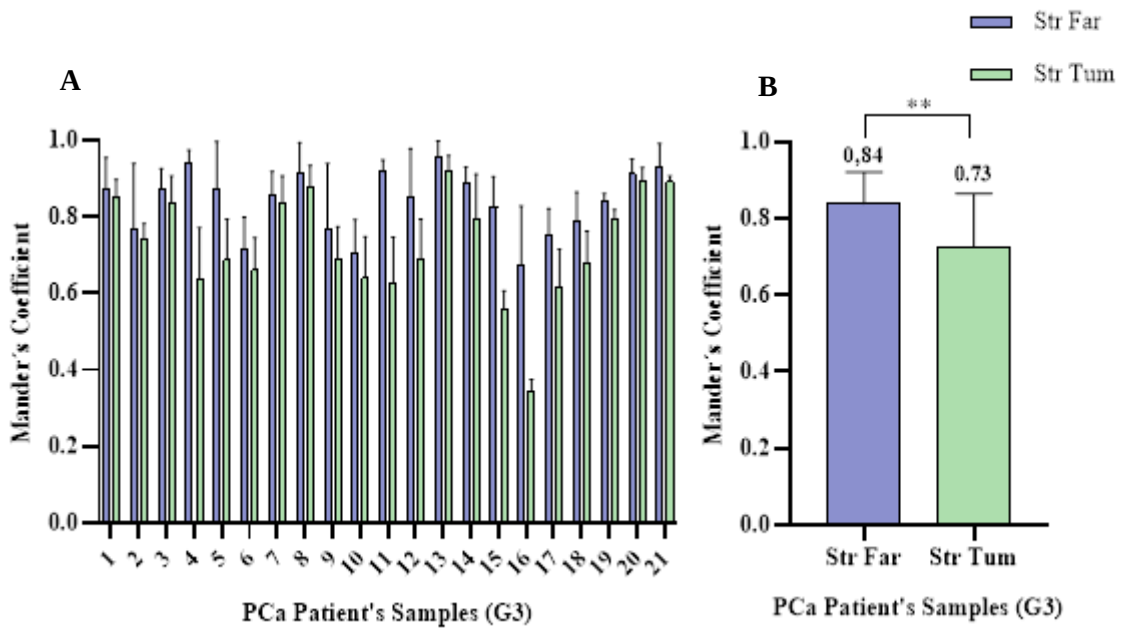

Figure 15: Co-localization Analysis between ASPA and Desmin in PCa Patient's Samples with Gleason Score 3. *(A) Manders Coefficient obtained in the 21 samples analysed, in the two compartiments; (B) Manders Coefficient obtained in the two types of ROIs analysed.*

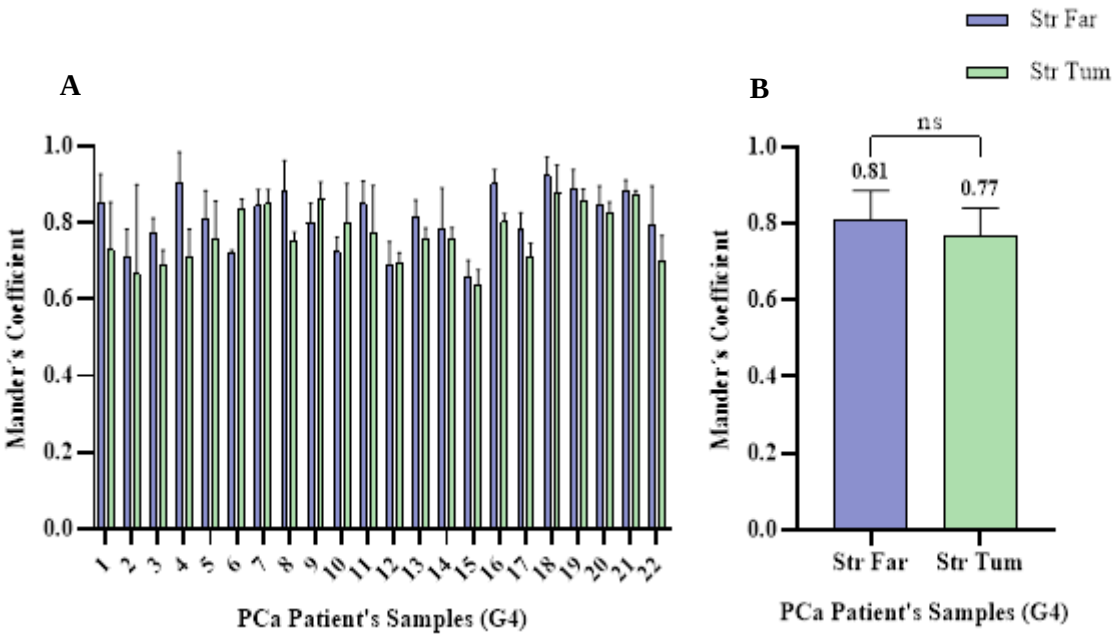

Figure 16: Co-localization Analysis between ASPA and Desmin in PCa Patient's Samples with Gleason Score 4. *(A) Manders Coefficient obtained in the 22 samples analysed, in the two compartiments; (B) Manders Coefficient obtained in the two types of ROIs analysed.*

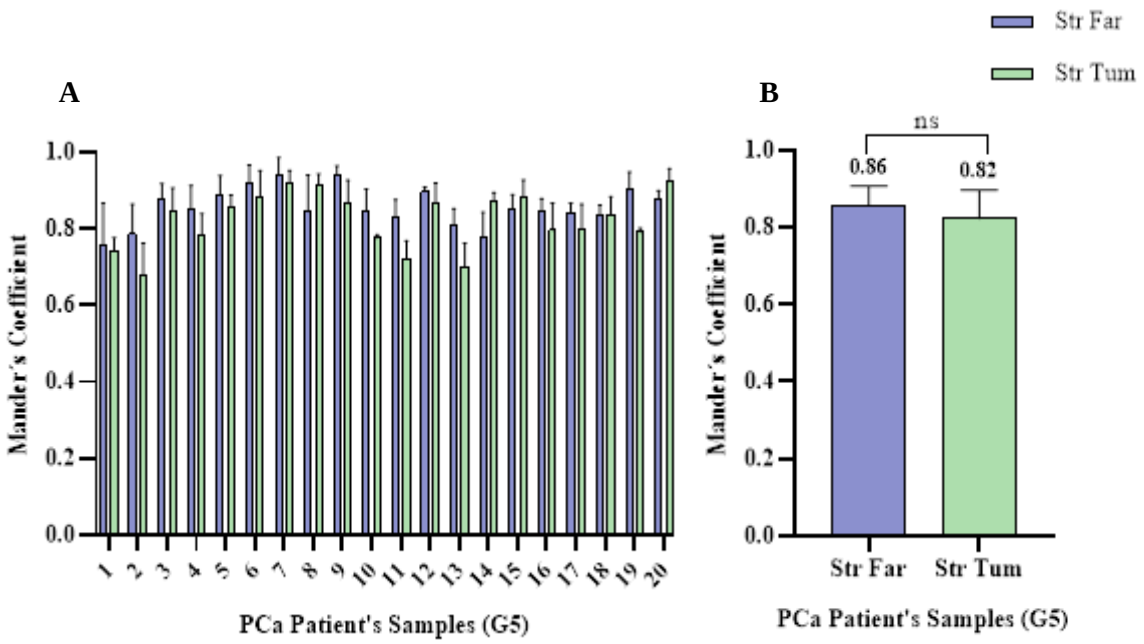

Figure 17: Co-localization Analysis between ASPA and Desmin in PCa Patient's Samples with Gleason Score 5. *(A) Manders Coefficient obtained in the 20 samples analysed, in the two compartiments; (B) Manders Coefficient obtained in the two types of ROIs analysed.*

Co-localization Analysis between Desmin and ASPA in the different disease groups, according

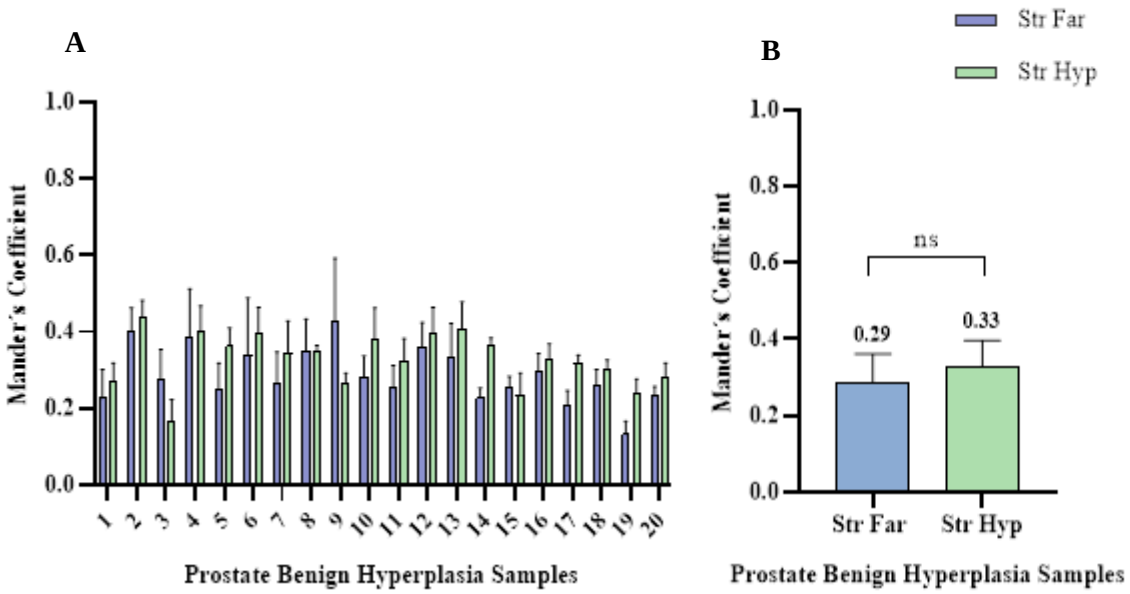

Figure 18: Co-localization Analysis betwee Desmin and ASPA in PBH Samples. *(A) Manders Coefficient obtained in the 20 samples analysed, in the two compartiments; (B) Manders Coefficient obtained in the two types of ROIs analysed.*

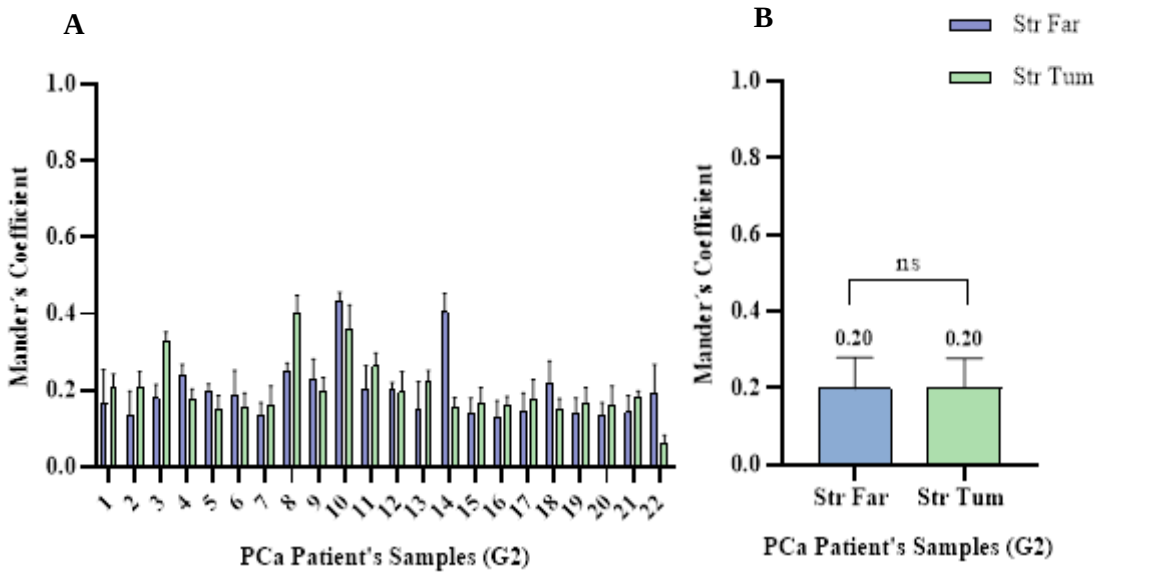

Figure 19: Co-localization Analysis between Desmin and ASPA in PCa Patient's Samples with Gleason Score 2. *(A) Manders Coefficient obtained in the 22 samples analysed, in the two compartiments; (B) Manders Coefficient obtained in the two types of ROIs analysed.*

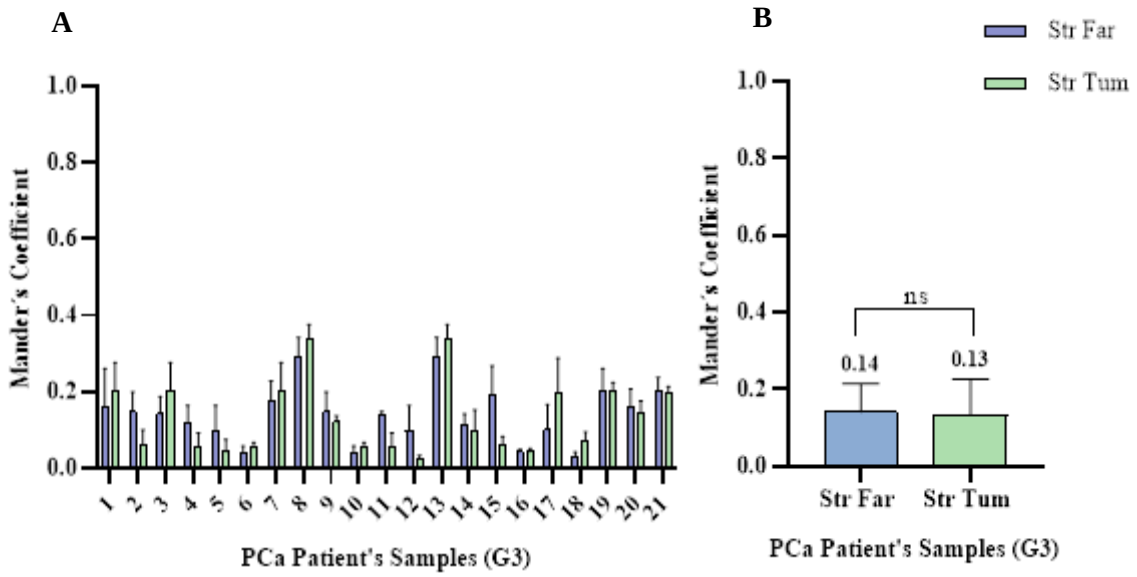

Figure 20: Co-localization Analysis between Desmin and ASPA in PCa Patient's Samples with Gleason Score 3. *(A) Manders Coefficient obtained in the 21 samples analysed, in the two compartiments; (B) Manders Coefficient obtained in the two types of ROIs analysed.*

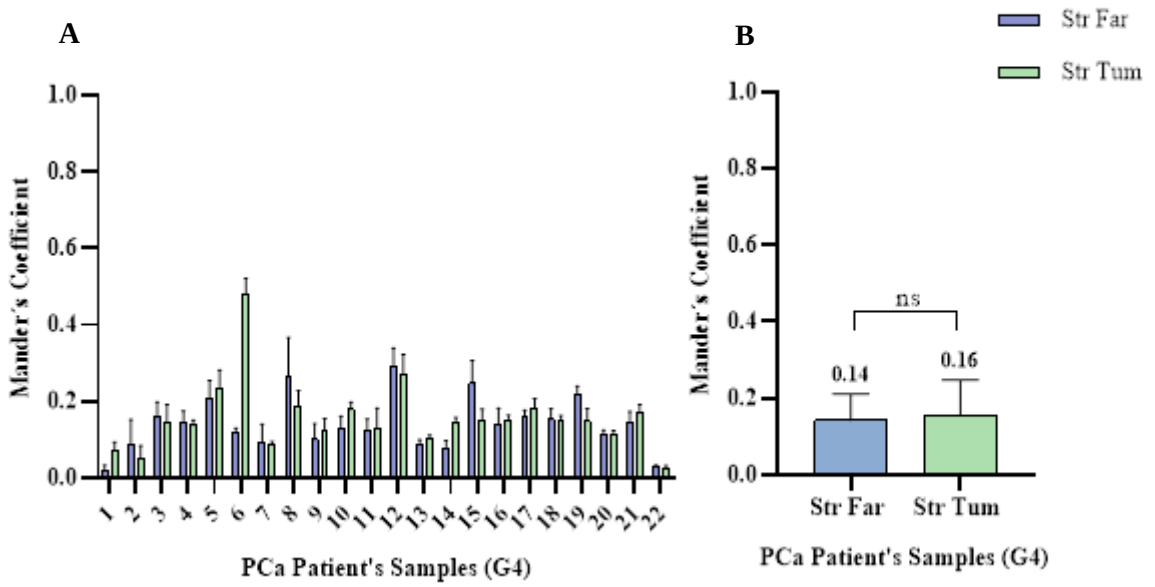

Figure 21: Co-localization Analysis between Desmin and ASPA in PCa Patient's Samples with Gleason Score 4. *(A) Manders Coefficient obtained in the 22 samples analysed, in the two compartiments; (B) Manders Coefficient obtained in the two types of ROIs analysed.*

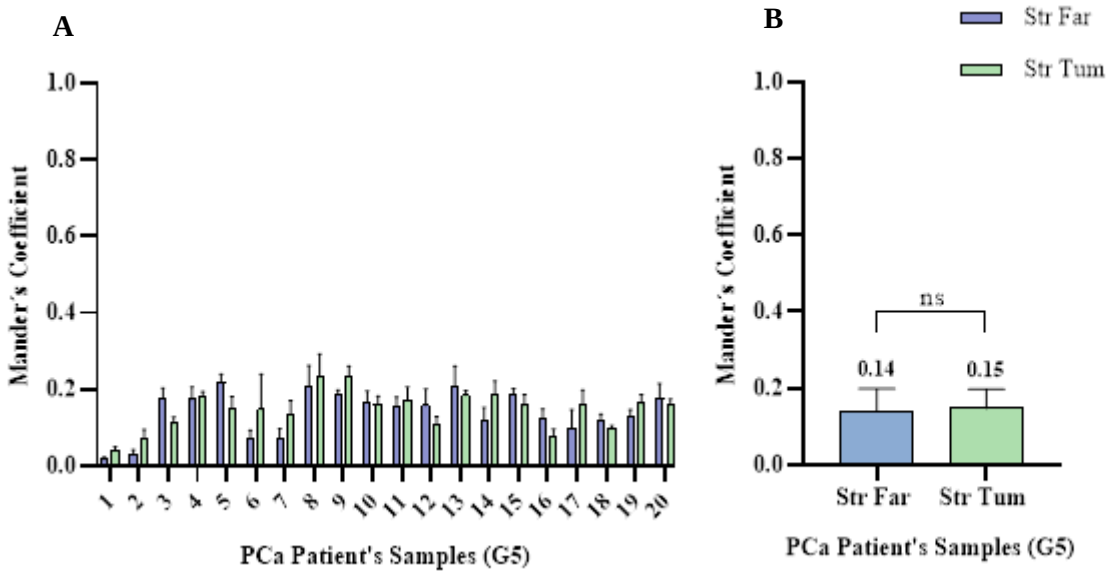

Figure 22: Co-localization Analysis between Desmin and ASPA in PCa Patient's Samples with Gleason Score 5. *(A) Manders Coefficient obtained in the 20 samples analysed, in the two compartiments; (B) Manders Coefficient obtained in the two types of ROIs analysed.*

Vascular Density in the different disease groups, according to the different compartments analysed

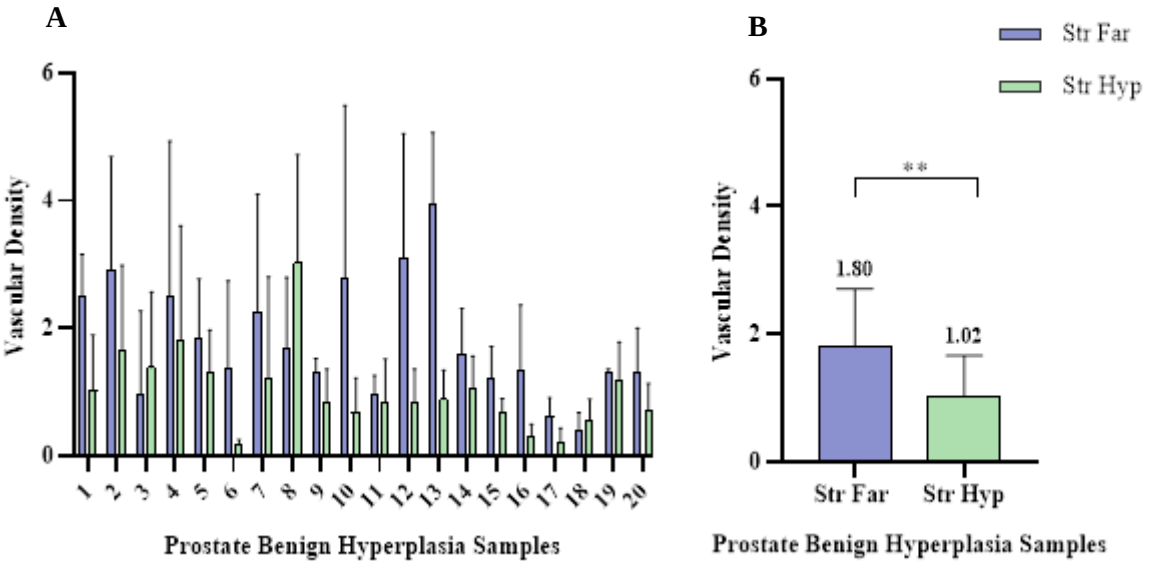

***Figure 23: Vascular Density in PBH Samples**. (A) Vascular Density in the 20 samples analysed, in the two compartiments; (B) Vascular Density obtained in the two types of ROIs analysed.*

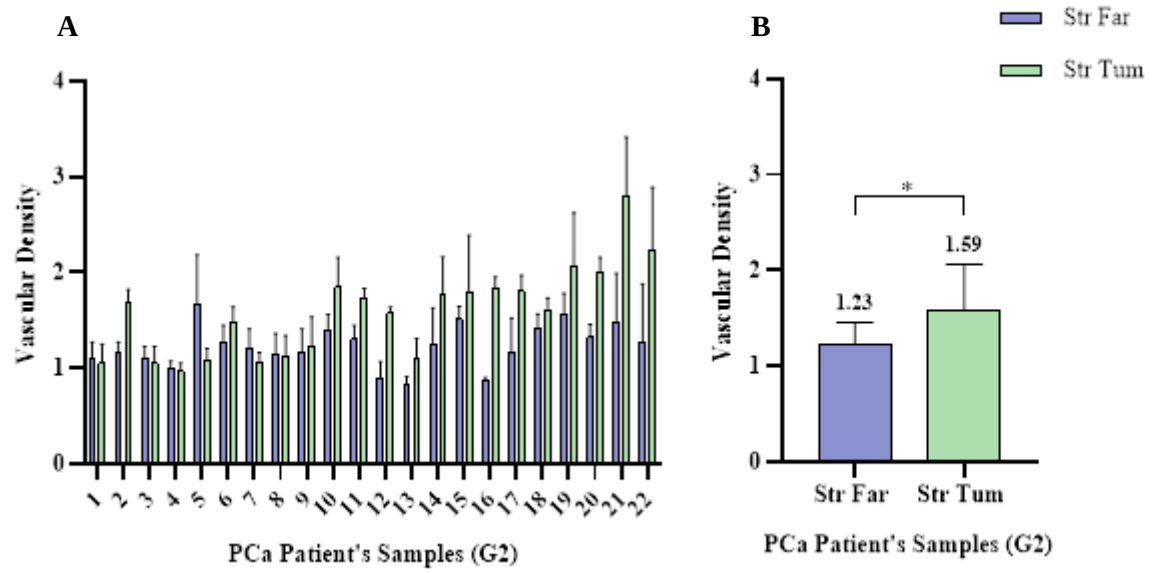

***Figure 24: Vascular Density in PCa Patient's Samples with Gleason Score 2.** (A) Vascular Density in the 22 samples analysed, in the two compartiments; (B) Vascular Density in the two types of ROIs analysed.*

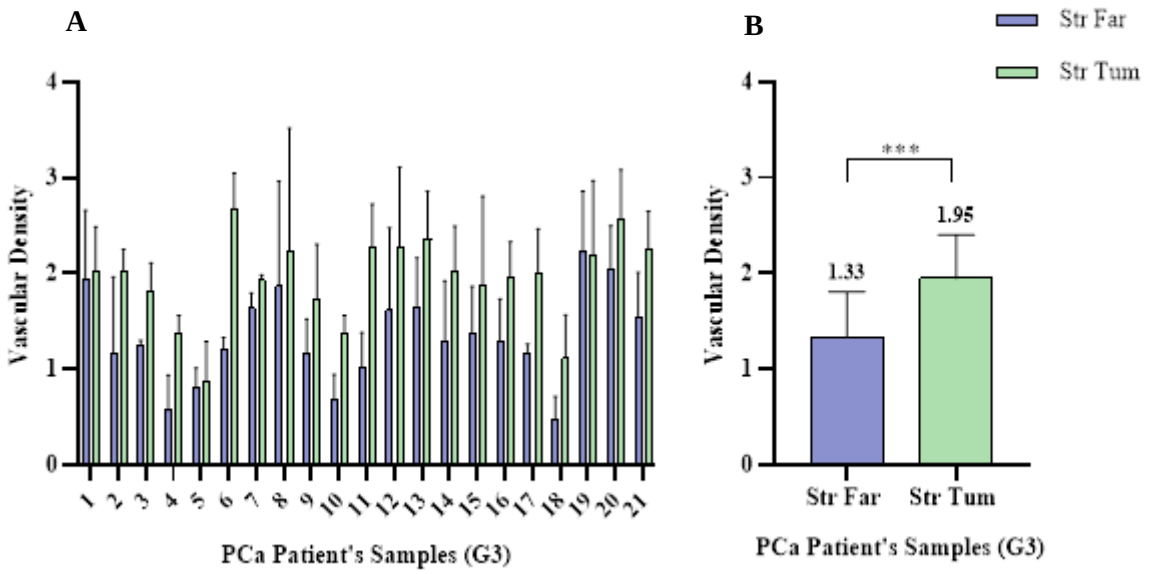

Figure 25: Vascular Density in PCa Patient´s Samples with Gleason score 3. *(A) Vascular Density in the 21 samples analysed, in the two compartiments; (B) Vascular Density obtained in the two types of ROIs analysed.*

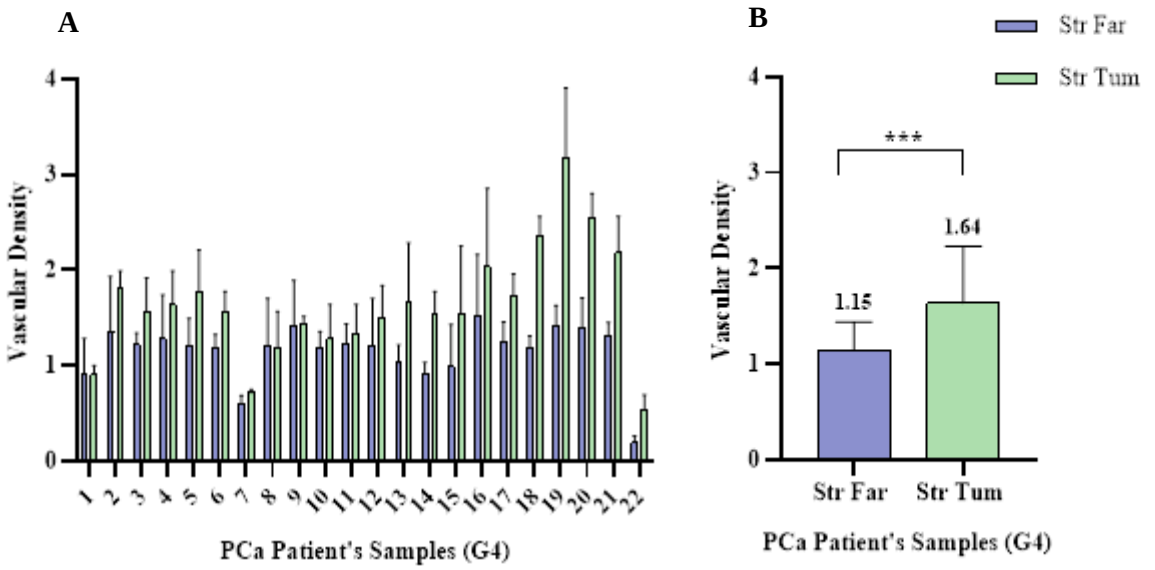

Figure 26: Vascular Density in PCa Patient´s Samples with Gleason score 4. *(A) Vascular Density in the 22 samples analysed, in the two compartiments; (B) Vascular Density obtained in the two types of ROIs analysed.*

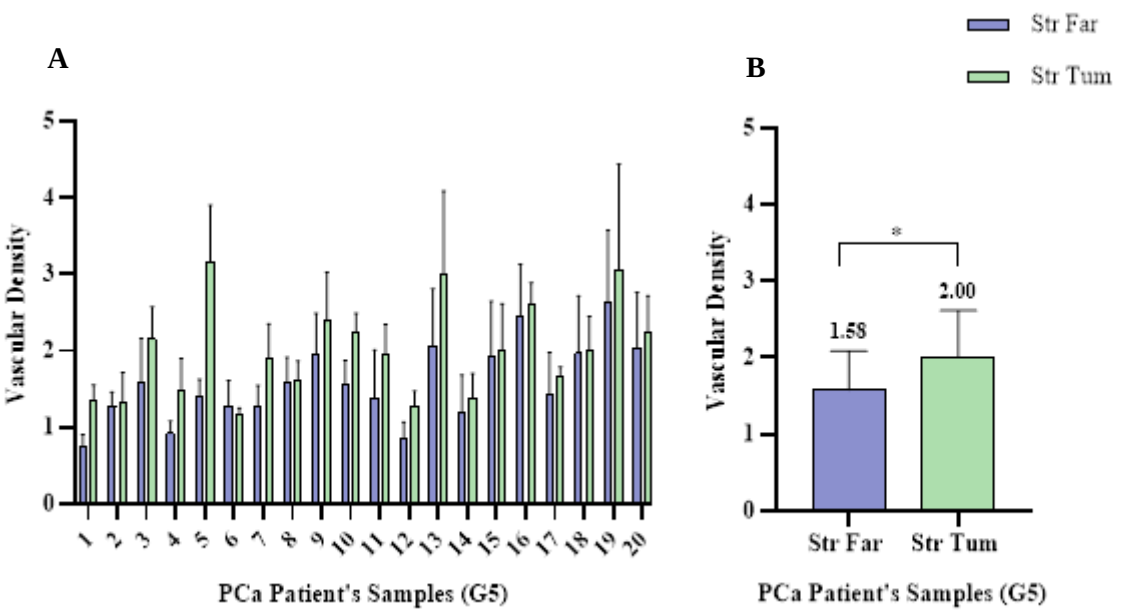

Figure 27: Vascular Density in PCa Patient´s Samples with Gleason score 4. *(A) Vascular Density in the 22 samples analysed, in the two compartiments; (B) Vascular Density obtained in the two types of ROIs analysed.*

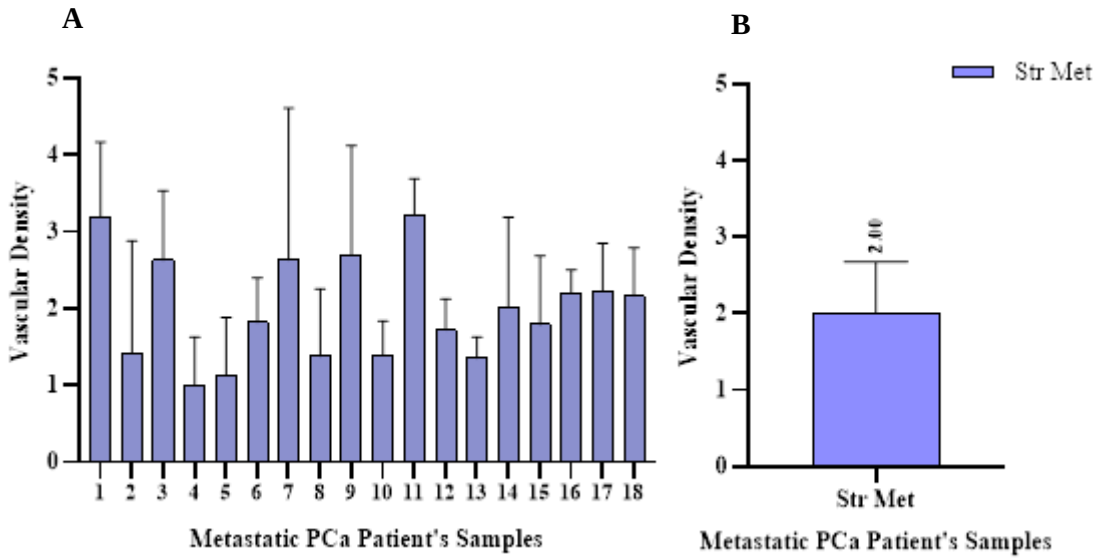

Figure 28: Vascular Density in Metastatic PCa Patient's Samples. *(A) Vascular Density in the 18 samples analysed, in the areas close to metastatic cells; (B) Vascular Density in the Str Met.*

Co-localization Analysis between ASPA and CD31 in the different disease groups, according to the different compartments analysed

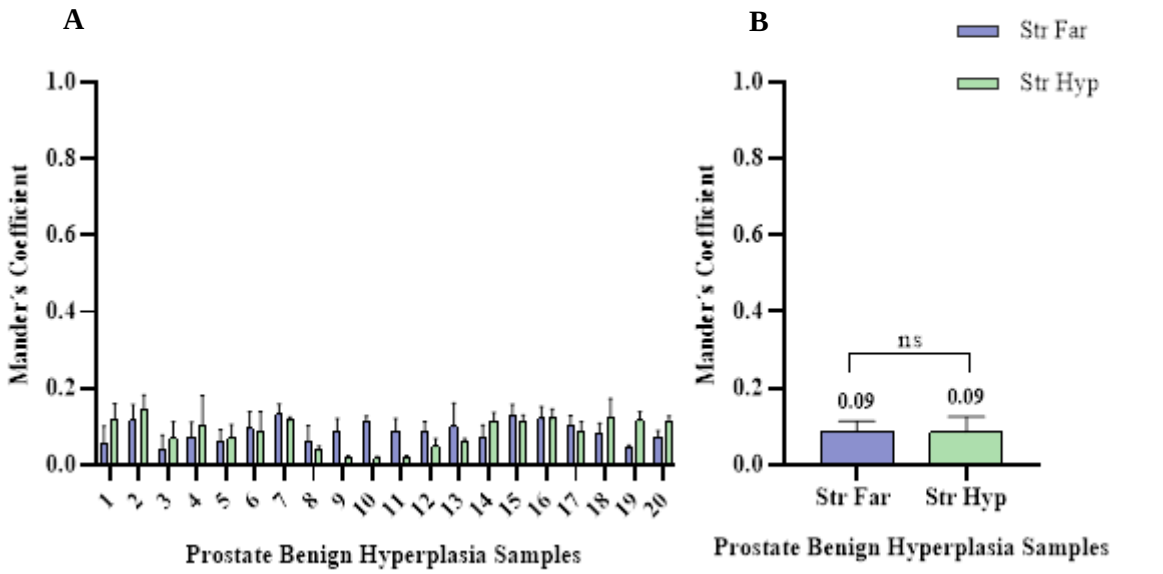

Figure 29: Co-localization Analysis betwee ASPA and CD31 in PBH Samples. *(A) Manders Coefficient obtained in the 20 samples analysed, in the two compartiments; (B) Manders Coefficient obtained in the two types of ROIs analysed.*

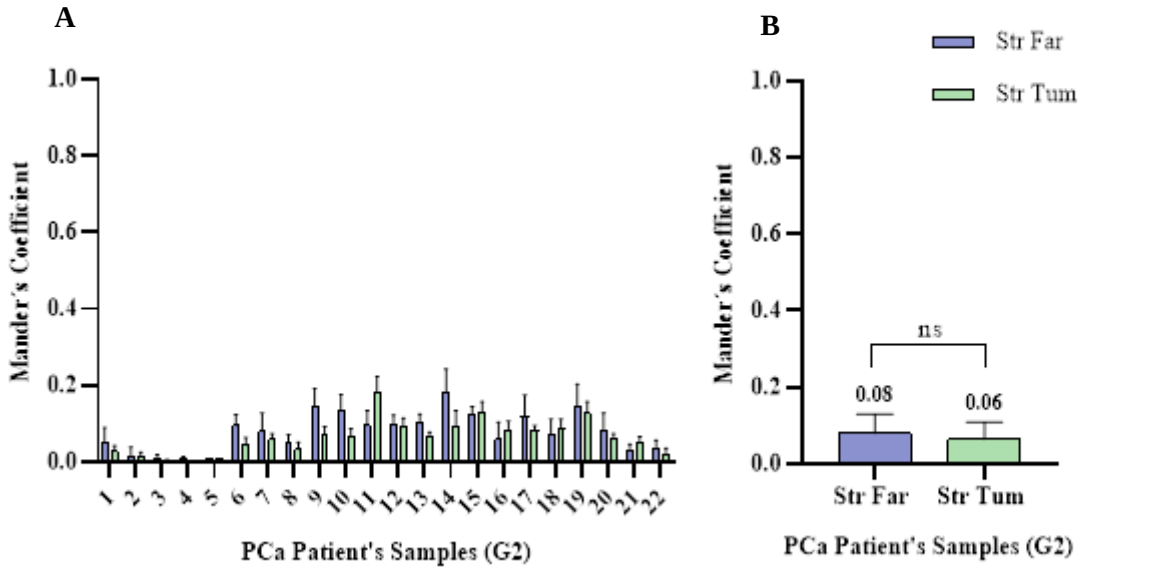

Figure 30: Co-localization Analysis between ASPA and CD31 in PCa Patient's Samples with Gleason Score 2*. (A) Manders Coefficient obtained in the 20 samples analysed, in the two compartiments; (B) Manders Coefficient obtained in the two types of ROIs analysed.*

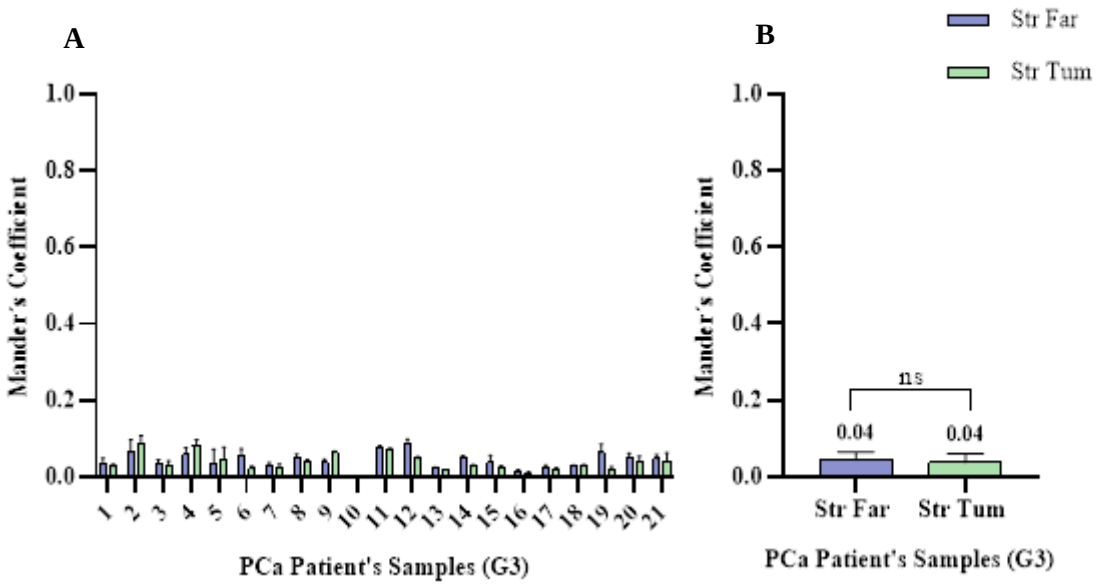

Figure 31: Co-localization Analysis between ASPA and CD31 in PCa Patient's Samples with Gleason Score 3. *(A) Manders Coefficient obtained in the 21 samples analysed, in the two compartiments; (B) Manders Coefficient obtained in the two types of ROIs analysed.*

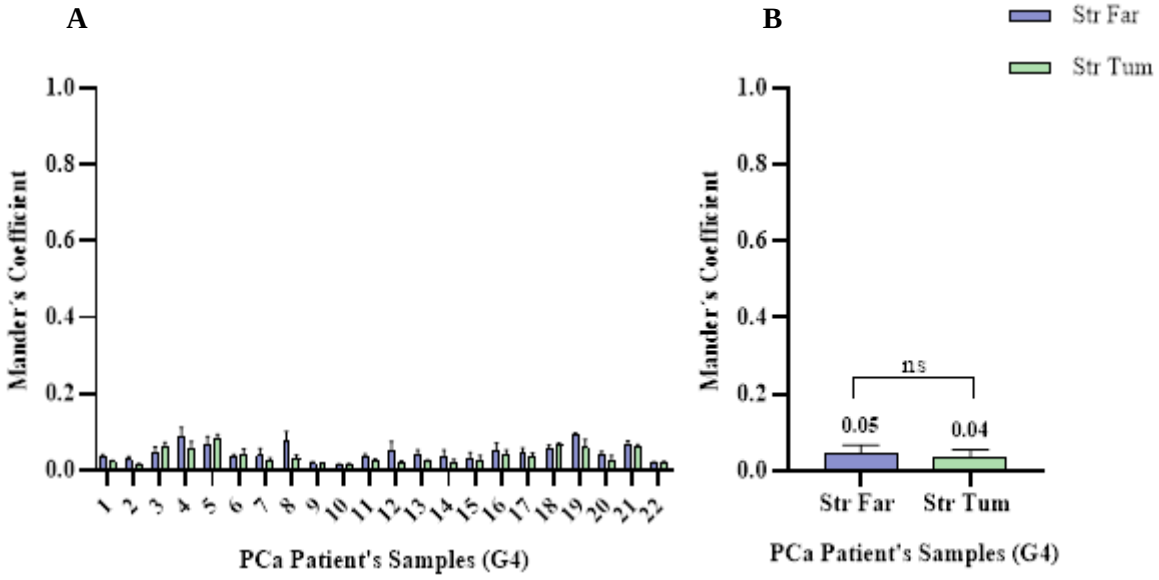

Figure 32: Co-localization Analysis between ASPA and CD31 in PCa Patient's Samples with Gleason Score 4*. (A) Manders Coefficient obtained in the 22 samples analysed, in the two compartiments; (B) Manders Coefficient obtained in the two types of ROIs analysed.*

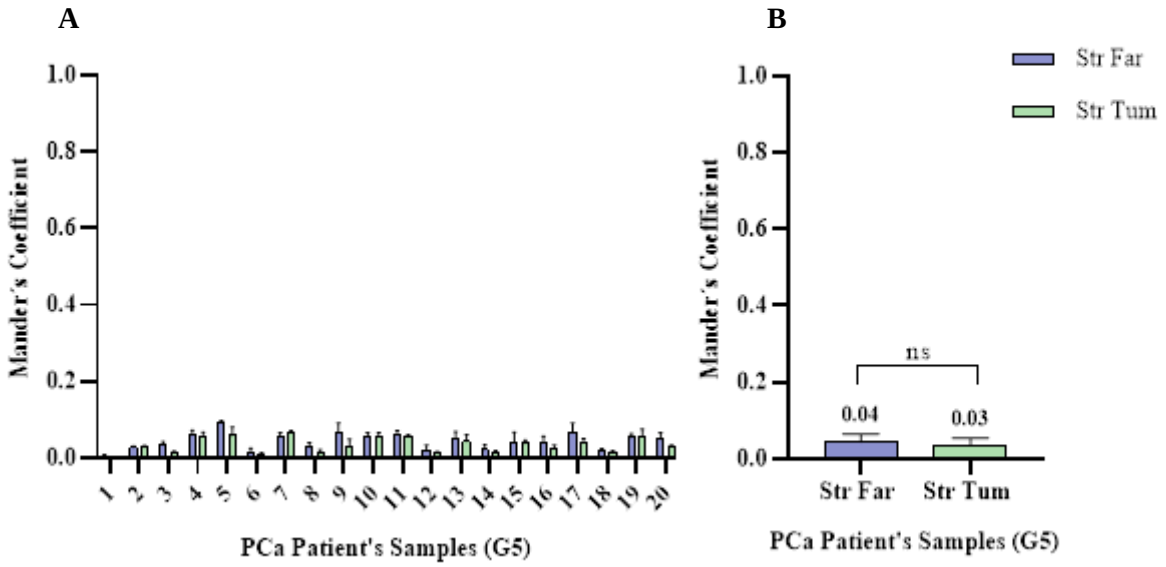

Figure 33: Co-localization Analysis between ASPA and CD31 in PCa Patient's Samples with Gleason Score 5. *(A) Manders Coefficient obtained in the 20 samples analysed, in the two compartiments; (B) Manders Coefficient obtained in the two types of ROIs analysed.*

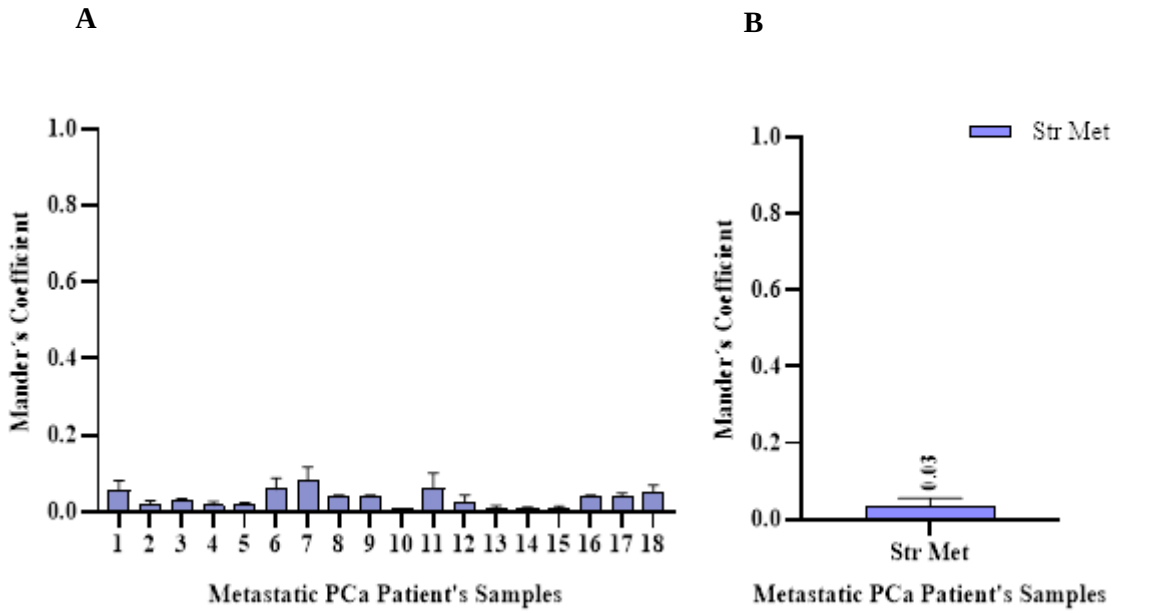

Figure 34: Co-localization Analysis between ASPA and CD31 in Metastatic PCa Patinet's Samples. *(A) Manders Coefficient obtained in the 18 samples analysed, in the areas close to the metastatic cells; (B) Manders Coefficient obtained in Str Met.*

CD68 positive cells in the different disease groups, according to the different compartments analysed

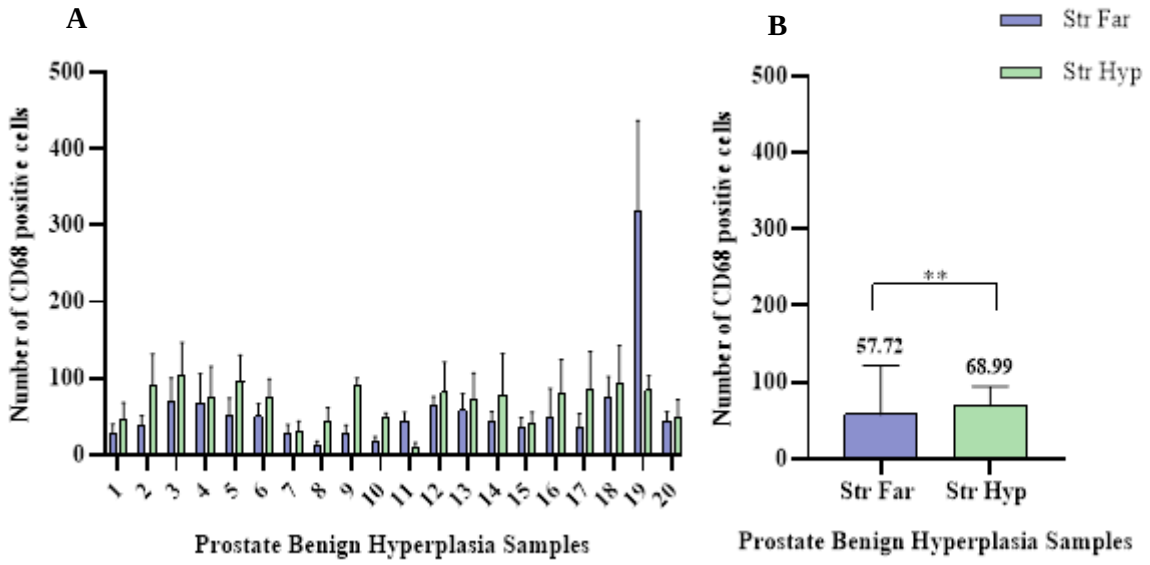

Figure 35: Number of CD68 positive cells in PBH Samples. *(A) Number of macrophages in the 20 samples analysed, in the two compartiments; (B) Number of macrophages obtained in the two types of ROIs analysed.*

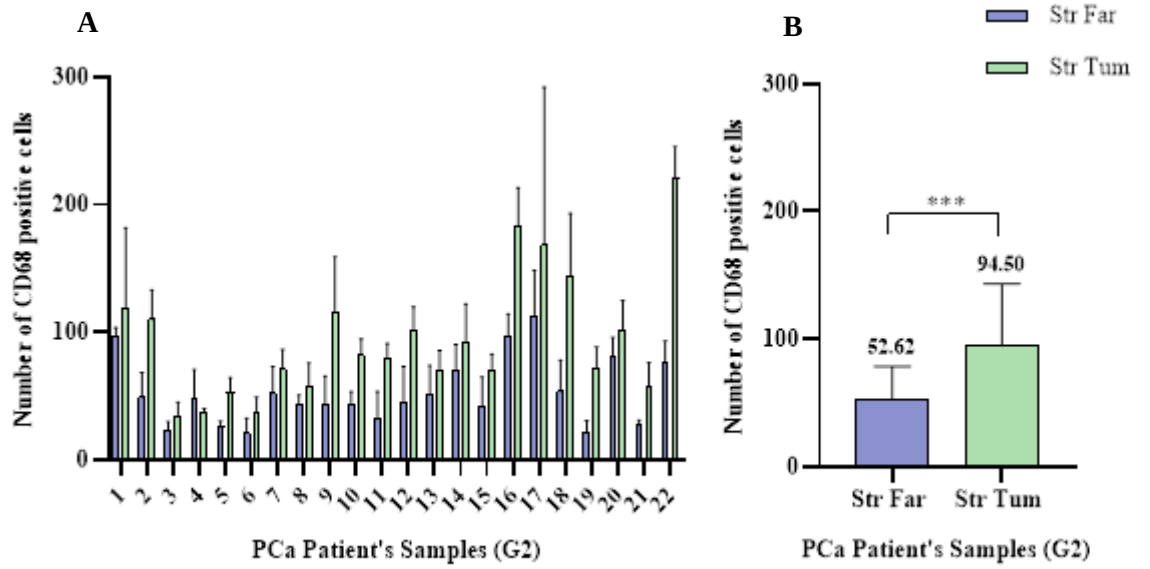

Figure 36: Number of CD68 positive cells in PCa Patient's Samples with Gleasson Score 2*. (A) Number of macrophages in the 22 samples analysed, in the two compartiments; (B) Number of macrophages obtained in the two types of ROIs analysed.*

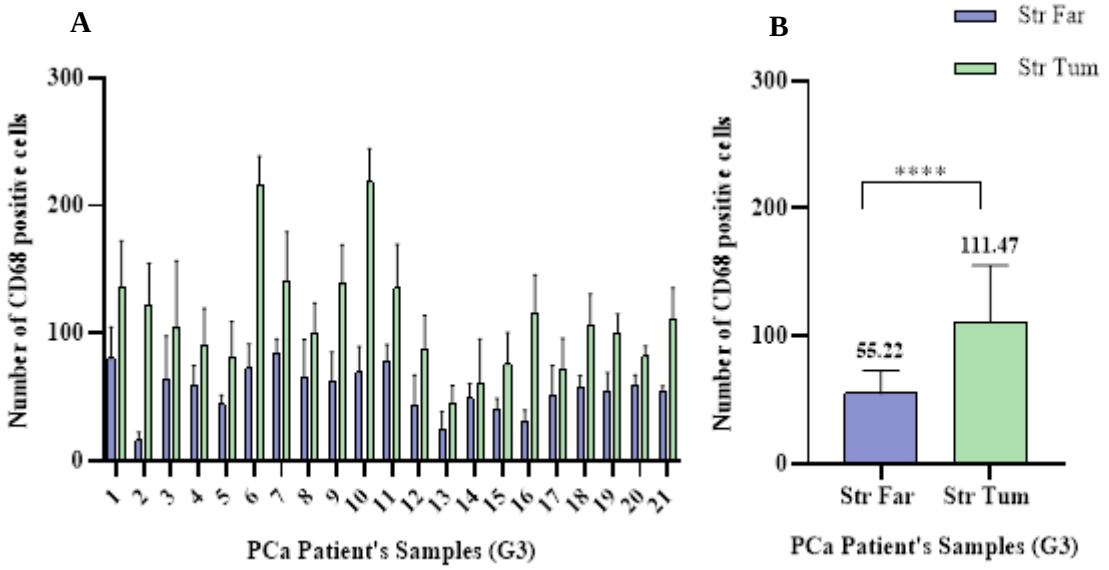

Figure 37: Number of CD68 positive cells in PCa Patient's Samples with Gleasson Score 3. *(A) Number of macrophages in the 21 samples analysed, in the two compartiments; (B) Number of macrophages obtained in the two types of ROIs analysed.*

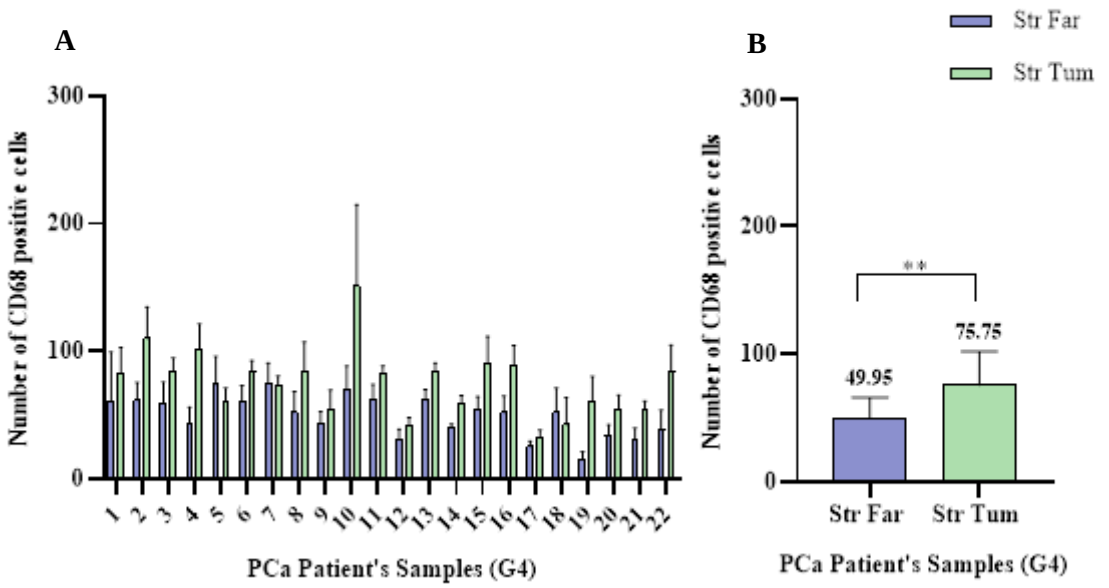

Figure 38: Number of CD68 positive cells in PCa Patient's Samples with Gleasson Score 4*. (A) Number of macrophages in the 22 samples analysed, in the two compartiments; (B) Number of macrophages obtained in the two types of ROIs analysed.*

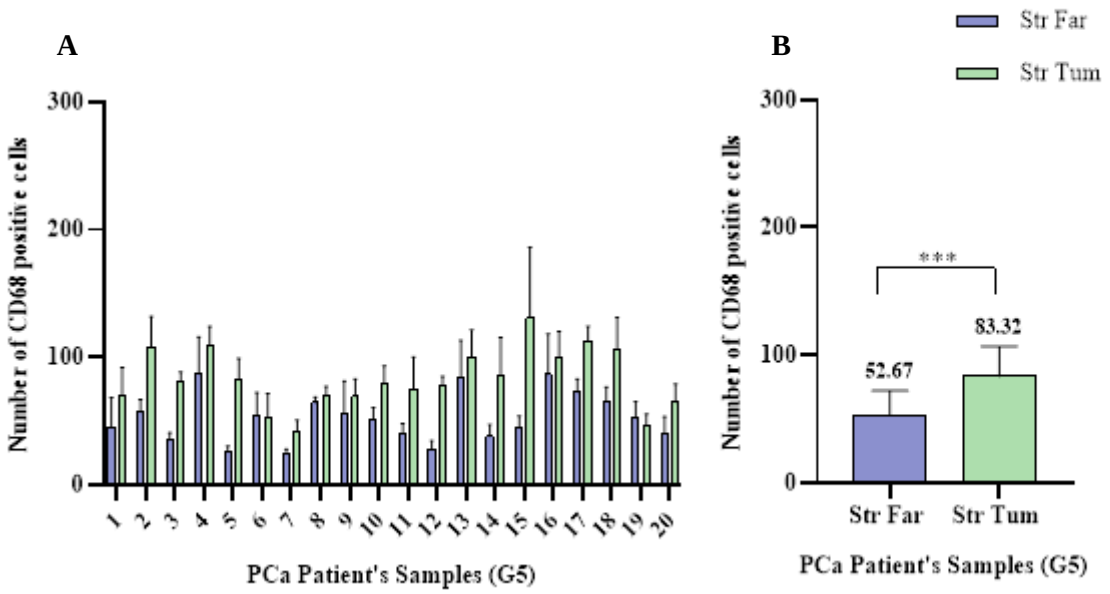

Figure 39: Number of CD68 positive cells in PCa Patient's Samples with Gleasson Score 5. *(A) Number of macrophages in the 20 samples analysed, in the two compartiments; (B) Number of macrophages obtained in the two types of ROIs analysed.*

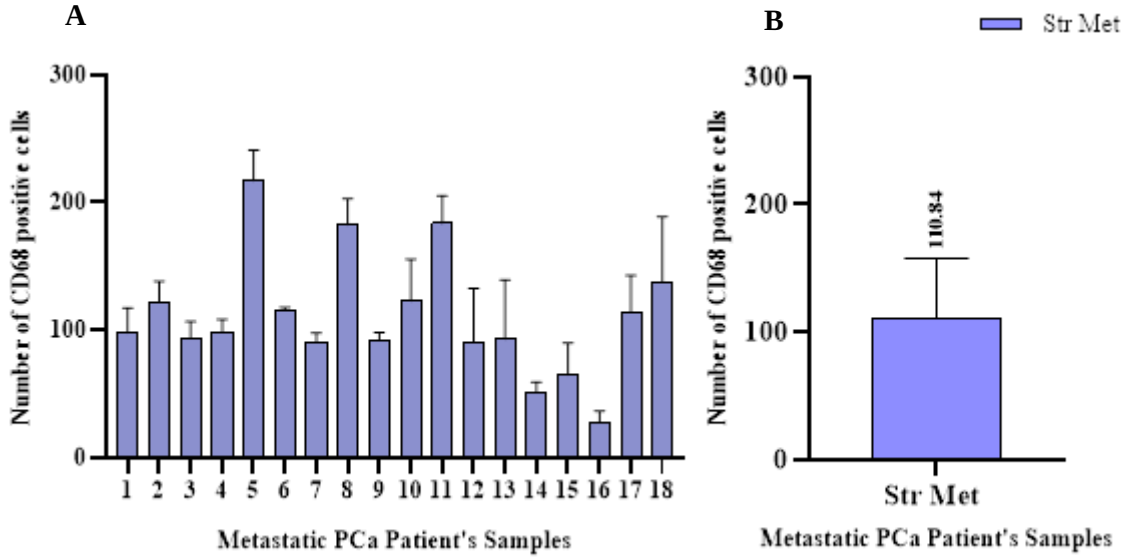

Figure 40: Number of CD68 positive cells in Metastatic PCa Patient´s Samples. *(A) Number of macrophages in the 180 samples analysed, in the areas close to the metastatic cells; (B) Number of macrophages obtained Str Met.*

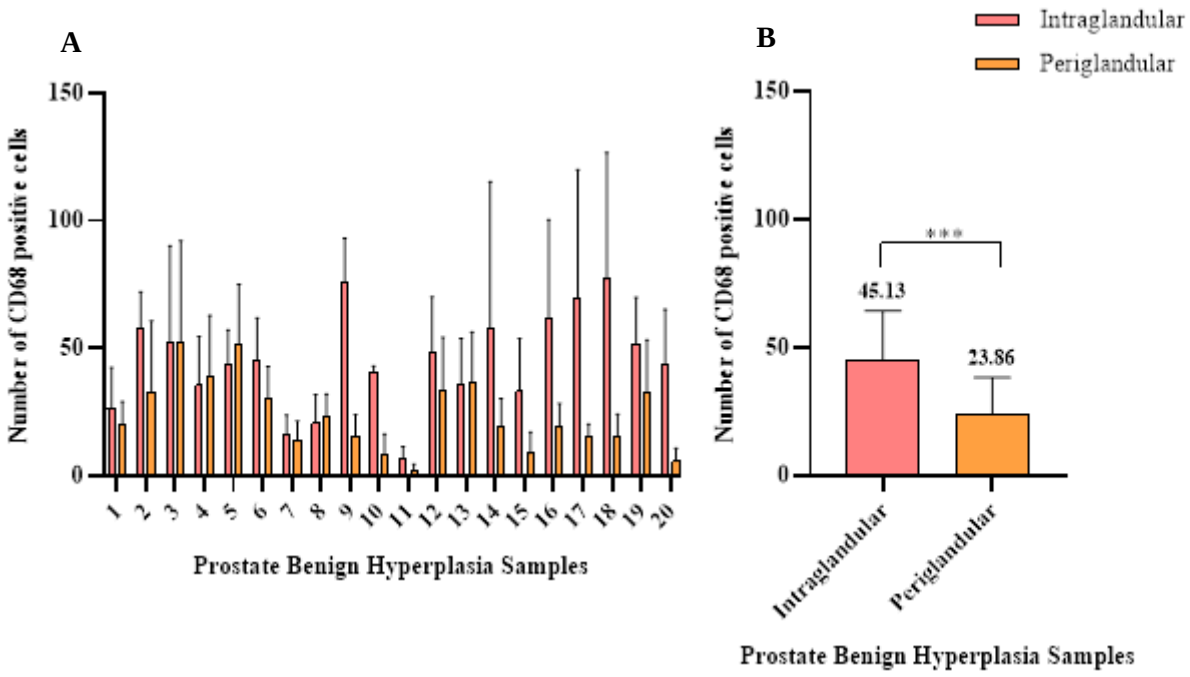

Figure 41: Number of CD68 positive cells in PBH Samples. *(A) Number of macrophages in the 20 samples analysed, in the Intraglandular and Periglandular areas; (B) Number of macrophages obtained in the two types of ROIs analysed.*

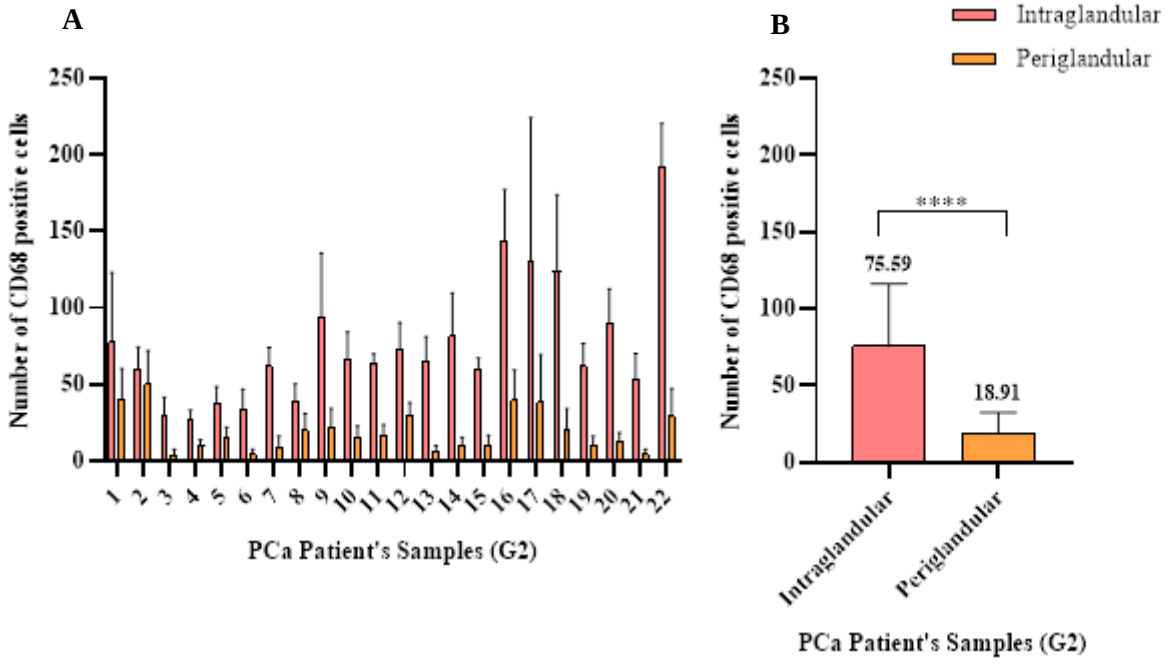

Figure 42: Number of CD68 positive cells in PCa Patient's Samples with Gleasson Score 2. *(A) Number of macrophages in the 22 samples analysed, in the Intraglandular and Periglandular areas; (B) Number of macrophages obtained in the two types of ROIs analysed.*

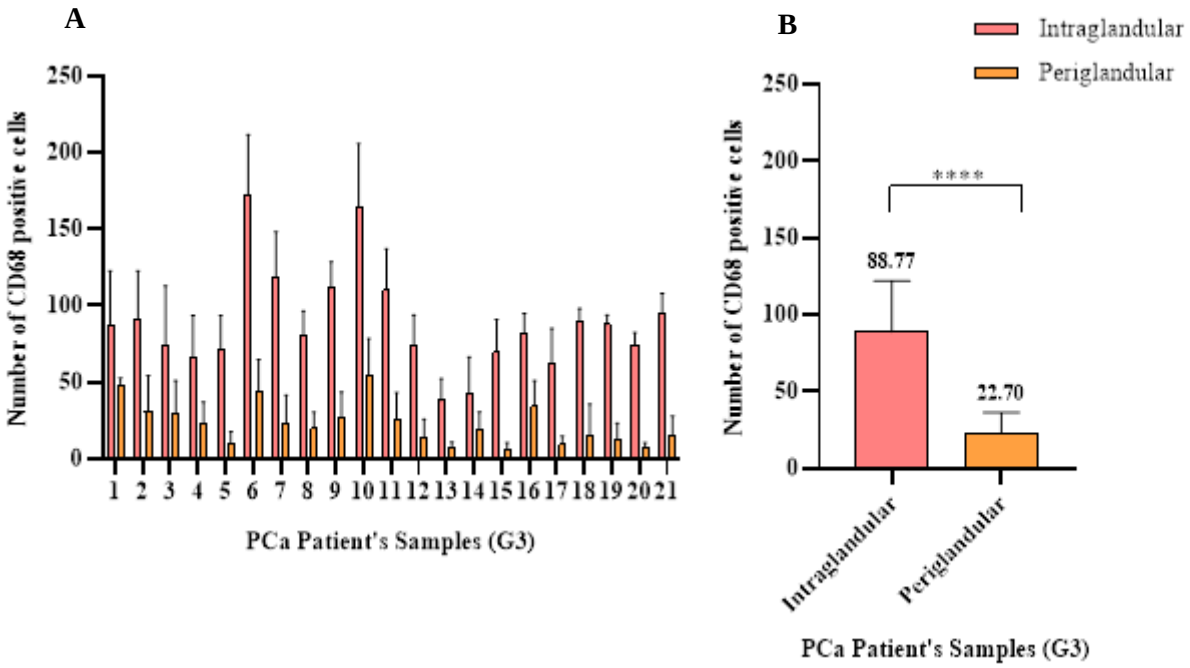

Figure 43: Number of CD68 positive cells in PCa Patient's Samples with Gleasson Score 3*. (A) Number of macrophages in the 21 samples analysed, in the Intraglandular and Periglandular areas; (B) Number of macrophages obtained in the two types of ROIs analysed.*

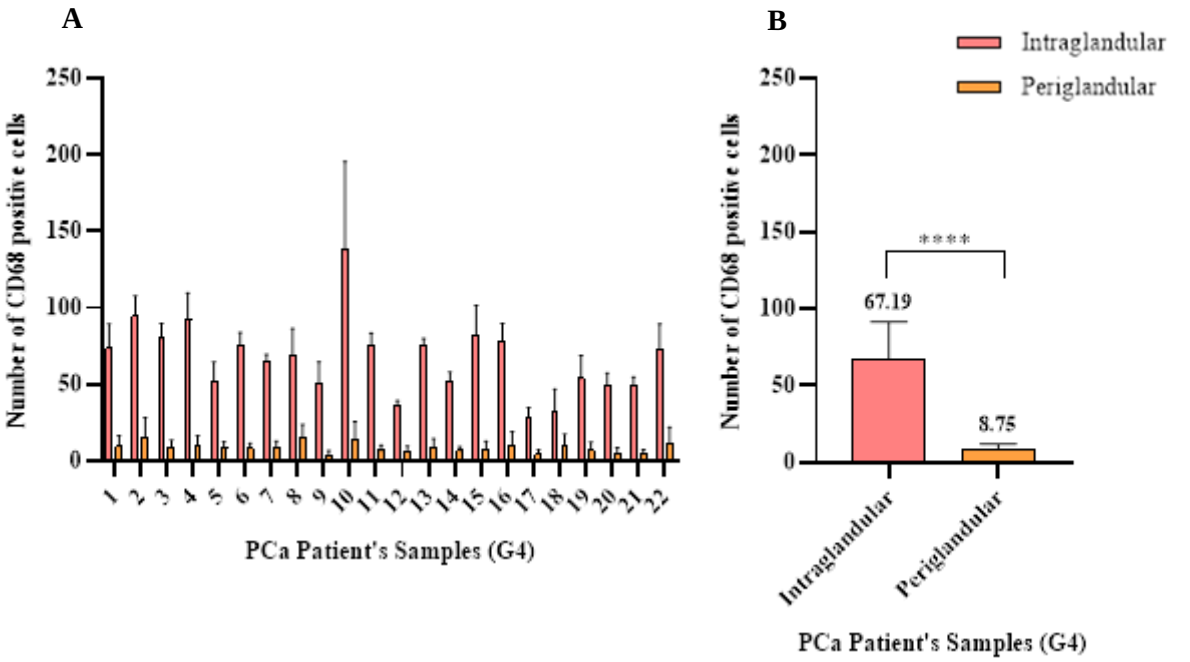

Figure 44: Number of CD68 positive cells in PCa Patient's Samples with Gleasson Score 4. *(A) Number of macrophages in the 22 samples analysed, in the Intraglandular and Periglandular areas; (B) Number of macrophages obtained in the two types of ROIs analysed.*

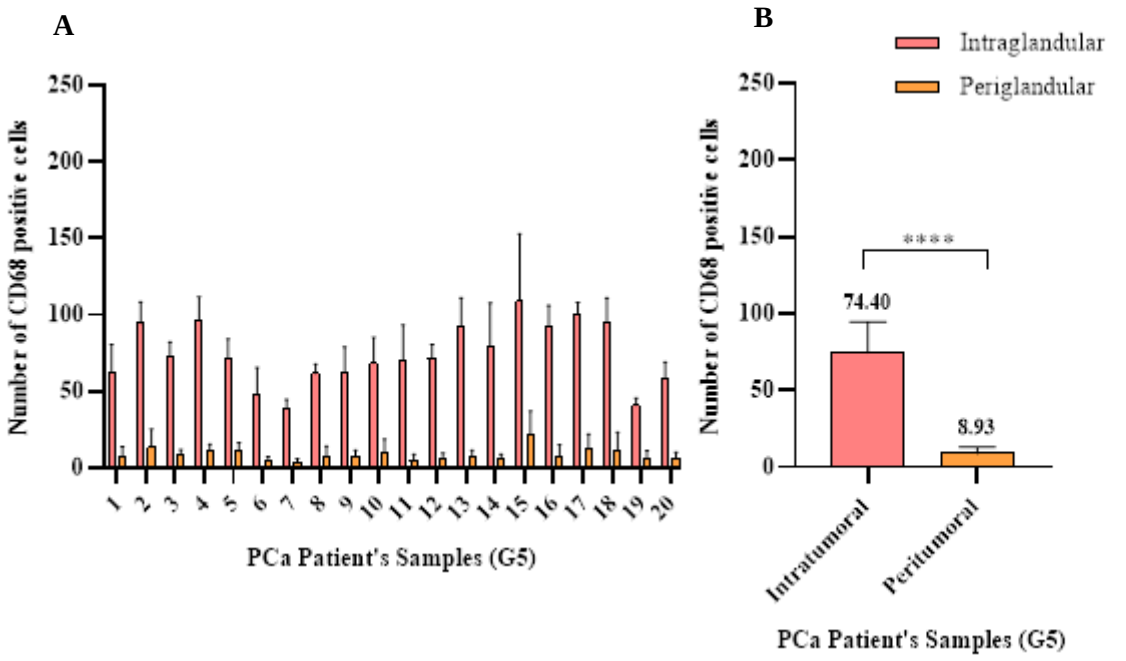

Figure 45: Number of CD68 positive cells in PCa Patient's Samples with Gleasson Score 2. *(A) Number of macrophages in the 20 samples analysed, in the Intraglandular and Periglandular areas; (B) Number of macrophages obtained in the two types of ROIs analysed.*

Statistical Analysis performed between the different samples' groups studied

Table 1: Summary table of statistical analysis performed regarding ASPA expression intensity in the Str close to prostatic glandular cells, for the different stage groups.

ASPA Expression Intensity Analysis (Str close to prostatic glandular cells)

Vs.	Hyp	G2	G3	G4	G5	Met
Hyp	-	****	****	****	****	****
G2	-	-	*	****	****	***
G3	-	-	-	****	****	*
G4	-	-	-	-	ns	ns
G5	-	-	-	-	-	*
Met	-	-	-	-	-	-

Table 2: Summary table of statistical analysis performed regarding ASPA expression intensity in the Str Far, for the different stage groups.

ASPA Expression Intensity Analysis (Str Far)

Vs.	Hyp	G2	G3	G4	G5
Hyp	-	****	****	****	****
G2	-	-	ns	****	****
G3	-	-	-	****	****
G4	-	-	-	-	ns
G5	-	-	-	-	-

Table 3: Summary table of statistical analysis performed regarding Desmin expression intensity in the Str close to prostatic glandular cells, for the different stage groups.

Desmin Expression Intensity Analysis (Str close to prostatic glandular cells)

Vs.	Hyp	G2	G3	G4	G5	Met
Hyp	-	*	ns	****	****	****
G2	-	-	**	**	**	****
G3	-	-	-	****	****	****
G4	-	-	-	-	ns	****
G5	-	-	-	-	-	****
Met	-	-	-	-	-	-

Table 4: Summary table of statistical analysis performed regarding Desmin expression intensity in the Str Far, for the different stage groups.

Desmin Expression Intensity Analysis (Str Far)

Vs.	Hyp	G2	G3	G4	G5
Hyp	-	**	ns	****	****
G2	-	-	***	*	****
G3	-	-	-	****	****
G4	-	-	-	-	ns
G5	-	-	-	-	-

Table 5: Summary table of statistical analysis performed regarding the co-localization between ASPA and Desmin in the Str close to prostatic glandular cells, for the different stage groups.

Co-localization: ASPA and Desmin Analysis (Str close to prostatic glandular cells)

Vs.	Hyp	G2	G3	G4	G5
Hyp	-	***	**	*	ns
G2	-	-	ns	ns	**
G3	-	-	-	ns	**
G4	-	-	-	-	ns
G5	-	-	-	-	-

Table 6: Summary table of statistical analysis performed regarding the co-localization between ASPA and Desmin in the Str Far, for the different stage groups.

Co-localization: ASPA and Desmin Analysis (Str Far)

Vs.	Hyp	G2	G3	G4	G5
Hyp	-	****	**	****	**
G2	-	-	ns	ns	ns
G3	-	-	-	ns	ns
G4	-	-	-	-	ns
G5	-	-	-	-	-

Table 7: Summary table of statistical analysis performed regarding the co-localization between Desmin and ASPA in the Str close to prostatic glandular cells, for the different stage groups.

Co-localization: Desmin and ASPA Analysis (Str close to prostatic glandular cells)

Vs.	Hyp	G2	G3	G4	G5
Hyp	-	****	****	****	****
G2	-	-	*	**	ns
G3	-	-	-	ns	ns
G4	-	-	-	-	ns
G5	-	-	-	-	-

Table 8: Summary table of statistical analysis performed regarding the co-localization between Desmin and ASPA in the Str Far, for the different stage groups.

Co-localization: Desmin and ASPA Analysis (Str Far)

Vs.	Hyp	G2	G3	G4	G5
Hyp	-	****	****	****	****
G2	-	-	*	*	ns
G3	-	-	-	ns	ns
G4	-	-	-	-	ns
G5	-	-	-	-	-

Table 9: Summary table of statistical analysis performed regarding the vascular density in the Str close to prostatic glandular cells, for the different stage groups.

Vascular Density Analysis (Str close to prostatic glandular cells)

Vs.	Hyp	G2	G3	G4	G5	Met
Hyp	-	***	****	***	****	****
G2		-	**	ns	*	*
G3			-	ns	ns	ns
G4				-	ns	ns
G5					-	ns
Met						-

Table 10: Summary table of statistical analysis performed regarding the vascular density in the Str Far, for the different stage groups.

Vascular Density Analysis (Str Far)

Vs.	Hyp	G2	G3	G4	G5
Hyp	-	*	*	*	ns
G2	-	-	ns	ns	*
G3	-	-	-	ns	ns
G4	-	-	-	-	**
G5	-	-	-	-	-

Table 11: Summary table of statistical analysis performed regarding the co-localization between ASPA and CD31 in the Str close to prostatic glandular cells, for the different stage groups.

Co-localization: ASPA and CD31 Analysis (Str close to prostatic glandular cells)

Vs.	Hyp	G2	G3	G4	G5	Met
Hyp	-	****	****	****	****	****
G2	-	-	*	*	**	*
G3	-	-	-	ns	ns	ns
G4	-	-	-	-	ns	ns
G5	-	-	-	-	-	ns
Met	-	-	-	-	-	-

Table 12: Summary table of statistical analysis performed regarding the co-localization between ASPA and CD31 in the Str Far, for the different stage groups.

Co-localization: ASPA and CD31 Analysis (Str Far)

Vs.	Hyp	G2	G3	G4	G5
Hyp	-	ns	****	****	****
G2	-	-	**	**	**
G3	-	-	-	ns	ns
G4	-	-	-	-	ns
G5	-	-	-	-	-

Table 13: Summary table of statistical analysis performed regarding the number of CD68 positive cells in the Str close to prostatic glandular cells, for the different stage groups.

CD68 positive cells Analysis (Str close to prostatic glandular cells)

Vs.	Hyp	G2	G3	G4	G5	Met
Hyp	-	ns	***	ns	*	**
G2	-	-	*	ns	ns	ns
G3	-	-	-	***	*	ns
G4	-	-	-	-	ns	***
G5	-	-	-	-	-	*
Met	-	-	-	-	-	-

Table 14: Summary table of statistical analysis performed regarding the number of CD68 positive cells in the Str Far, for the different stage groups.

CD68 positive cells Analysis (Str Far)

Vs.	Hyp	G2	G3	G4	G5
Hyp	-	ns	ns	ns	ns
G2	-	-	ns	ns	ns
G3	-	-	-	ns	Ns
G4	-	-	-	-	ns
G5	-	-	-	-	-

Table 15: Summary table of statistical analysis performed regarding the number of CD68 positive cells in the intraglandular regions, for the different stage groups.

Intraglandular CD68 positive cells Analysis

Vs.	Hyp	G2	G3	G4	G5
Hyp	-	**	****	**	****
G2	-	-	*	ns	ns
G3	-	-	-	*	ns
G4	-	-	-	-	ns
G5	-	-	-	-	-

Table 16: Summary table of statistical analysis performed regarding the number of CD68 positive cells in the periglandular regions, for the different stage groups.

Periglandular CD68 positive cells Analysis

Vs.	Hyp	G2	G3	G4	G5
Hyp	-	ns	ns	****	****
G2	-	-	*	**	*
G3	-	-	-	****	****
G4	-	-	-	-	ns
G5	-	-	-	-	-

Medians of the Biomarkers Expression

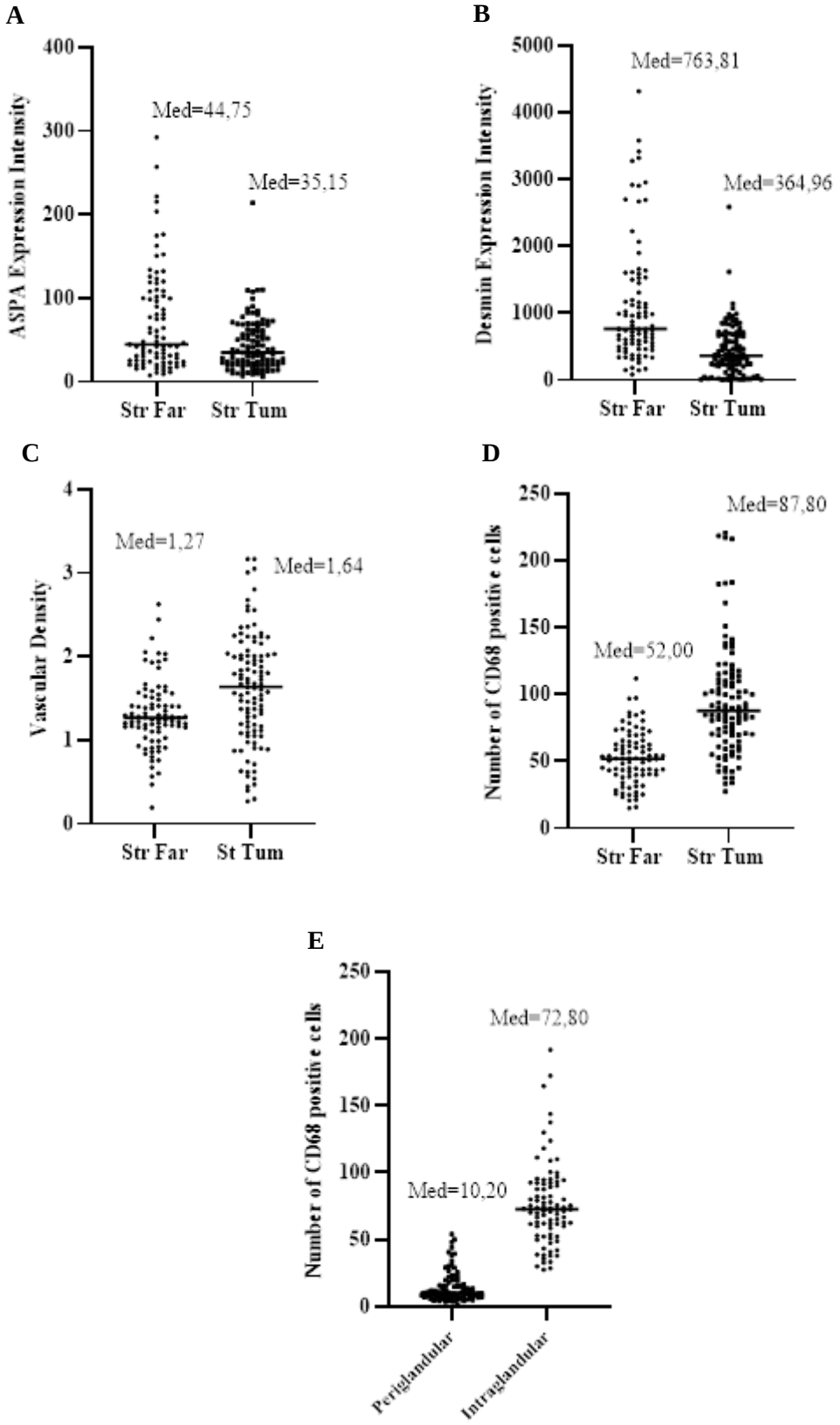

Figure 46: Distribution of the results obtained for each Biomarker studied in the all samples from the cohort analysed. *Representation of the median values of ASPA expression (A), Desmin expression (B), vascular density (C) and number of CD68 positive cells in the four compartiments evaluated (D and E).*

Analysis of the influence of clinico-pathological data variables in the patients' survival

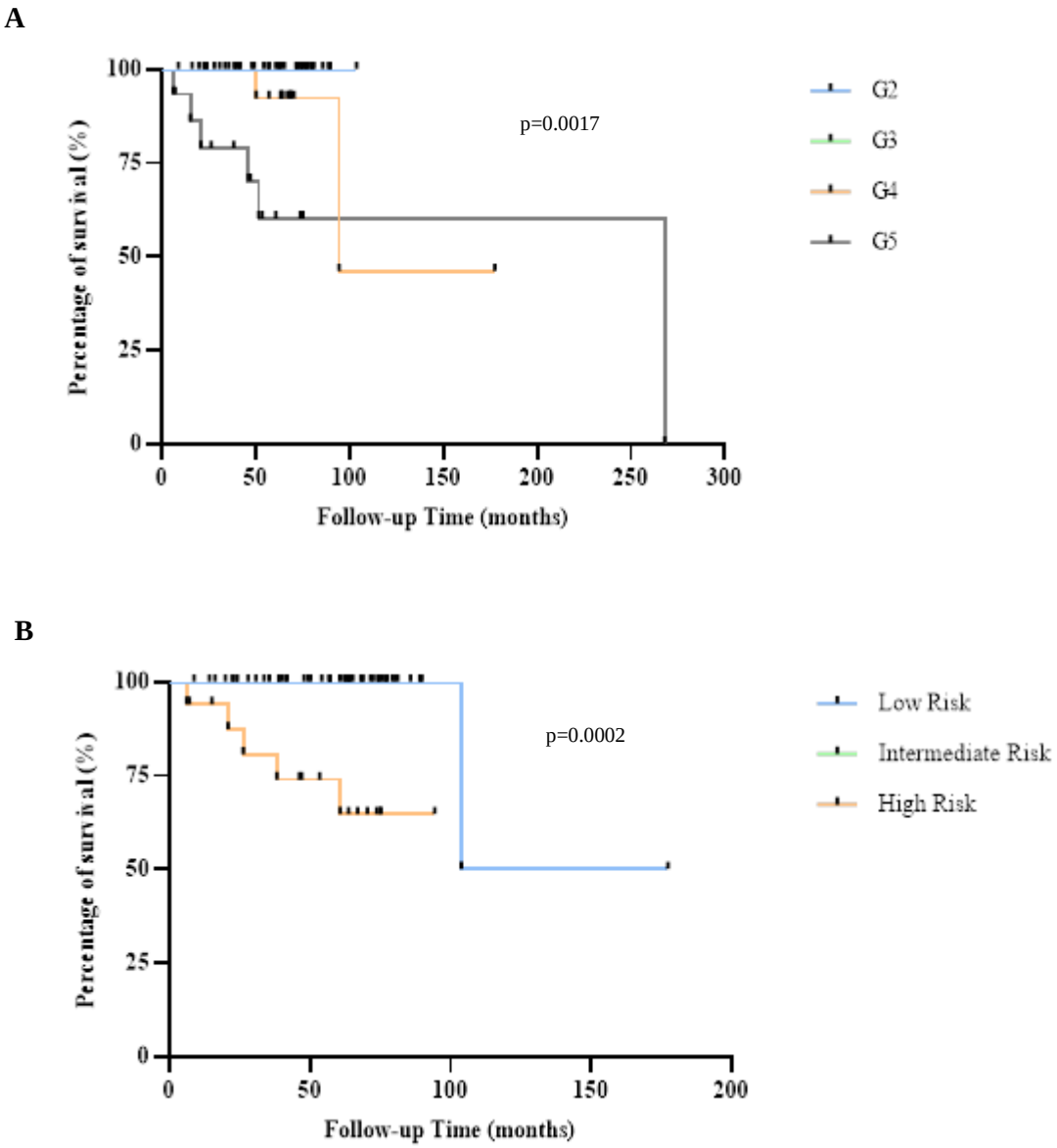

Figure 47: Cohort stratification according to PCa grade groups DSFS (A) and according levels of PSA based on D'Ámico classification DSFS (B).

Correlation of ASPA expression with clinico-pathological data

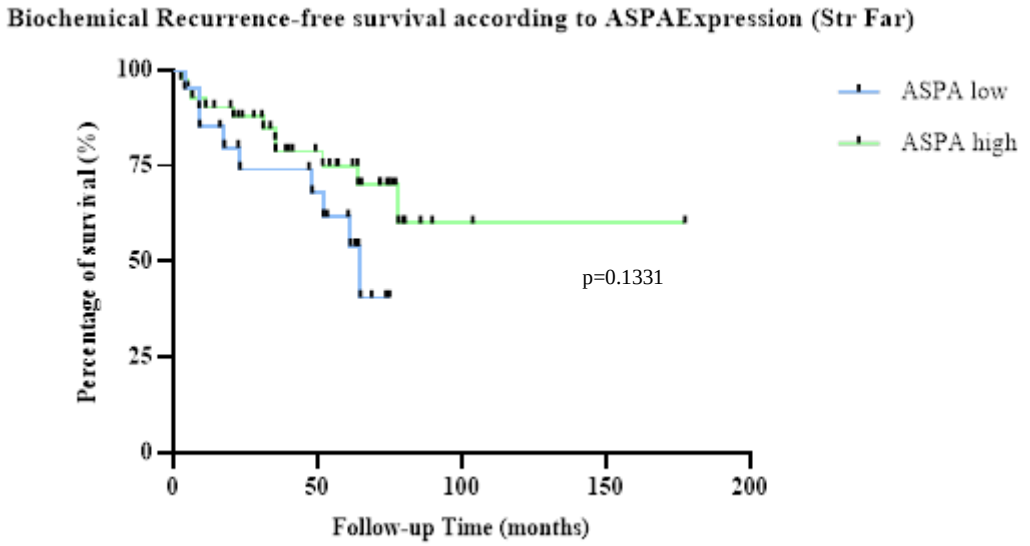

Figure 48: Correlation of ASPA expression with clinico-pathological data. *BRFS according to ASPA expression in the Str Far.*

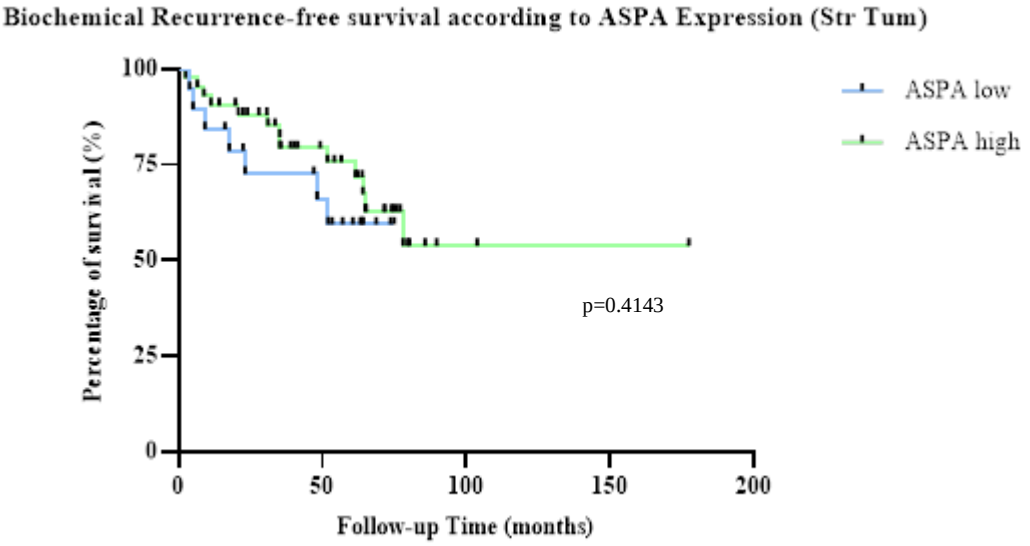

Figure 49: Correlation of ASPA expression with clinico-pathological data. *BRFS according to ASPA expression in the Str Tum.*

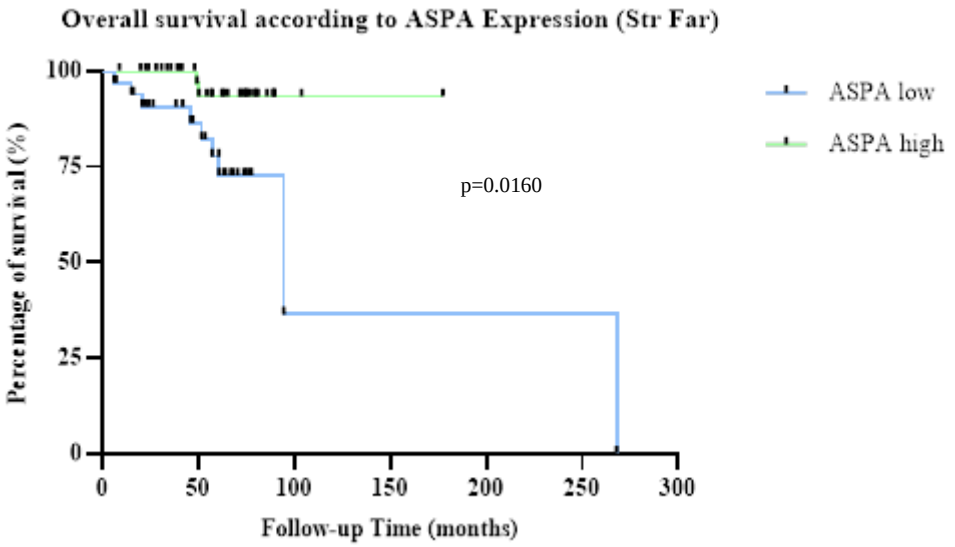

Figure 50: Correlation of ASPA expression with clinico-pathological data. *OS according to ASPA expression in the Str Far.*

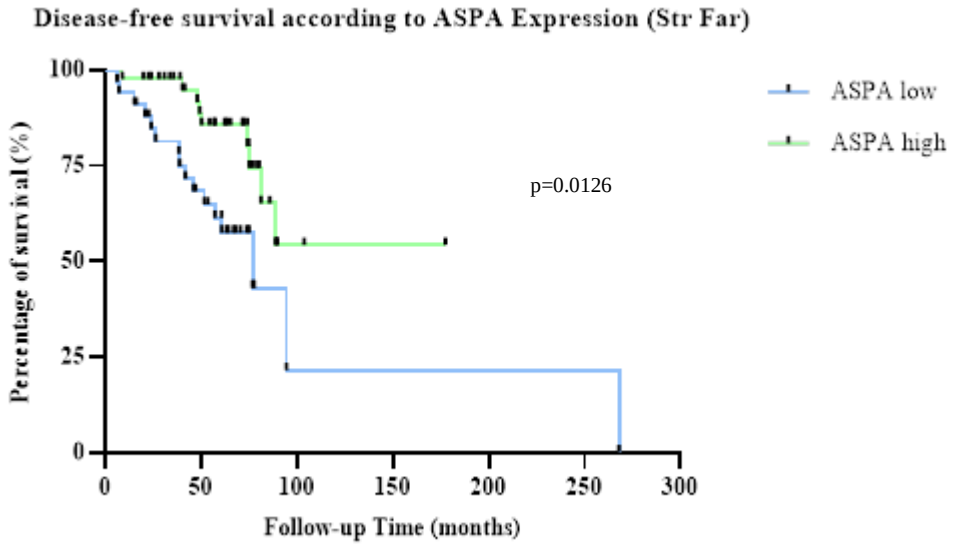

Figure 51: Correlation of ASPA expression with clinico-pathological data. *DFS according to ASPA expression in the Str Far.*

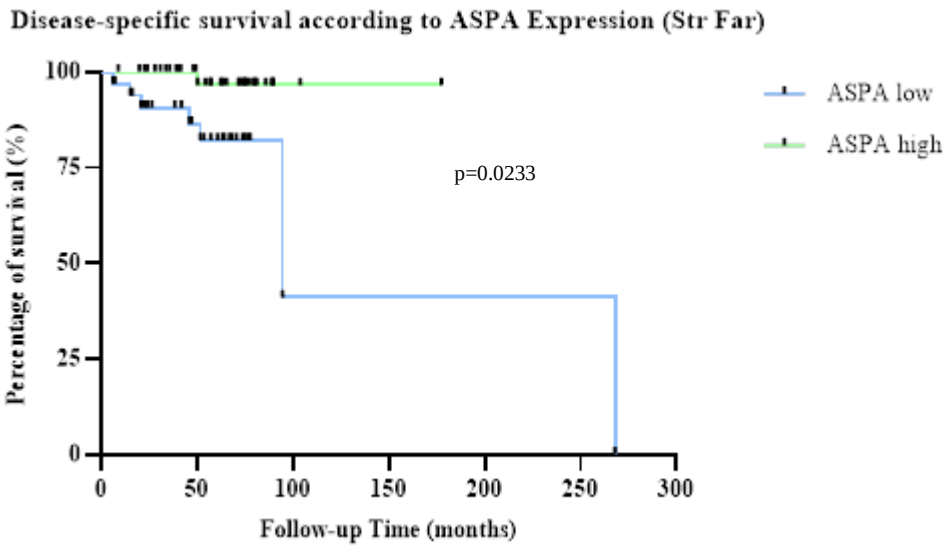

Figure 52: Correlation of ASPA expression with clinico-pathological data. *DSFS according to ASPA expression in the Str Far.*

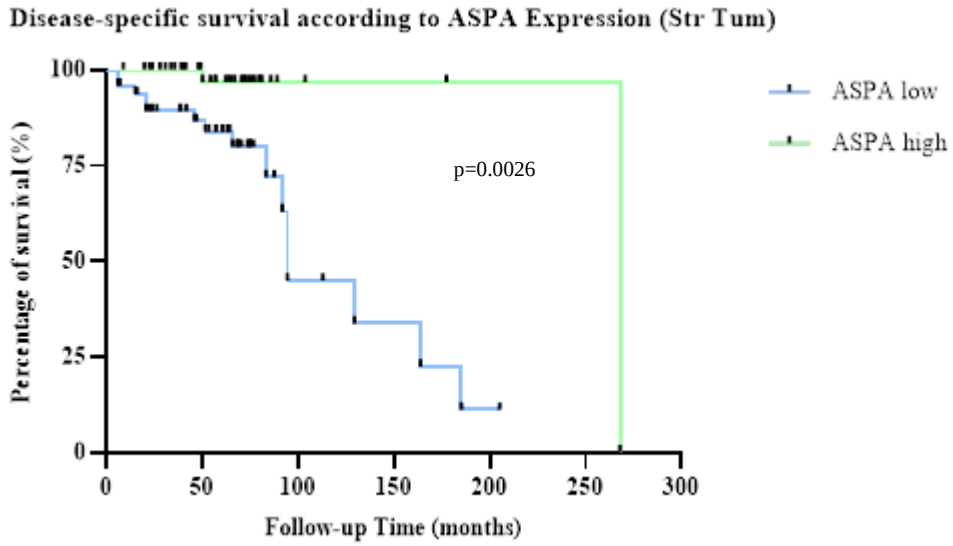

Figure 53: Correlation of ASPA expression with clinico-pathological data. *DSFS according to ASPA expression in the Str Tum.*

Correlation of Desmin expression with clinico-pathological data

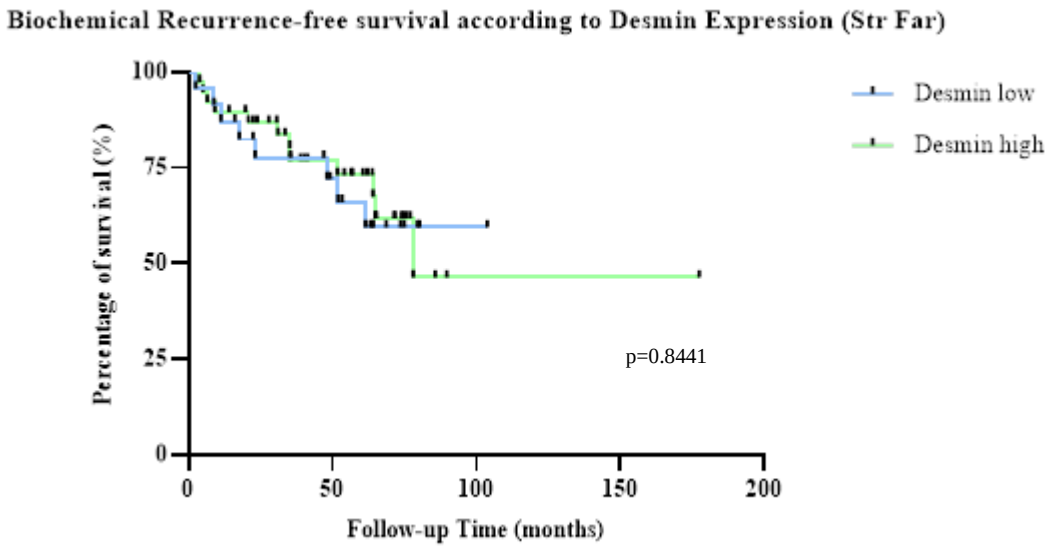

Figure 54: Correlation of Desmin expression with clinico-pathological data. *BRFS according to Desmin expression in the Str Far.*

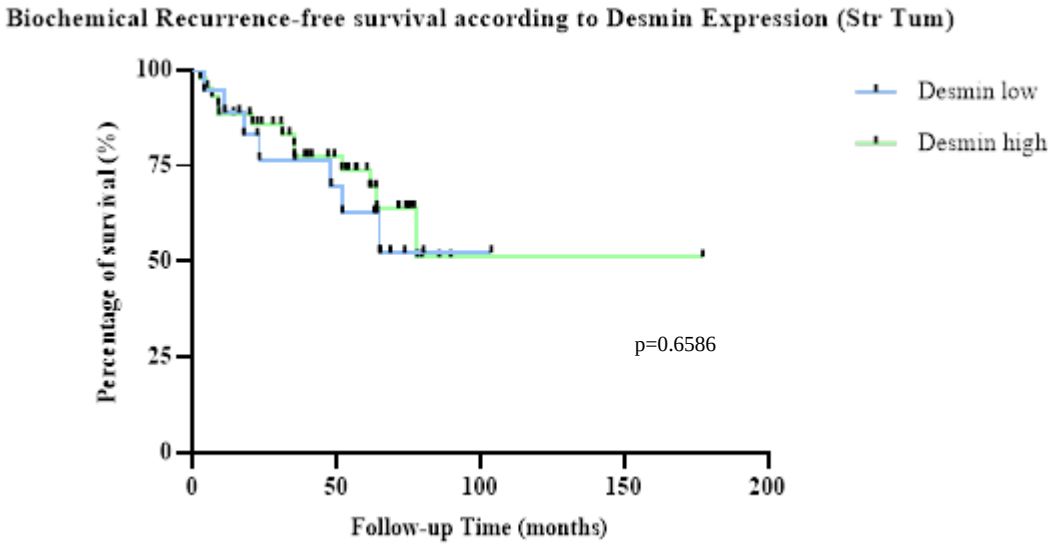

Figure 55: Correlation of Desmin expression with clinico-pathological data. *BRFS according to Desmin expression in the Str Tum.*

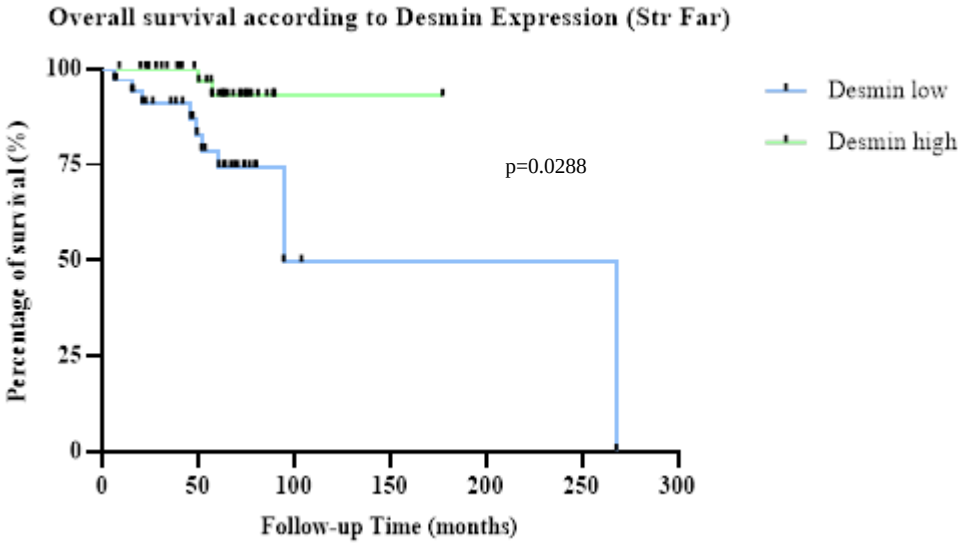

Figure 56: Correlation of Desmin expression with clinico-pathological data. *OS according to Desmin expression in the Str Far.*

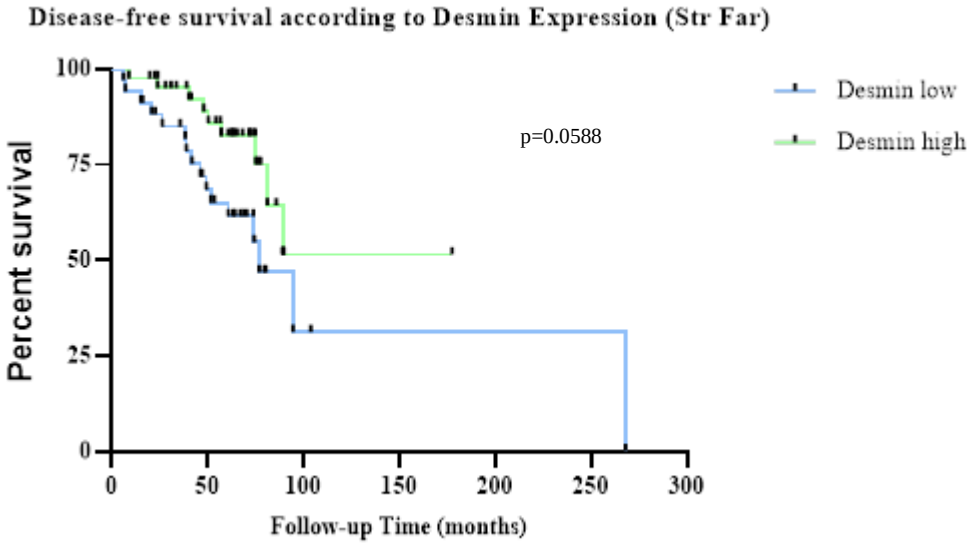

Figure 57: Correlation of Desmin expression with clinico-pathological data*. DFS according to Desmin expression in the Str Far.*

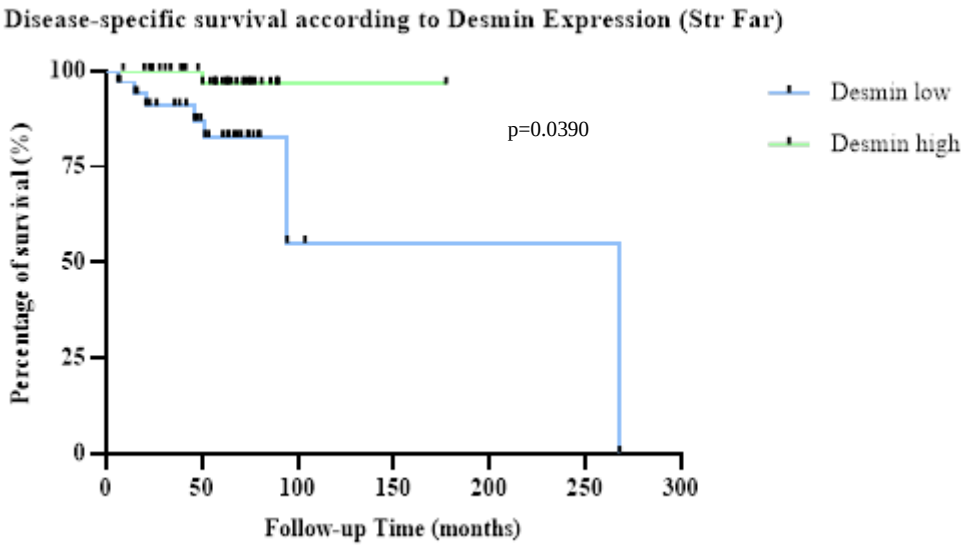

Figure 58: Correlation of Desmin expression with clinico-pathological data*. DSFS according to Desmin expression in the Str Far.*

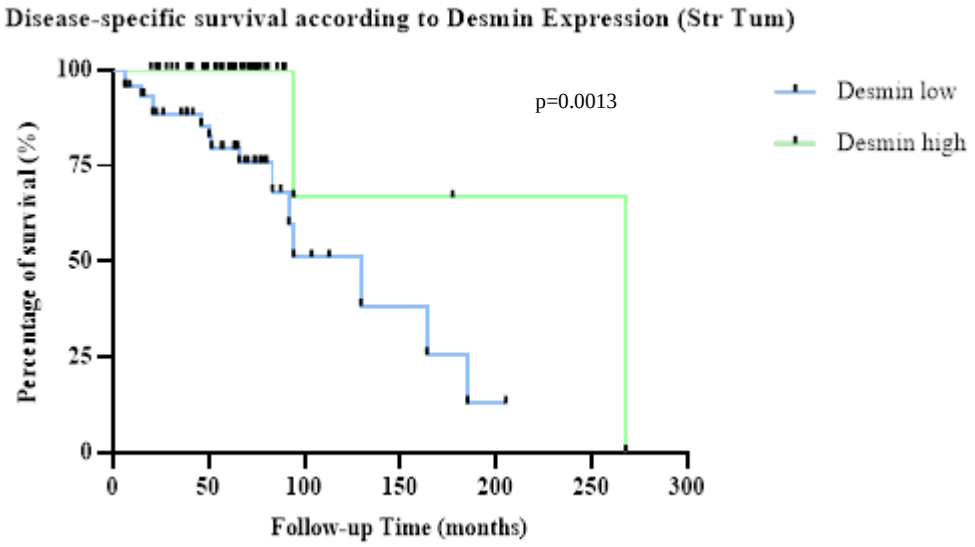

Figure 59: Correlation of Desmin expression with clinico-pathological data. *DSFS according to Desmin expression in the Str Tum.*

Correlation of Vascular Density with clinico-pathological data

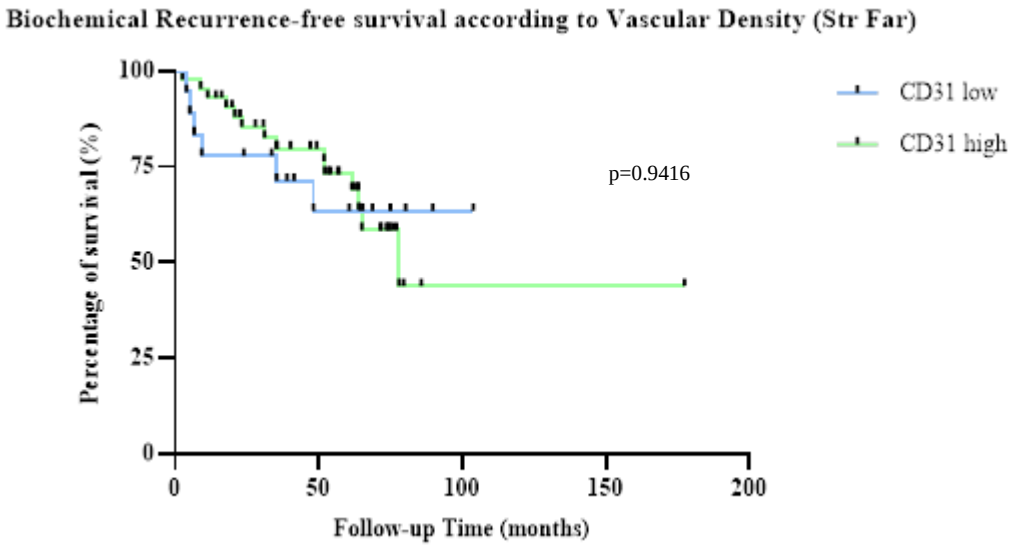

Figure 60: Correlation of Vascular Density with clinico-pathological data. *BRFS according to Vascular Density in the Str Far.*

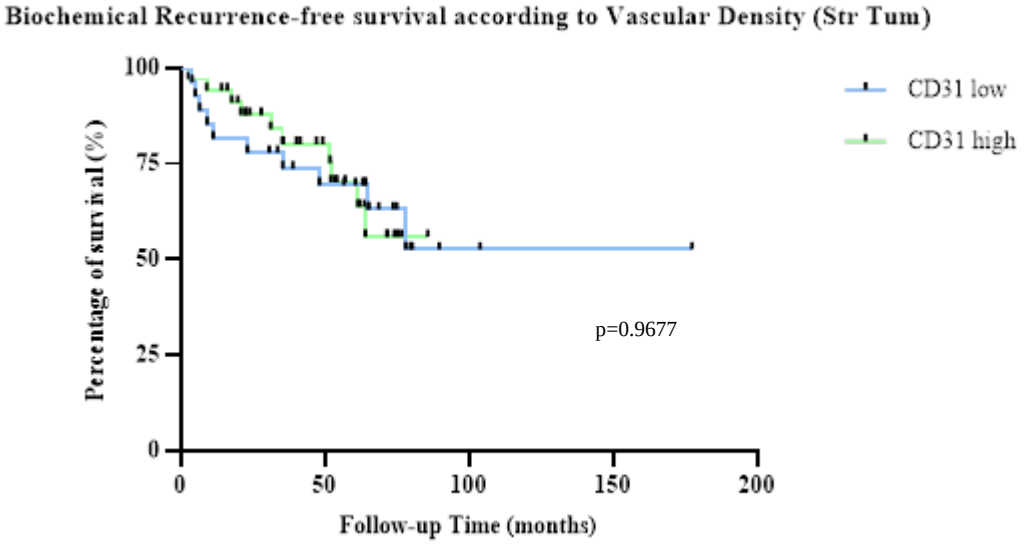

Figure 61: Correlation of Vascular Density with clinico-pathological data*. BRFS according to Vascular Density in the Str Tum.*

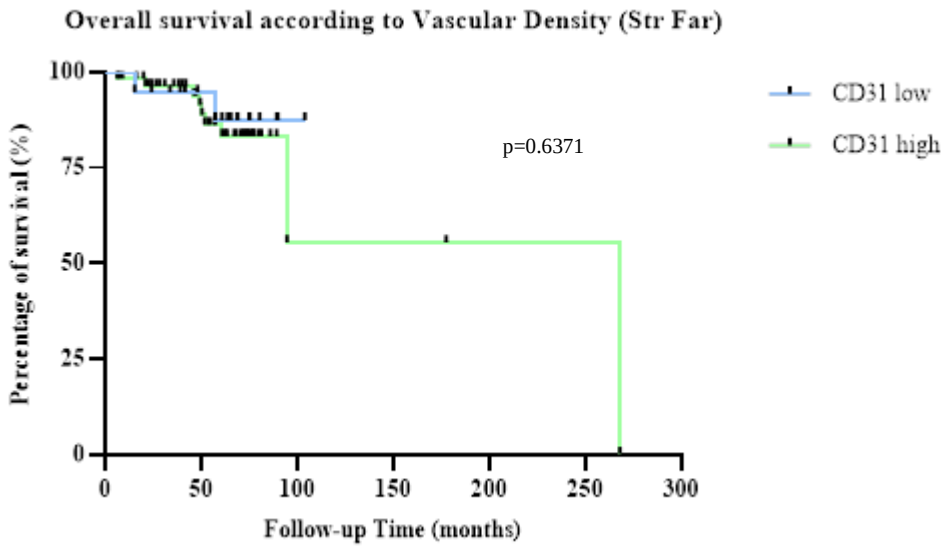

Figure 62: Correlation of Vascular Density with clinico-pathological data*. OS according to Vascular Density in the Str Far.*

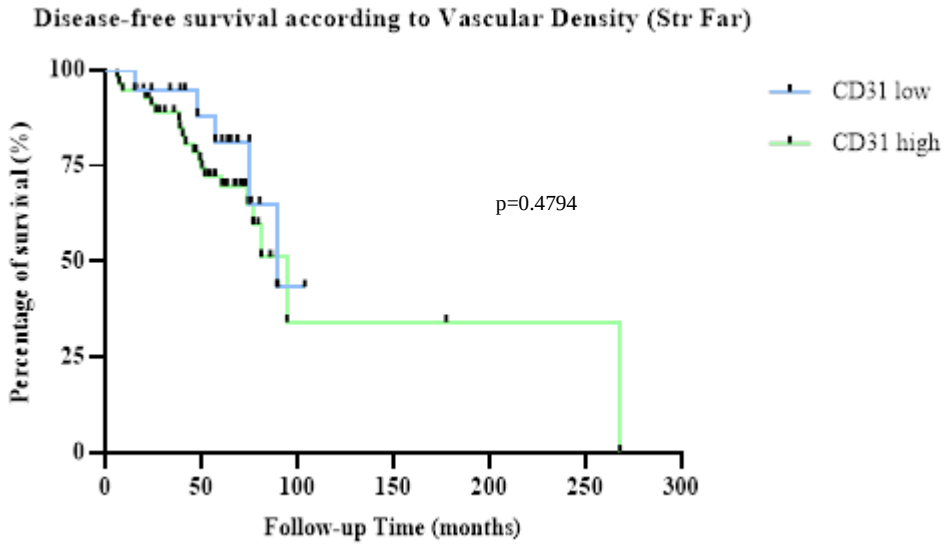

Figure 63: Correlation of Vascular Density with clinico-pathological data. *DFS according to Vascular Density in the Str Far.*

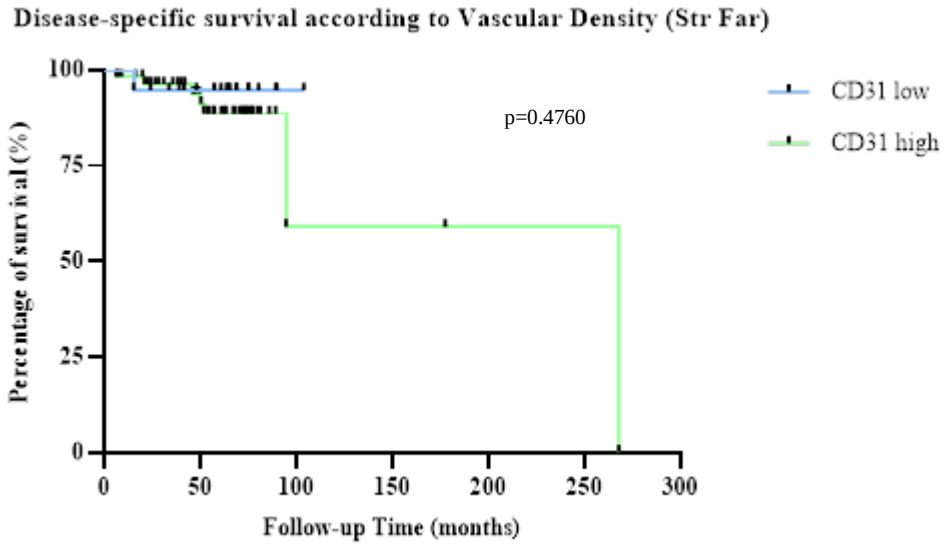

Figure 64: Correlation of Vascular Density with clinico-pathological data. *DSFS according to Vascular Density in the Str Far.*

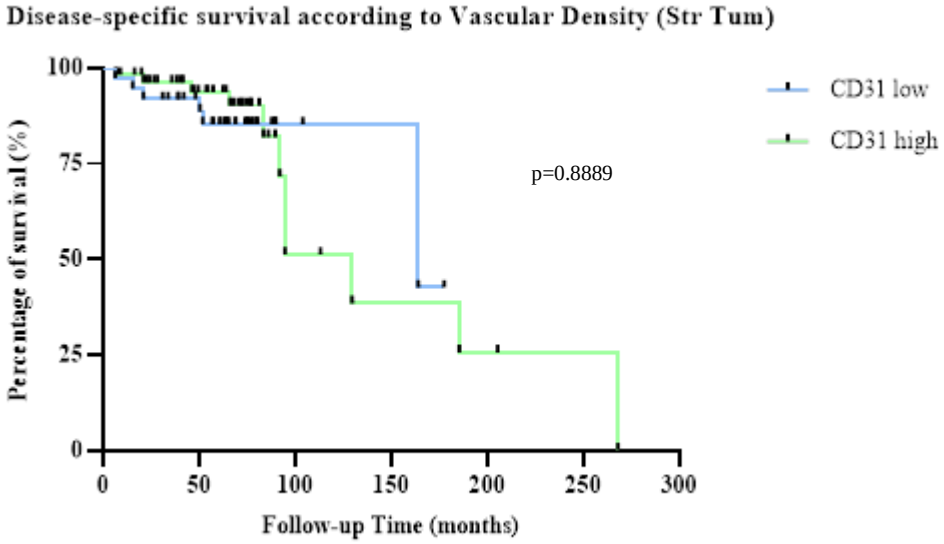

Figure 65: Correlation of Vascular Density with clinico-pathological data. *DSFS according to Vascular Density in the Str Tum.*

Correlation of CD68 positive cells numbers with clinico-pathological data

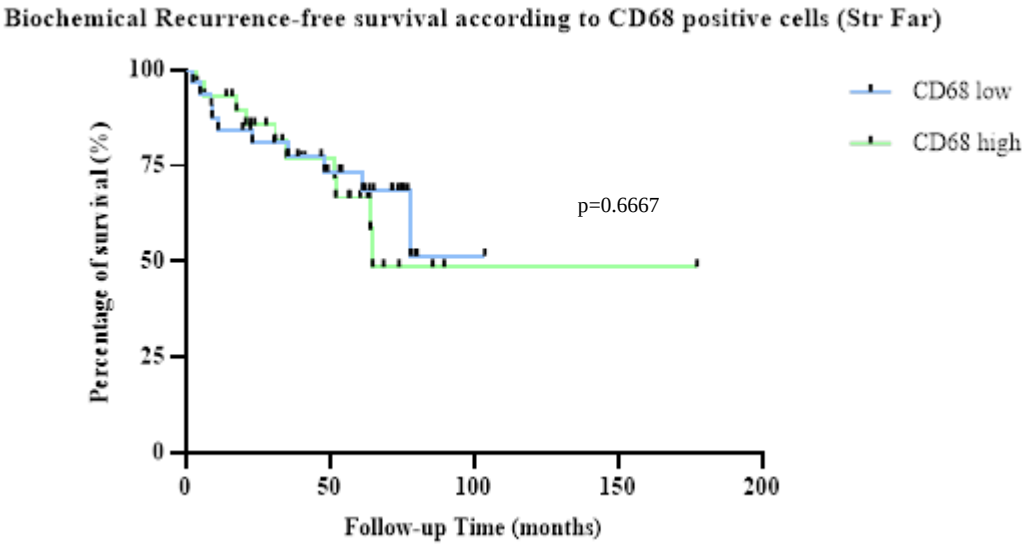

Figure 66: Correlation of CD68 positive cells with clinico-pathological data. *BRFS according to CD68 expression profile in Str Far.*

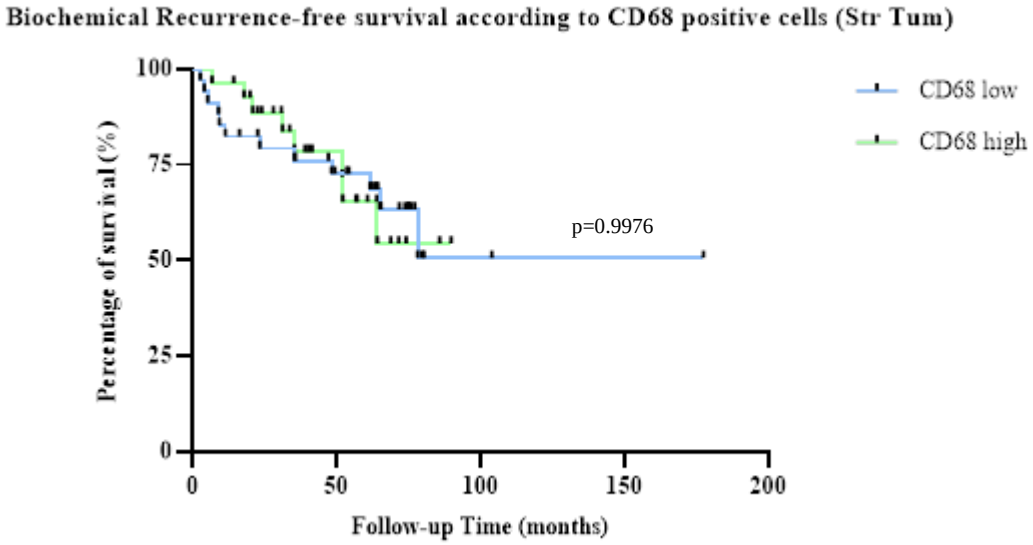

Figure 67: Correlation of CD68 positive cells with clinico-pathological data. *BRFS according to CD68 expression profile in Str Tum.*

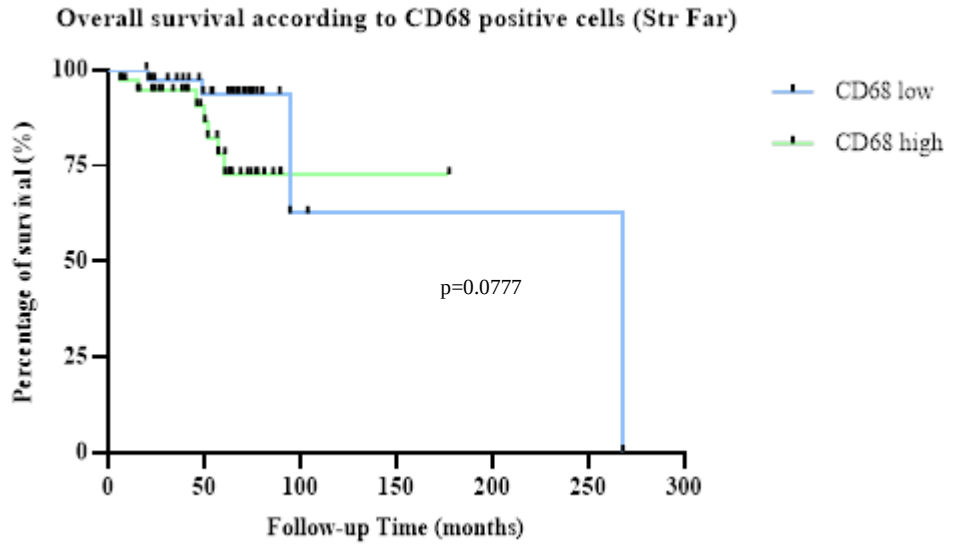

Figure 68: Correlation of CD68 positive cells with clinico-pathological data*. OS according to CD68 expression profile in Str Far.*

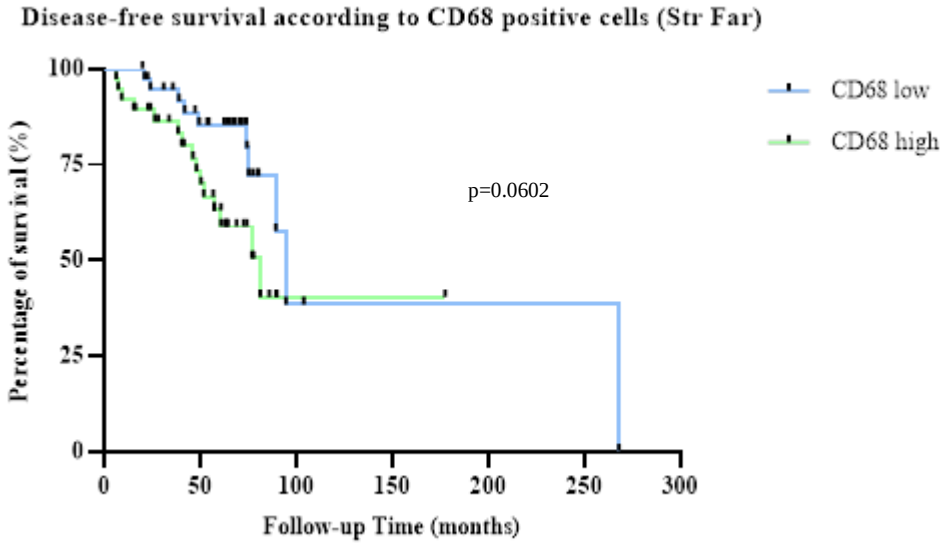

Figure 69: Correlation of CD68 positive cells with clinico-pathological data. *DFS according to CD68 expression profile in Str Far.*

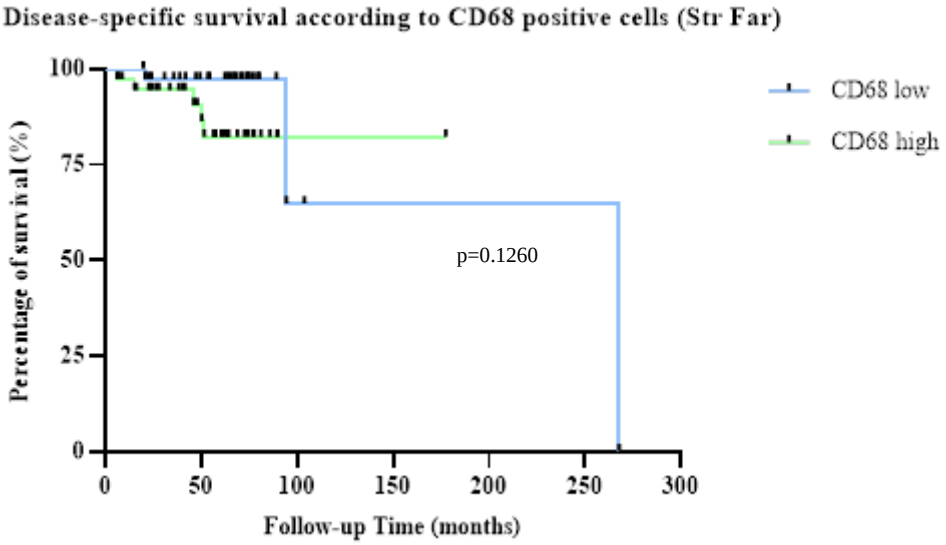

Figure 70: Correlation of CD68 positive cells with clinico-pathological data. *DSFS according to CD68 expression profile in Str Far.*

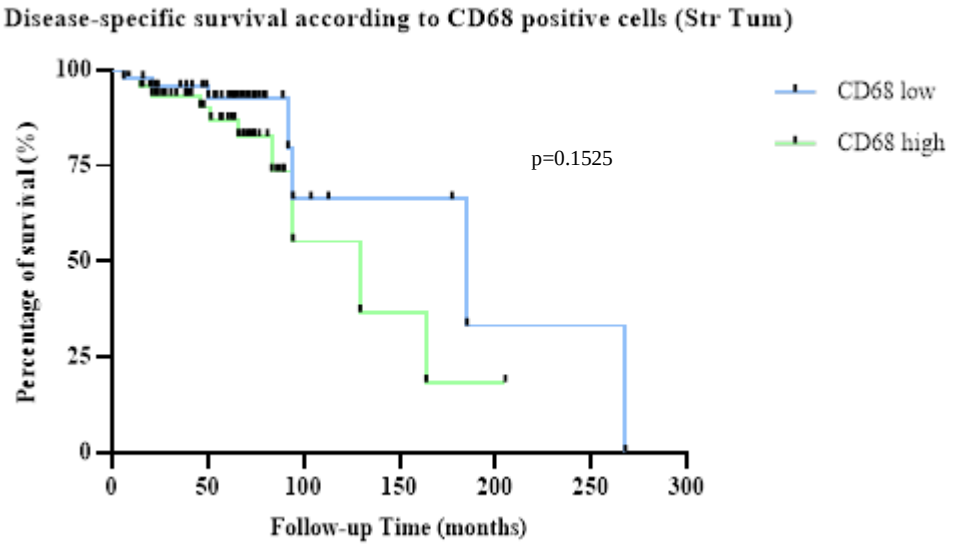

Figure 71: Correlation of CD68 positive cells with clinico-pathological data. *DSFS according to CD68 expression profile in Str Tum.*